EXPERIMENTAL VALIDATION OF A NOVEL STRUCTURAL HEALTH MONITORING
STRATEGY FOR BOLTED PIPELINE JOINTS

by

Julie L. Briand

Submitted in partial fulfilment of the requirements
for the degree of Master of Applied Science

at

Dalhousie University
Halifax, Nova Scotia
August 2010

DALHOUSIE UNIVERSITY

DEPARTMENT OF CIVIL AND RESOURCE ENGINEERING

The undersigned hereby certify that they have read and recommend to the Faculty of Graduate Studies for acceptance a thesis entitled "Experimental Validation of a Novel Structural Health Monitoring Strategy for Bolted Pipeline Joints" by Julie L. Briand in partial fulfillment of the requirements for the degree of Master of Applied Science.

Dated: August 18, 2010

Supervisor: _____

Readers: _____

                     _____

                     _____

DALHOUSIE UNIVERSITY

DATE: August 18, 2010

AUTHOR: Julie L. Briand

TITLE: Experimental Validation of a Novel Structural Health Monitoring Strategy for Bolted Pipeline Joints

DEPARTMENT OR SCHOOL: Department of Civil and Resource Engineering

DEGREE: M.A.Sc.   CONVOCATION: October   YEAR: 2010

Permission is herewith granted to Dalhousie University to circulate and to have copied for non-commercial purposes, at its discretion, the above title upon the request of individuals or institutions.

_____
Signature of Author

The author reserves other publication rights, and neither the thesis nor extensive extracts from it may be printed or otherwise reproduced without the author's written permission.

The author attests that permission has been obtained for the use of any copyrighted material appearing in the thesis (other than the brief excerpts requiring only proper acknowledgement in scholarly writing), and that all such use is clearly acknowledged.

*To Stephen Buchholz, who supported me through
my uncertainty, self-doubt and discontent;
you have my gratitude and love.*

*To Stephen Buchholz, who supported me through
my uncertainty, self-doubt and discontent;
you have my gratitude and love.*

TABLE OF CONTENTS

LIST OF TABLES

LIST OF FIGURES

LIST OF ABBREVIATIONS AND SYMBOLS USED

Latin Alphabet

c_1	The first IMF
c_i	IMFs
c_n	n^{th} IMF derived from sifting process
CGWT	Cylindrical Guided Wave Technique
DAQ	Data Acquisition
$d\left(\frac{C}{N}\right)$	Matrix of piezoelectric strain coefficients
E	EMD energy of an IMF
E	Modulus of elasticity
E_{avg}	Average EMD energy of multiple impacts, for one sensor
$E_{Damaged}$	EMD energy of an IMF calculated for the damaged state of the system
$E_{Healthy}$	EMD energy of an IMF calculated for the healthy state of the system
E_{max}	Maximum EMD energy of multiple impacts, for one sensor
E_{min}	Minimum EMD energy of multiple impacts, for one sensor
EMD	Empirical Mode Decomposition
EMD-EDI	EMD Energy Damage Index
FFT	Fast Fourier Transform
FRF	Frequency Response Functions
h_1	Difference between the signal $x(t)$ and mean m_1 in the first sifting
h_{1k}	Difference between the signal h_{1k} and the mean m_{1k} in the kth sifting
HHT	Hilbert-Huang Transform
I	Second area moment of Inertia
IMF	Intrinsic Mode Function
L	Length
m_1	Mean of the upper and lower envelopes in the first sifting
m_{1k}	Mean of the upper and lower envelopes in the kth sifting process
m	Mass
NDE	Non-Destructive Evaluation
PVC	Polyvinyl Chloride
PZT	Piezoceramic, Lead Zirconate Titanate
r_1	Residual after extraction of first IMF
r_n	n^{th} residual derived after extraction of nth IMF
SEM	Spectral Element Model

SD	Standard Deviation	
SHM	Structural Health Monitoring	
SMA	Shape Memory Alloy	
$s^E \left(\dfrac{m^2}{N} \right)$	Matrix of mechanical compliance coefficients	
t	Time	
UT	Ultrasonic Testing	
VBDD	Vibration Based Damage Detection	
VBDT	Vibration Based Damage Testing	
$x(t)$	Continuous time signal	

Greek Symbols

ω	Angular instantaneous frequency
ν	Poisson's ratio
$\varepsilon^T \left(\dfrac{F}{m} \right)$	Matrix of dielectric permittivity

ACKNOWLEDGMENTS

ABSTRACT

The early detection of damage of in-service structural or mechanical systems is of vital importance. With early detection, the damage may be repaired before the integrity of the system is jeopardized, avoiding possible monetary losses, environmental impacts, injury and death. With this goal in mind, many structural health monitoring techniques have been developed which use a combination of sensors and algorithms to collect, process and interpret data to detect damage in a structure. This thesis presents work completed in support of the experimental validation of a novel structural health monitoring technique developed with the aim of providing improved qualitative results compared to those methods currently available.

This novel method is based on the detection of changes within the dynamic characteristics of a structure due to damage. In the developed methodology, the free vibration response of the structure is monitored and collected through piezoceramic sensors before and after the occurrence of damage. Subsequently, this novel method uses the decomposition part of the Hilbert-Huang Transform (HHT), known as Empirical Mode Decomposition (EMD), to decompose the free vibration signatures of a structure into a collection of oscillatory modes, called Intrinsic Mode Functions (IMFs). Next, an index, called the EMD Energy Damage Index, is created based on the energy change of the IMFs measured from the healthy-state baseline. The index therefore reflects any deviations in the structural integrity of the structure thereby providing a means to detect the presence of damage.

As part of an effort to establish the integrity and limitation of this novel damage detection method, a series of experimental testing on mechanically bolted joints was performed. The damage detection of bolted joints is an important issue due to their wide use in aerospace, mechanical and structural systems. Wherever bolted systems exist in environments which impose vibration, shocks or thermal cycling on the threaded fasteners, they are at risk of self-loosening caused by such dynamic loads. Four different bolted joint systems were tested under different conditions including a steel pipe with an 8-bolt flanged joint, a pressurized steel pipe with a 12-bolt flanged steel joint, an in-service steel pipe with a 12-bolt flanged joint and a PVC pipe with an 8-bolt flanged joint.

The proposed methodology was generally successful in detecting the inflicted damage in all cases. Numerous parameters were investigated such as impact location, sensor location, hammer tip type, frequency bandwidth, intrinsic mode functions, and boundary conditions. Two significant conclusions to this work include the necessity of establishing a method to determine which frequency band has the most sensitivity to damage and the requirement of excitation consistency.

CHAPTER 1

INTRODUCTION

1.1 STRUCTURAL HEALTH MONITORING

With passing time, the majority of systems undergo some form of deterioration which may advance to a point of jeopardizing the integrity of the system. However, with early detection and maintenance, the health condition of the system may be improved, thereby prolonging its life span and avoiding possible monetary losses, environmental impacts, injury and death. Therefore, an ideal objective is to have continuous, real-time knowledge of the integrity of in-service structures. With such knowledge, users are given confidence in the optimal usage of the structure and are able to reduce costs, minimize system downtime and avoid catastrophic failures while manufacturers are able to improve their products (Chang, 1999). Consequently, the development of diagnostic techniques to provide early detection and monitoring of new and existing systems is of vital importance.

Recent sensing technology improvements coupled with current developments in computations and communications have resulted in considerable interest in the creation of reliable and efficient health monitoring strategies (Chang, 1999). The term created to describe this relatively new, interdisciplinary field of engineering is Structural Health Monitoring (SHM).

According to Chang (1999), the objective of structural health monitoring technology is to develop autonomous systems which continually monitor and inspect structures for the purpose of detecting damage while minimizing labour involvement. For the purposes of SHM of mechanical and structural systems, damage may be defined as changes to the material and/or geometric properties of infrastructure systems, including changes to boundary conditions and system connectivity which may adversely affect the current or future performance of the system (Worden et al., 2007).

Conventional understanding of SHM entails a five step process to determine the damage state in a system (Farrar and Worden, 2007; Rytter, 1993):

I) Existence: Is there damage in the structure?

II) Location: Where is the damage in the structure?

III) Type: What kind of damage is present?

IV) Extent: How severe is the damage?

V) Prognosis: What is the remaining service life of the structure?

An SHM methodology must include a damage detection technique to fulfill the first four steps. Accurate performance of the damage detection method depends upon the sensitivity of the sensors and the interpretation algorithm of the damage sensitive features (Chang, 1999). The extent and efficiency with which the above questions are fulfilled is an excellent method of evaluating the superiority of the damage detection method and the SHM procedure overall.

The process of SHM involves observation of a system and periodic collection of response measurements, the subsequent extraction of damage sensitive features and finally an analysis to determine the health state of the structure (Farrar and Worden, 2007). It is important to note that SHM analysis uses changes in the damage sensitive features occurring between the previously assessed healthy state and the newly monitored state to detect damage. Not only is SHM useful for aging infrastructure, but it is an essential tool to establish system integrity after an extreme event such as an earthquake.

Structural Health Monitoring requires knowledge of many different disciplines including structures, materials, computation, signal processing, statistics and sensor technology. With such an interdisciplinary field, the body of work performed to date is very large and widespread. In an effort to provide a starting point for new SHM researchers, Worden et al. (2007) have summarized the fundamental truths of SHM by defining the following axioms based on the decades of previous work performed:

- *Axiom I*: All materials have inherent flaws or defects;

- *Axiom II*: The assessment of damage requires a comparison between two system states.

- *Axiom III*: Identifying the existence and location of damage may be done without performing a comparison between the healthy and damaged states, but identifying the type of damage present and the damage severity can generally only be done when data is available from both the damaged and undamaged structures.

- *Axiom IVa*: Sensors cannot measure damage. Feature extraction through signal processing and statistical classification is necessary to convert sensor data into damage information.

- *Axiom IVb*: Without intelligent feature extraction, the more sensitive a measurement is to damage, the more sensitive it is to changing operational and environmental conditions;

- *Axiom V*: The length and time-scales associated with damage initiation and evolution dictate the required properties of the SHM sensing system.

- *Axiom VI*: There is a trade-off between the sensitivity to damage of an algorithm and its noise rejection capability.

- *Axiom VII*: The size of damage that can be detected from changes in system dynamics is inversely proportional to the frequency range of excitation.

Novel SHM techniques are constantly being developed and evolved in a response to demands to increase the serviceable life of our deteriorating infrastructure. With the large investments in developing new infrastructure there is a considerable market for SHM strategies that provide detailed integrity information capable of providing early warnings of structural deficiencies. Furthermore, reliable SHM strategies that replace scheduled maintenance and periodic inspection routines will decrease the extensive labour and system downtime costs (Chang, 1999). An effective and efficient SHM strategy is one that includes a damage detection method capable of detecting and quantifying global damage as well as local damage.

Many conventional damage detection methods are no longer considered efficient because they require prior knowledge of the damage location and onsite access to each damaged location. These localized methods include: visual inspection, Liquid Penetrant

Testing (PT), Magnetic Particle Testing (MT), Ultrasonic Testing (UT), Magnetic Flux Leakage (MFL), Radiography Testing (RT), Eddy-current testing and thermal field testing. Furthermore, these methods entail undesirable expenses due to their heavy reliance on equipment and/or requirement of highly skilled operators (Rezaei, 2010).

In response to the limitations of the localized damage detection methods, Vibration-Based Damage Testing (VBDT) methods have emerged as an alternative option over the past three decades. Damage detection using VBDT methods is based on the fact that modal properties such as frequencies, mode shapes, and modal damping of a structure are functions of physical properties like mass, stiffness, and damping. When defects or damages occur in a structure, all or some of these physical properties change and lead to variations in the modal characteristics.

In contrast to conventional methods, VBDT techniques examine the general behavior of the structure and provide information on the overall, global, health state of the system. This feature makes this type of method perfect for integration with an SHM methodology. The observation of the system could then be accomplished continuously or periodically based on a collection of response measurements from an array of sensors attached to or embedded within the structure.

This global monitoring ability has made VBDT techniques an incredibly attractive research topic for various industries. Doebling et al. (1998) noted that the response to VBDT methods has been in part due to media coverage of spectacular structural failures, economic concerns and recent technical advancements. The history of quantifiable structural VBDT methods dates back to the mid 1970's when the oil industry spent considerable effort to develop the technology for their offshore platforms.

Since then, the aerospace, infrastructure and composite fields have joined the oil industry in developing VBDT techniques. Doebling et al. (1996) and Sohn et al. (2003) have performed extensive literature reviews which detail the first two and a half decades of work in the field of VBDT for structural and mechanical systems. However, despite the dedicated body of research, it is Brownjohn's belief (2007) that the effectiveness of VBDT methods still remains to be proven in practical applications of civil infrastructure such as bridges, dams, buildings, towers, offshore installations, nuclear installations and tunnels.

1.2 VIBRATION-BASED SHM

Table 1 lists the different categories of VBDT methods that have been developed to date. Each of these methods has its own advantages and disadvantages.

Table 1-1 Vibration based damage detection categories and methods (adapted from Lee et al., 2004).

Category		Methodology
Modal Parameters	Natural Frequencies	• *Frequency change* • *Residual force optimization*
	Mode Shapes	• *Mode shape changes* • *Modal strain energy* • *Mode shape derivatives*
Structural Matrix Methods	Stiffness Based	• *Optimization techniques* • *Model updating*
	Flexibility Based	• *Dynamically measured flexibility*
Machine Learning	Genetic Algorithm	• *Stiffness parameter optimization* • *Minimization of the objective function*
	Artificial Neural Network	• *Back propagation network training* • *Time delay neural network* • *Neural network systems identification with neural network damage detection*
Other techniques		• *Time history analysis* • *Evaluation of frequency response functions (FRF)*

Natural frequency analysis, used for damage sensitive feature extraction, has been the most common method in the field of VBDT. Natural frequency based methods rely on the premise that structural damage causes a reduction in the structural stiffness, which in turn changes the resonant frequencies. However, extensive research has proven that natural frequencies are a poor damage indicator, because they generally have low damage sensitivity (Lee et al., 2004) and they do not convey any spatial information that could be used for damage localization (Farrar et al., 2001).

Methods based on the evaluation of mode shapes have been more successful in detection and localizing damage. In general, mode shapes are able to provide spatial information about the structure which can be used to localize damage. However, these methods have two major practical drawbacks which make mode shape methods an

unappealing choice. According to Doebling et al. (1996), there is a lot of difficulty in taking satisfactory mode shape measurements; as well as obtaining the number of measurements required to provide sufficient resolution for damage localization.

Structural matrix methods, which are mainly based on the investigation of structures` stiffness and flexibility matrices, have also been investigated for damage detection applications. In these approaches, a change in the stiffness or flexibility matrix before and after damage is considered as an indication of damage. Structural matrix methods also suffer from practical issues in terms of an inability to take precise and complete measurements of all modes of a structure (Lee et al., 2004).

Machine learning refers to computational intelligence methods which have learning capability (Adeli and Hung, 1995). Among these methods, neural networks and genetic algorithms have drawn attention of many researchers for structural damage identification due to their ability to cope with uncertainty, insufficient information and noise (Adeli and Hung, 1995). However, these techniques have four major challenges in practical applications: brittleness, lack of Meta knowledge, knowledge acquisition, and validation (Melhem and Nagaraja, 1996).

The last category listed in Table 1 refers to VBDT methods that incorporate time history analysis and the frequency response of structures. Within this category, statistical processes are used to analyze the time history signals in order to identify damage assuming that changes in the mean and/or variance of the structure's vibration pattern result from damage. The statistical methods are limited to identification of change in the statistical parameters and do not convey any information about location nor damage severity (Lee et al., 2004).

Methods based on the frequency response functions (FRF) are an extension of mode shape curvature methods (Lee et al., 2004). The FRF of a structure in all frequencies in the measurement range is used to detect changes in stiffness assumed to be caused by damage (Lee et al., 2004). In practice, FRFs have the advantage of measurement simplicity as opposed to mode shapes; however, experimental studies on the FRF based damage detection method have demonstrated unreliability (Lee et al., 2004).

1.3 MOTIVATION

The limitations of the majority of the previous VBDT methods has prompted the emergence of a new category of time history analyses which includes damage detection methods using signal processing techniques such as the Hilbert-Huang Transform (HHT). The objective of these methods is the extraction of damage metrics based on parameters obtained from the chosen signal processing technique.

Introduced by Huang et al. (Huang et al., 1998), the HHT is in part based on the Empirical Mode Decomposition (EMD). Empirical Mode Decomposition decomposes a real signal into a collection of simpler modes or Intrinsic Mode Functions (IMFs). Each IMF has unique characteristics and represents a major component of the original signal. Damage sensitive features can subsequently be extracted from the IMFs and used for damage identification.

The advantages of HHT are its simplicity, its ability to deal with non-stationary and nonlinear signals, and its capability of extracting buried details within a signal (Rezaei, 2010). HHT can provide a lot of information about the structural dynamic behavior of the system which allows damage sensitive features to be discovered and utilized. Recently, SHM methods incorporating the HHT have been growing in popularity and have been successfully applied in various damage detection applications.

One SHM methodology based on HHT that has recently been developed is a novel damage index, referred to as the Empirical Mode Decomposition-Energy Damage Index (EMD-EDI), created by Cheraghi et al. (2005). This index uses the energy of the first IMF of the response signals before and after damage. The index, therefore, reflects any deviations in the structural integrity of the structure, thereby providing a means to detect the presence of damage.

Cheraghi et al. (2005) investigated the validity of this method by conducting an experiment on adhesively bonded joints in simply supported plastic pipes. Further experimental studies using the same method were completed by Cheraghi and Taheri (2007) to detect corrosion defects in a cantilevered aluminum pipe, Rezaei and Taheri (2009) to detect corrosion damage in a cantilevered steel pipe, Rezaei and Taheri (2010b) to detect notches in beams, and Rezaei and Taheri (2010a) to detect mid-span girth weld

cracks in a steel pipe. The EMD-EDI has not yet been experimentally validated for use with bolted pipeline joints.

1.4 OBJECTIVE

The object of this thesis was to explore the application of the Empirical Mode Decomposition Energy Damage Index, coupled with the use of piezoelectric sensors, and its integrity for detecting damage in bolted pipeline joints. This study serves to further expand the previous work accomplished on this method by focusing on a different type of structural damage than has been studied to date. For the purpose of this study, experimental testing on four different bolted pipeline joints was completed using two different materials (namely steel and PVC). The type of damage considered was loss of clamping force, the most common cause of bolted joint failure. This was achieved by bolt loosening and/or removal.

1.5 THESIS LAYOUT

This thesis is divided into seven chapters; of the seven, three chapters include publications generated in the course of this thesis.

Chapter 2 guides the reader through a detailed literature review which begins with an introduction to bolted joints, which is then followed by a summary of the joint failure problems facing owners or uses of bolted joint systems. Next, the traditional damage detection methods used for bolted joints are outlined. Subsequently, the topic of structural health monitoring, as applied to bolted joints, is addressed including the use of piezoelectric transducers in SHM. Afterward, an overview is presented of the Hilbert-Huang transform and its application to structural health monitoring. Concluding the chapter is a presentation of the EMD-EDI, followed by its application to pipelines for the purposes of structural health monitoring.

Chapter 3 details the experimental investigation performed on an 8-bolt steel pipe joint, using three different combinations of piezoceramic sensors. The objective of this study was to detect varying degrees of loosened bolts using the EMD-EDI. A description of the experimental setup, vibration testing procedure, data analysis and damage

detection process is presented. The experimental set-up involved a simply supported steel pipe jointed at the mid-section using an 8-bolt flanged joint.

Chapter 4 presents a conference paper entitled "Detection of an in-Service Condensation Pipeline Joint" which was written for the SPIE 2010 conference in San Diego, California. This paper details the experimental testing performed on an in-service joint located underground at the Central Services, Dalhousie University. The objective of this study was to detect varying degrees of loosened bolts using the EMD-EDI. A description of the experimental setup, vibration testing procedure, data analysis and damage detection process is presented.

Chapter 5 is a prepared journal article entitled "Damage Detection of a Pressurized Steel Pipeline Joint using an Empirical Mode Decomposition-Based Energy Damage Index". The objective of this study was to detect loosened bolts using the EMD-EDI, and it presents a detailed description of the experimental setup, vibration testing procedure, data analysis and damage detection process. The experimental set-up involved a free hanging pressurized steel pipe jointed at the mid-section using a 12-bolt flanged joint.

Chapter 6 provides an in depth report on the experimental tests performed on an 8-bolt PVC bolted pipeline joint. Once again, the objective of this study was to detect loosened bolts using the EMD-EDI. A detailed description of the experimental setup, vibration testing procedure, data analysis and damage detection process is presented. The experimental set-up involved a free hanging PVC pipe jointed at the mid-section using an 8-bolt flanged joint. The same tests were also complete for a cantilevered boundary condition.

As a conclusion to this thesis, Chapter 7 summarizes the experimental work completed, and gives a review of the conclusions arrived at throughout this work. Furthermore, recommendations for future work are suggested.

CHAPTER 2

LITERATURE REVIEW

2.1 BOLTED JOINTS

Bolted joints are the most commonly used components employed in the construction of civil structures and mechanical systems (Jiang et al., 2003). Often, bolts are the fastener of choice because they are a simple, low-cost, method of joining two components together, particularly in situations where disassembly and reassembly is expected to be necessary. Moreover, if a specific clamping force is required, there is little other choice beyond that of a bolted joint (Bickford, 1995). However, even after centuries of widespread use, bolted joints are still not well understood.

The bolted joint is still widely viewed as a low-tech, low priority item and its perceived importance is directly reflected in the awareness and attitudes of many of those responsible for the integrity of bolted joint connections (Metzger, 2004). There is little or no difference between the function of a welded joint and a bolted joint, nor between the consequences of potential failure of either joint. Nevertheless, for many years industry has set extensive controls over material choice, weld specifications, technician training and integrity testing of the welding operation, whilst in many cases effectively ignoring bolted joints (Metzger, 2004; Noble, 2006).

Due to inadequate awareness of the problems and issues related to bolted joints in the past, there have been many failures, including some catastrophic events. Oil drilling platforms have tipped over, airplane engines have failed, roofs have collapsed and astronauts have died because of bolted joint failures (Bickford, 1995). The Energy Institute of Great Britain reported that leaking joints were the main cause of hydrocarbon releases on UK Continental Shelf offshore installations and that similar concerns existed for many onshore facilities handling petroleum and other dangerous substances (Energy Institute (Great Britain), 2007).

Some of these failures have led to extensive news coverage. All of these failures have resulted in monetary losses for the involved parties. These impacts have led to industries becoming increasingly aware of the potential hazards posed by bolted joints and has resulted in a great deal of research into the mechanisms of bolted joint failures. It is now known that the failure of a bolted joint involves a large number of variables that are difficult if not impossible to predict and/or control (Bickford, 1995).

2.2 BOLTED JOINT FAILURE

There are three basic, overall factors which determine the reliability of a bolted connection and the probability of a joint failing in-service (Corbett, 1998):

1. Joint design
2. Bolt/component quality
3. Achieving design bolt tension during installation

Assuming a joint is correctly designed for the in-service loadings, and the components provided are initially satisfactory, achieving the correct bolt tension during installation may be reasonably difficult. Corbett (1998) states that "90% of all bolted joint failures can be attributed to incorrect bolt tightening" because "the vast majority of bolted joints in engineering are tightened in an uncontrolled manner". This may explain why the durability of a system is often proportional to the number of bolted joints used (Jiang et al., 2003).

The first few factors that may affect in-service bolt tension have one common link; they do not have anything to do with the joint itself. The first significant variable that affects the life of the bolted joint is the technicians that assemble the joint. The answers to whether the technicians are well trained, if they are adequately supervised and if they actually care about what they are doing would have a considerable impact on the joint integrity. Furthermore, the conditions that the technician has to work under to perform the assembly also have a major impact. Can the technician easily see and reach all the bolts in the joint; and, do the environmental conditions favor good concentration?

Common assembly errors made by bolting mechanics are as follows (Noble, 2006):

- Fitting the wrong gasket
- Not inspecting gasket for handling/storage damage
- Application of grease to gasket
- Not lubricating bolt threads
- Not lubricating nut spot face
- Using an incorrect lubricant
- Leaving dirt or grit on gasket face
- Greasing the groove on a ring type joint
- Re-using gaskets or rings
- Fitting nuts the wrong way so that stampings gall the flange face
- Not setting bolts correctly for tightening
- Leaving tape on gaskets
- Not inspecting and cleaning flange faces

When the joint is assembled or reassembled, time should be set aside for the joint components to be individually inspected for the correct specification and damage so that future joint problems may be prevented at the source. A prior history of the joint will also aid in preventing future problems.

A bolted joint ready for service needs to have attained the designed clamping force, which is reached by achieving the correct bolt tension in all the bolts of the joint. The following list presents additional factors which have a considerable effect on the final in-service bolt tension and thus the clamping force and the integrity of the joint. Four of these factors will be expanded on further in the following sections.

1. *Initial preloads*: the load developed in the bolts from torquing or tensioning during the initial tightening process.

2. *Sequence/procedure*: the procedure that is used to tighten the bolts of a joint can significantly affect the final in-service bolt tension such as if the bolts are tightened all in one pass at the final torque or in several passes in increments.

3. *Residual preloads*: the preload left in the bolts at the end of the assembly process after embedment, elastic interactions and short-term relaxation.

4. *External loads*: there may be external loading acting on the joint which may add or subtract from the bolt tension. Loadings such as pipeline pressure, weight of additional structural components, etc. If these loadings are not taken into consideration in the design, the clamping force may not be sufficient to maintain joint integrity.

5. *Service conditions*: the local environment surrounding the joint may cause substantial problems in the operating conditions. Conditions such as severe temperatures may cause differential expansion or contraction, or a wet environment to cause corrosion.

6. *Long-term relaxation*: relaxation may be caused by corrosion, stress relaxation or creep, and vibration.

7. *Component quality*: proper size, material, and satisfactory condition.

When a joint is assembled and put into service, there are hundreds of factors that can modify the initial and residual preload in the individual fasteners (Bickford and Nassar, 1998). Without trained technicians familiar with these variables a joint may be put into service without a sufficient clamping force. Consequently, the bolted joint will be unable to withstand the necessary loadings and will have, at the minimum, a shortened life span before leakage and or failure occurs.

2.2.1 Initial Preload

An incorrect preload on the bolts may cause a variety of joint problems affecting the behavior and life of the bolted joint. According to Bickford (1995), the following list summarizes the main issues resulting from incorrect preload:

1. *Static failure of the fastener*: the application of too much preload may cause the bolt to break or the threads to strip.

2. *Static failure of the joint member*: excessive preload may crush, gall, warp or fracture joint members (such as castings and flanges).

3. *Vibration loosening of the nut*: in most applications, proper preload can eliminate vibration induced loosening of the nut.

4. *Fatigue failure of the bolt*: a higher preload on the bolt will usually improve the fatigue life of the fastener.

5. *Stress corrosion cracking*: may cause bolt breakage and is encouraged by a high preload if it is above a specific threshold.

6. *Joint separation*: a low preload may allow the joint to separate, resulting in leakage and/or joint failure.

7. *Joint slip*: inadequate preload may cause the joint to slip under shear loads causing misalignment, cramping, fretting corrosion, fatigue, or bolt shear.

Too much preload may be just as troublesome as too little preload. Furthermore, a uniform preload for all the fasteners in a joint is also important to prevent joint failure. Factors contributing to an incorrect initial preload include friction, embedment, nonparallel joint surfaces and the method used for bolting the joint.

2.2.1.1 FRICTION

Even though a bolted joint would not work without friction, it is also a significant factor that contributes to a smaller preload than desired if torque is used to assemble the joint. Figure 2-1 illustrates the relationship between torque, friction and the resulting bolt tension.

Ninety percent of the torque applied to tighten a bolt is typically absorbed by friction. Approximately 50% is lost to interface friction between the nut and joint, and another 40% is lost to friction between the nut and the bolt thread surfaces. Figure 2-1 suggests that only 10% of the applied torque is actually converted into bolt preload and that any increase in friction has a significant impact on the amount of torque converted to bolt tension.
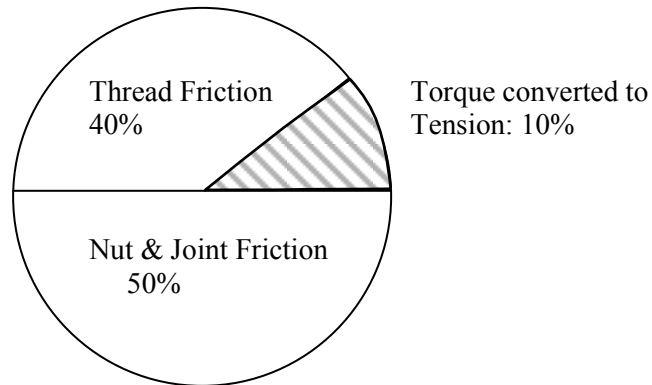
Figure 2-1 Relative relationship between torque, friction and bolt tension (adapted from Bickford, 1995).

Listed below are factors that affect the torque-preload relationship by possibly affecting the available friction (Bickford, 1998b):

- Lubrication: amount, type, temperature and location
- The hardness of the bolt, nut, joint members, washers
- Surface finishes of each part
- The type of materials used for each part
- The thickness, condition, consistency and type of plating
- The manufacturing process used to form the threads
- The thread form
- Hole finish, alignment, concentricity
- Burrs around edges of holes
- Whether or not the holes have been countersunk
- Type, number, size, location, and hardness of washers used
- Fit of wrench on nut or bolt
- The order in which the torque is applied to the nut or bolt

Additional geometric factors that may affect the friction and therefore the final bolt preload are (Bickford, 1998b):

- Fit between threads: tighter-fitting threads result in larger contact areas than loose fitting threads. Higher contact pressure result in greater friction forces.

- Hole clearance: larger holes with greater clearance will reduce the contact area between the joint face and the bolt head/nut face increasing the contact pressure.

- Hole perpendicularity: the angle of the bolt hole to the joint face will affect how well the bolt head and nut sit against the joint and if any increase in contact pressure would occur.

- Angle of threads: if the thread angle of the nut does not perfectly match the thread angle of the bolt, the contact area would be reduced.

- Hole interference: if the holes in the mating surfaces are misaligned, then when the bolt is tightened, it will scrape against the hole wall, contributing additional friction to the tightening process.

Further factors that also have an effect on friction will be mentioned throughout the following sections.

2.2.1.2 EMBEDMENT

In some situations, as shown in Figure 2-2, there may be hole interference due to an undersized bolt hole caused by manufacturing tolerances in the flange and/or bolt. Additionally, the interference may be caused by flange misalignment. These frictional and/or embedment constraints cause some of the tension in the bolt to be lost as the bolt is forced past the walls of the hole, thereby reducing the final joint clamping force.
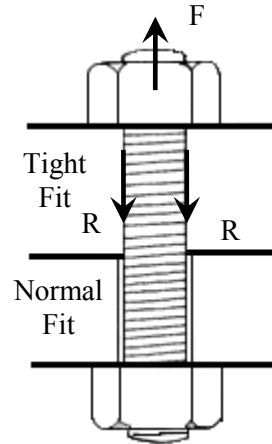
Figure 2-2 Bolt hole interference (adapted from Bickford, 1995).

2.2.1.3 NONPARALLEL JOINT SURFACES

Another factor that can reduce the clamping load is misalignment of the mating flanges of the joint. If the flanges are initially nonparallel or simply too far apart, and the bolt tightening process is relied upon to bring flanges into contact with each other, it would require torque to advance the flanges towards each other. If this additional required torque was not taken into account by the designer, then there would not be sufficient torque left to provide the desired clamping force.

2.2.1.4 BOLTING METHOD

The type of tool used to tighten the joint will have a significant impact on the final preload of each bolt, if the bolts are not being inspected for the final tension. Table 2-1 lists the accuracy of a variety of bolting methods. If a method such as direct tension indicators and ultrasonic extensometers are being used then even a crude bolting method can yield accuracy within ±2% (Sturdevant, 1998). It should also be kept in mind that the torque accuracies listed above are for a midscale reading, the variation in torque accuracy at the lower and high end of the gauge scale will be even greater.

Table 2-1 Bolting method accuracy (adapted from Sturdevant, 1998).

Bolting Tool	Torque Accuracy (%)	Preload Accuracy (%)
Hydraulic torque wrench	±3-5	±23-28
Hand wrench with torque multiplier	Unknown	±70-150
Pneumatic impact wrench	Unknown	-300 to +150
Manual slugging wrench	Unknown	-48 to +50
Hydraulic stud tensioners	N/A	±20
Dial or click torque wrench	±5	±60-80

2.2.2 Residual Preload

The common assumption made when bolting a joint is that there is an equal and opposite relationship between the applied preload, or tension in the bolts, and the clamping force between joint members (Bickford, 1998a). However, there are multiple factors that may contribute to an incorrect residual preload in the bolts at the end of the assembly process.

2.2.2.1 SHORT-TERM RELAXATION

During a relatively short period of time after bolts are initially tightened, individual bolts will invariably lose some of their tension due to relaxation. Bickford (1998a) explains that this short-term relaxation generally occurs in a component, such as a bolt or gasket, or a portion of a component (such as the threads in a nut) that is loaded past its yield point. Once past the yield point, creep will begin to occur resulting in joint relaxation. Although there is no specifically known duration during which this occurs, the general pattern of relaxation is illustrated in Figure 2-3.
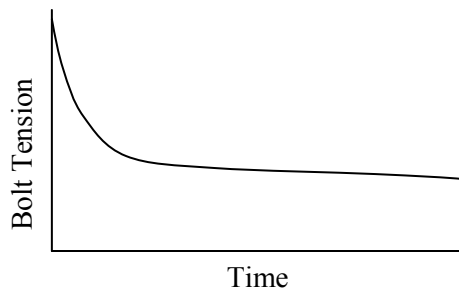
Figure 2-3 General trend of short-term relaxation (adapted from Bickford, 1995).

18

There are many causes and contributing factors to the amount of relaxation a joint will experience. Therefore, it is incredibly difficult to predict how much relaxation will occur in any specific joint.

2.2.2.1.1 Sources of Short-Term Relaxation

One of the most common causes of short-term relaxation is embedment (Bickford, 1998a). The surfaces of any component are never perfectly flat; under magnification, the surfaces of bolt threads, bolts, washers, nuts and flanges are uneven with a series of high points and low points (Figure 2-4 (a) and (b)). If the surface unevenness is sufficiently large, when loading is initially applied the high points of a surface will undergo extremely large pressures since they only constitute a small portion of the surface.

Consequently, plastic deformation will occur and the high points will flatten until a sufficient amount of the surface is in contact thus decreasing the concentrated pressure and stabilizing the system. Embedment is of particular concern with new parts since the surfaces have not suffered any wear; previously used parts do not suffer from as much embedment. If embedment occurs with a conical joint surface (Figure 2-4 (c)), the diminished bolt tension is even greater than that for a flat joint surface (Bickford, 1998a).

a)   b)   c)
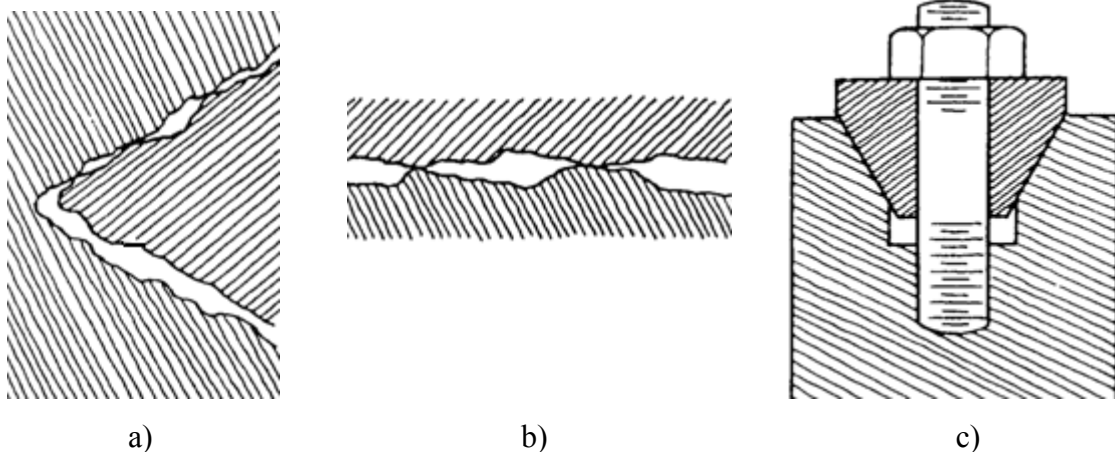
Figure 2-4 Embedment **a)** Thread **b)** Joint surface **c)** Conical joint surface (adapted from Bickford, 1995).

An additional cause of short-term relaxation is the geometry of the nuts and bolts. An undersized bolt or oversized nut will result in little contact between threads and therefore may results in substantial plastic deformation. Moreover, if the thread engagement length

is too short, the thread contact area will be insufficient resulting in excessive relaxation. Furthermore, Bickford states (1998a) that the contact faces of nuts and bolt heads are never exactly perpendicular to the axis of the threads or to the axis of the bolt hole. Consequently, there will be little contact between threads, illustrated in Figure 2-5, causing plastic deformation.
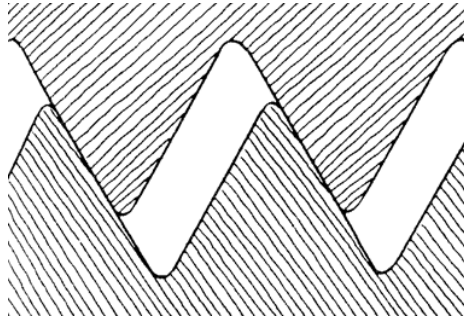
Figure 2-5 Poor thread engagement (adapted from Bickford, 1995).

Loss of preload may also come from the geometry of the bolt hole. If the fillet joining the body and head of the bolt contacts the edge of the bolt hole as shown in Figure 2-6 (a), the edge of the bolt hole will break down when the bolt is tightened. Once it does, the amount of stretch in the bolt will lessen, and bolt tension will decrease. As well, if a bolt is paired with an oversized hole without the benefit of a washer (illustrated in Figure 2-6 (b)), there will only be a small contact surface available for the bolt/nut head.

a)   b)
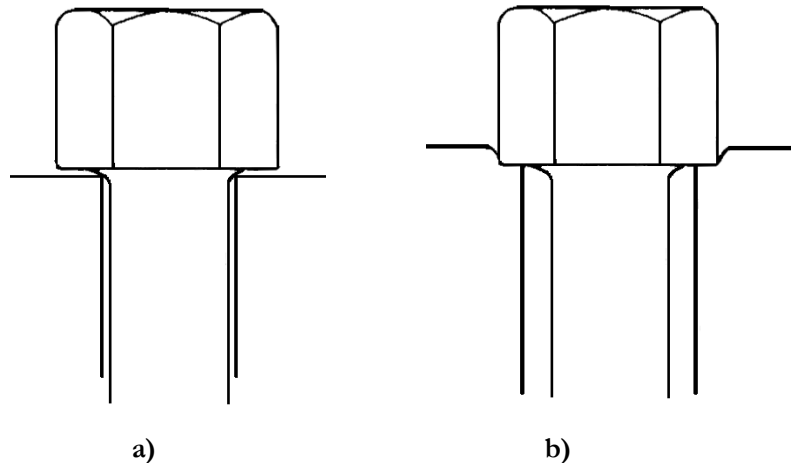
Figure 2-6 Poor geometry **a)** Contact of edge with fillet **b)** Oversized bolt hole (adapted from Bickford, 1998a).

20

Depending on the surface material, the bolt/nut head may embed in the joint surface causing relaxation.

If a part is soft, due to a manufacturing error, such as improper heat treatment or using incorrect material, creep and relaxation will again occur. If a fastener is bent as it is tightened, as in the case of flange misalignment, one side of the fastener will undergo higher stresses. If these stresses exceed the material's yield limit, the bend in the fastener will cause greater than normal embedment (Bickford, 1998a).

2.2.2.1.2 FACTORS AFFECTING SHORT-TERM RELAXATION

The degree of relaxation that will occur in a particular bolt or joint as a whole depends on some secondary factors in addition to the primary causes listed above. The effects of all the relaxation sources listed above will be greater in a more complicated joint. A joint that has more members and more contact surfaces will suffer from more relaxation. It is also important to remember that relaxation takes time. Joints that are tightened very quickly will not have any time to relax during the process. If the bolts of a joint are tightened in passes, the components are given time to stabilize which allows the necessary bolt tension to be reached.

An additional factor may be the process of tightening one bolt at a time (Prodan, 1974, as cited in Bickford, 1998a). The initially tightened bolt may undergo higher concentrated stress levels resulting in a greater level of relaxation for that fastener. Furthermore, if joint members are bent out of shape, tightening one bolt may cause additional stress in other fasteners, possibly resulting in further relaxation.

Another of these factors is bolt length. Because of a smaller thread to length ratio, long, thin bolts will relax to a lesser degree than shorter bolts with a larger diameter. If both bolts have the same amount of threads, the embedment will be the same for both; however, preload loss is proportional to the change in length, so shorter bolts will cause greater preload losses. Bushings are often used to take advantage of this fact by effectively increasing the length of the joint which allows longer bolts to be used, resulting in less joint relaxation (Bickford, 1998a).

2.2.2.2 ELASTIC INTERACTIONS BETWEEN BOLTS

During the assembly of a multi-bolt joint, tightening one bolt will cause changes in the preload of the other bolts in the joint. The term used by Bibel (1998) to describe this phenomenon is "elastic interactions". When one bolt is tightened, the joint is compressed, allowing the previously tightened bolts to relax a little. With each subsequently tightened bolt, each previously tightened bolt will react the same way. A technician unaware of this fact may assume a joint has the correct preload if the correct tightening procedure is not followed.

2.2.3 Service Conditions

Depending upon the design of the joint and the chosen components, the environmental conditions may have a significant impact on the joint once it is put in-service. For example, gaskets may be fatigued by fluctuating internal pressures, or they may be chemically altered or suffer changes in their elasticity and strength due to heat. Elevated temperatures will reduce component strength and thermal fluctuations may cause differential expansions and contractions in various joint components changing the loading conditions and possibly contributing to eventual joint failure. Anything that causes a gasket to shrink may cause a loss of clamping force, leading to joint instability and gasket blow out.

Components are also susceptible to hydrogen embrittlement. Hydrogen embrittlement can occur during the manufacturing process or during in-service operation by processes such as electroplating and cathodic protection. Hydrogen embrittlement is caused by the diffusion of hydrogen atoms into a material and their subsequent assembly in cavities which exerts pressure on the material. The buildup in pressure causes the material to become brittle and susceptible to cracking.

In addition to temperature fluctuations, pressure fluctuations, chemical alterations and hydrogen embrittlement, two more environmental causes of component damage are fatigue and corrosion.

2.2.3.1 BOLT FATIGUE

If a joint is subject to cyclic loading, the affect that bolt fatigue could have on the life of the joint must be considered. Proper maintenance of the clamping load on the joint is extremely important to bolt fatigue life. Kull (1998) states that in well designed joints, where the clamping load has been maintained, the bolts may only see 5-10% of the total load on the joint. Therefore, all of the factors that reduce the required clamping force would have an effect on bolt fatigue life.

Joint design, the surrounding environment, and the type of loading on the joint will all have an effect on the bolt fatigue. The joint stiffness ratio describes the relationship between the elasticity and geometry of the bolted members to those of the bolt. The stiffer the joint and the more elastic the bolt, the less variable load the bolt would see when a working load is imposed on the joint (Kull, 1998). Accordingly, soft gasketed joints may have shorter fatigue lives than metal joints having a greater stiffness.

Environment conditions such as high, low or fluctuating temperatures and/or a corrosive situation may also reduce bolt fatigue life. If the in-service loading results in the transverse movement of the joint (evidence of insufficient clamping force), the bolts may loosen significantly, thus affecting bolt fatigue life (Junker, 1972).

If plated bolts need to be used for a corrosive environment or if the bolt threads have been damaged in any way, the fatigue life of the bolt is also reduced (Kull, 1998). Any manufacturing defect in the bolt will also have an effect, including any anomalies in the geometric configuration of the bolt.

2.2.3.2 CORROSION

Corrosion is the deterioration of a material due to electrochemical reactions with its surrounding environment. There are many different types of corrosion that may occur in a joint:

- *General (uniform corrosion)*: occurs over the entire exposed surface of the metal due to microscopic anodes and cathodes.
- *Galvanic corrosion*: occurs when two dissimilar metals are in electoral contact and one metal corrodes preferentially.

23

- *Pitting corrosion*: localized corrosion due to high localized energy at inhomogeneities in the structure.

- *Crevice corrosion*: occurs in crevices where liquid may gather and become stagnant. Crevice corrosion is commonly found under rivets, bolts, gaskets and between valve disks and seats.

- *Intergranular corrosion*: occurs at grain boundaries and weakens the alloy.

- *Stress corrosion cracking (SCC)*: may occur unexpectedly when a metal experiences tensile stress in a corrosive environment. The stress may be from assembly, in-service loadings or manufacturing residuals. This type of corrosion is very chemically specific; only certain combinations of metal and environmental conditions would result in SCC.

- *Fretting corrosion*: occurs at the contact surfaces of components under load. When components are not designed to move relative to one another as may happen with vibration and/or joint slippage, metal fragments or surface oxides may break loose and become an abrasive, wearing away the contact surface due to the load.

Corrosion may be controlled by using corrosion resistance materials, protective coatings, inhibitors, and cathodic protection. Furthermore, the design of the joint itself would have a large impact; whether dissimilar metals are used side by side, or there are any drainage options for stagnant liquid, if corrosion is taken into account when designing the thickness of the components, and if the production of areas of high stress concentration is avoided.

2.2.4 Long-Term Relaxation

There are several factors affecting long-term in-service bolt tension relaxation. Among these are creep, stress relaxation and dynamic loadings. Creep, the tendency of a solid material to slowly deform under constant loading, may occur in materials after long term exposure to levels of stress that are below the yield strength of the material. Stress relaxation, which is temperature dependant, occurs when the elastic deformation becomes

plastic or permanent and the loss of elasticity lowers the clamping force. Another factor affecting long-term relaxation is the self-loosening of bolts from dynamic loadings.

Joints must often exist in environments where they are subjected to dynamic loadings. Fasteners in a joint may loosen (self-loosen) if they are exposed to vibration and/or shocks, thermal cycles, and flexing of joint members. The self-loosening phenomenon is also observed if the joint undergoes external transverse or shear loading, or any type of cyclical loading that causes relative slip at the joint. The two most common modes of failure of threaded fasteners subjected to dynamic loads are fatigue and vibration induced loosening (Pai and Hess, 2002) and vibration is the most common cause of self-loosening (Bickford, 1995).

Since 1945, there has been a great deal of experimental research into the causes of dynamic bolt self-loosening. It has been found that loosening begins with a gradual relaxation of the initial preload until a critical clamping force is reached. During this early stage, preload loss is due to material deformation (Jiang et al., 2003). Once the critical point is reached, the nut will begin to rotate and back off the bolt; this would occur very rapidly. For further detailed explanation of the research performed on the mechanisms of self-loosening as well as methods of arresting this failure mode, the reader is referred to the Handbook of Bolts and Bolted Joints, (Bickford and Nassar, 1998).

2.3 DAMAGE DETECTION METHODS FOR BOLTED JOINTS

Until recently, the damage detection methods used to detect joint problems have all required individual effort, time and training on the part of a technician. Table 2-2 lists the types of damages previously mentioned and the typical inspection techniques used for damage detection. The majority of these techniques fall under the category of non-destructive evaluations (NDE). Non-destructive testing are methods which allow the examination, and evaluation, of structures, materials, and components without causing any damage or destruction to the object being tested while providing a means to ensure product reliability and quality (CINDE, 2010).

Table 2-2 Inspection techniques for joint damage (adapted from Energy Institute (Great Britain), 2007).

Damage Type	Typical Conditions	Inspection Technique
General corrosion	Exposed Areas	Visual, sample removal, Cylindrical Guided Wave technique
Galvanic Corrosion	Dissimilar metals (flanges, bolts, gaskets)	Visual
Localised bolt corrosion	Dissimilar metals, exposed areas	Sample removal, visual, Phased Array UT*, CGWT**
Crevice corrosion	Exposed areas	Visual, sample removal
Fatigue	Joints subject to vibration, cyclic loading	Visual, Phased Array UT
Creep	High temperature applications	Time-of-flight UT
Stress corrosion cracking	A combination of a chloride-containing environment, susceptible material and tensile stress	Phased Array UT
Hydrogen embrittlement	Hydrogen can form on surface during manufacturing or be caused by Cathodic Protection	Visual, highlighting any corroded High Strength Fasteners for replacement
Flange face	Pipework containing a corrosive medium, dissimilar materials	Intrusive visual, UT

*UT stands for Ultrasonic Testing; **CGWT stands for Cylindrically Guided Wave Technique

If damage evaluation is not feasible or possible through non-destructive techniques, then a sample of bolts may be removed for destructive testing. For bolts that have been removed for one reason or another, black light testing can be used to detect stress cracking of threads and body of bolts to be reused.

2.3.1 Visual Inspection

Visual inspection is the most common method of performing non-destructive damage detection. A straightforward method, it relies on the inspector's experience and judgment for accurate damage assessment. The only equipment necessary for a visual inspection is a magnifying glass or a microscope if desired by the inspector. This method has several limitations, in that only the external parts of the joint are visible to the inspector. Therefore, visual assessment could only detect obvious damage such as extremely loose

bolts and surface corrosion. Any damage extending beyond the surface or damage without any signs on the joint surface will remain unnoticed.

2.3.2 Cylindrical Guided Wave Technique (CGWT)

The cylindrical guided wave technique can be used to detect corrosion wastage and cracks in cylindrical objects. The CGWT employs transducers to emit a continuous or pulse-wave signal. Low-frequency ultrasound waves are guided down the length of the cylindrical component being tested by its boundaries. The reflected signals that the transducers receive are then used to detect and locate damage based on arrival times, velocities and frequencies. However, because this method is based on the constant cross-section of the object being tested, it cannot differentiate between damages. The CGWT requires skilled operators due to subjective results. The advantages to CGWT are that only a small section of a pipeline needs to be accessed in order to test a relatively large area. This permits testing of buried or insulated components.

2.3.3 Ultrasonic Testing (UT)

Ultrasonic testing uses pulses of ultrasonic waves to detect defects or flaws due to their different acoustic nature (CINDE, 2010); it can be used to test any material that transmits mechanical vibrations for damage. Ultrasonic testing requires expensive equipment and well trained operators; operators should have sufficient experience since the interpretation of results is often difficult. Concerning bolted joints, ultrasonic testing may be used to test flange faces for corrosion and erosion using shear wave transducers. Phased Array Ultrasonic Testing may also be used to detect thread wear and cracking through the use of a transducer array which allows the creation of a visual image of the inspected material. Time of flight Ultrasonic Testing (TOF) is used to measure bolt preload by determining bolt elongation. Likewise, it can also be used to detect creep. Time of flight UT works by introducing a sonic pulse at one end of a bolt and measuring the time until the echo of the signal returns from the opposite end.

2.4 STRUCTURAL HEALTH MONITORING

A vast amount of civil infrastructure has been built over the last century such as buildings, bridges, dams, water supply lines, tunnels, and off-shore platforms. Over time, these structures withstand damage caused by fatigue, earthquakes, strong winds, traffic and other environmental impacts, causing deterioration. Early detection of any structural damage or deterioration prior to local failure may prevent a catastrophic failure of the entire structure (Park et al., 2006) thereby keeping the general public from harm.

With the current increased interest in ascertaining the safety and the serviceability of aged structures combined with the economics of repair and maintenance, efficient structural health monitoring methods have become essential. Because bolts are among the most prevalent form of fastening employed in structures, they make an attractive subject for the field of structural health monitoring (Mascarenas et al., 2005). Furthermore, with industries focused on the most efficient and economical design of products, redundancy is no longer such an attractive option which puts more emphasis on the need for a well developed SHM system.

The traditional method of inspecting bolted joints has been by visual assessment or other assessment that require onsite personnel. For a system with a limited number of bolted joints, these methods work well and are relatively efficient. However, when one considers that some systems, such as an offshore oil platform, can contain up to 15,000 bolted joints on critical services alone, the need for an online system becomes clear (Noble, 2006). In comparable situations, individual inspections would be extremely labor-intensive and expensive; they may also possibly expose the inspectors to hazardous conditions and uncomfortable working environments (Ritdumrongkul et al., 2004). Additionally, there may be a need for a system shutdown in order for the inspection to take place at the cost of production.

2.4.1 Piezoelectric Sensors

A very important consideration for an online structural health monitoring system is the choice of sensors. Over the past several decades, there has been significant advancement in sensing technology. There are currently a variety of sensors that may be used with

structural health monitoring systems. Commonly used sensors are optical fiber sensors, accelerometers, displacement transducers, velocity transducers, and piezoelectric sensors.

When selecting a sensor, it is important to keep in mind that the sensor should be robust enough to remain in good condition under various loading and environmental conditions (Noman, 2008). Furthermore, according to Park et al. (2006), sensors used to monitor structures should be inexpensive as many are required, should preferably be wireless with some data processing capabilities, and should have minimal power requirements. These capabilities will aid in the development of an efficient and low-cost SHM systems. It is also important to consider the capability of the sensor to measure the desired component of a particular quantity (acceleration, velocity and displacement), noise factor and the effect the sensor's mass may have on dynamics of the structure (Lee et al., 2004).

Piezoelectric transducers are widely used in the field of structural health monitoring. Their appeal comes from numerous advantageous properties such as their small size and light weight. In addition, piezoelectric sensors are attractive because they do not require excitation, they have a high signal to noise ratio, and they can be easily bonded to a structure. Furthermore, they have a fast response, high sensitivity, linear behavior, high operational bandwidth (Riley, 2005), and can operate over a large temperature range. Conversely, piezoelectric transducers have a drawback in that they are brittle due to their crystalline structure and are relatively weak in tension and shear (Rezaei, 2010).

Piezoelectric transducers operate on the basis of the electromechanical coupling exhibited by piezoelectric materials. Piezoelectric materials exhibit electromechanical coupling: they produce an electrical displacement with an application of mechanical stress, and can produce mechanical strain from an application of an electrical field (Leo, 2007). The mechanical-to-electrical coupling is known as the direct effect and the electrical-to-mechanical coupling is known as the converse piezoelectric effect. Piezoelectric sensors and actuators take respective advantage of the direct and converse piezoelectric effects. Piezoelectric self-sensing actuators have the capability of acting as both a sensor and an actuator, thereby providing a significant reduction in the number of system components for certain applications (Ritdumrongkul and Fujino, 2006).

There are three categories of piezoelectric materials: naturally occurring materials such as quartz and Rochelle salt, and two types of synthetic materials. The synthetic piezoelectric materials have greater electromechanical abilities due to their manufacturing process. The synthetics are piezoelectric polymers such as polyvinylidene fluoride, and piezoceramics such as barium titanate and lead zirconate titanate (PZT), which is the most widely used piezoelectric material (Leo, 2007).

Accordingly, piezoelectric transducers are available in two forms: piezoceramics and piezoelectric polymers. Piezoceramic sensors are available in different shapes such as plates and disks; they have a high stiffness but low cost. In contract, piezoelectric polymer patches are available in a variety of sizes as flexible, thin films. However, the polymers have greater electromechanical ability but are also more expensive than their counterparts.

Due to the benefits of piezoelectric sensors, they have been widely used in structural health monitoring methods by surface bonding or embedment. The following sections will highlight many applications of piezoelectric transducers in the field of structural health monitoring.

2.4.2 SHM Applied to Bolted Joints

To surmount the issues surrounding traditional non-destructive evaluation methods described earlier, there has been a great deal of research performed in the development of real-time, in-service, structural health monitoring systems over the past decade. Many non-destructive evaluation (NDE) techniques for bolted joints have been and are currently being developed for structural health monitoring.

For example, Lovell and Pines (1998) conducted a preliminary experimental and analytical investigation into using continuum wave models for the damage assessment of a single bolt lap joint. The system consisted of two aluminium beams bolted together and fixed at either end. Damage was created by altering the torque used to tighten the bolt. Piezoceramic actuators were employed to excite the structure in vibration, and piezoelectric strain sensors were used to monitor vibration around joint. Lovell et al. determined that their method was capable, but would be costly due to the number of sensors, actuators and other diagnostic tools required.

The objective of Stinemates et al. (2002) was to demonstrate that finite element analysis can be used to define the parameters of a structural health monitoring system. They used a finite element model to analyze a three story building with loosened bolts and validated their FEM model by comparing mode shapes and weights to the actual set-up.

Park et al. (2005) proposed the use of a PZT-induced Lamb waves-based method for the structural health monitoring of jointed steel plate-type structures. Their experimental set-up consisted of two steel plates on simple supports connected by eight bolts. Using two PZT patches for transmitter/sensor of the lamb waves, they used the Time-of-flight and wavelet coefficient as damage features to detect bolt removal.

With the goal in mind of developing a method to detect damage in a structure from ambient excitation, Nichols et al. (2007) performed experiments on a composite beam bolted at either end to two steel plates. Excitation was provided by means of an electrodynamic shaker located at mid-span and damage was bolt loosening. Damage assessment was made using the Pierson-Moskowitz distribution and in the presence of strongly varying temperatures.

Further work using auto-regressive modeling was completed by Fasel et al. (2008). Experiments and numerical analyses were performed to detect bolt preload reduction using chaotic structural excitation with a damage detection algorithm based on auto-regressive modeling. Signals were applied to the structure using macro fiber composite (MFC) patches.

2.4.3 Impedance-Based Structural Health Monitoring

Impedance-based structural health monitoring takes advantage of the direction relation between the electrical impedance of a bonded PZT patch to the mechanical impedance of the host structure. By monitoring the host structure's mechanical properties using the measured electrical impedance, changes in the structural integrity may be determined through changes in the electrical impedance. Impedance-based methods rely on high frequency structural excitations, providing a high sensitivity to minor defects.

However, due to the complexities of the damaged structures and the difficulties in high-frequency analysis, only limited information about the nature of damage can be

obtained (Yan et al., 2007). Damage location is ascertained due to the known localized detection area surrounding each sensor and the damage severity is qualitatively assessed using a damage index which measures the change in the impedance before and after damage (Ritdumrongkul and Fujino, 2006).

As a qualitative health monitoring method, the electromechanical impedance method has been widely studied (Yan et al., 2007) and bolted joints make an attractive subject due to their localized damage. For instance, Park et al. (2001) performed preliminary experimental testing on a single bolt lap-joint in an effort to monitor bolt preload loss in real time. The system consisted of two joined beams suspended from one end using fishing wire. To supplement the preload monitoring, they used a shape memory alloy (SMA) washer to restore preload loss to the joint. They successfully illustrated that the impedance method in conjunction with an SMA actuator may be used for condition monitoring and repair until a more permanent repair is possible.

To improve upon this method and make it more economically feasible, Peairs et al. (2002) experimentally investigated the use of a low cost impedance method which uses a digital signal analyzer with a Fast Fourier transform (FFT) function instead of the very expensive impedance analyzer. The low cost method was tested on the same set-up used by Park et al. (2001) as well as on a model pipeline with bolted joints. Peairs et al. were as able to detect preload loss as successfully as they could using the traditional method.

Mascarenas et al. (2005) conducted experimental research using a piezoelectric (PZT) enhanced washer in conjunction with the impedance method to detect the self-loosening mode in a moment-resisting portal frame. They used mechanical impedance matching between the PZT enhanced washers and the joint connections to detect changes in the bolt preloads. Their results demonstrated that the proposed device is only useful after large preload losses.

Park et al. (2006) explored the use of an active sensing device which consisted of a miniaturized impedance measuring chip and a self-sensing macro-fibre composite patch together with the use of the electro-mechanical impedance method to detect and quantify damage. Experimental validation was performed using a system consisted of four bolts joining together two aluminium plates. Park et al. illustrated that their method has good damage detection capability by providing consistent results according to repeated

loosening and tightening. However, it was determined that this method had difficulty determining the damage location.

Also using the impedance-based method coupled with another method, Rutherford et al. (2007) employed a non-linear feature identification technique for structural damage detection. The non-linear features associated with the electro-mechanical impedance measurements are extracted using the frequency domain autoregressive model. The experimental set-up was very similar to that of Mascarenas et al. (2005).

To improve on the conventional impedance method and create a quantitative analysis, two different approaches have been proposed, one based on neural networks and the other on wave-propagation modeling (Park et al., 2003). Lopes et al. (2000) combined the impedance based SHM technique with an artificial neural network. The artificial neural networks were integrated with the aim of further characterizing the structural damage. Lopes et al. (2000) experimentally investigated these combined methods on a quarter scale bridge section with bolted joints, and were successfully able to locate and estimate damage severity. The damage was inflicted by loosening bolts.

Ritdumrongkul and Fajino (2006) presented the use of PZT actuator-sensors in conjunction with a spectral element method (SEM) model for damage characterization. They performed laboratory experiments on a suspended two-joint and four-joint aluminum beam where damage was simulated by loosening bolts. Once the impedance was measured, numerical models of the structures were formulated in order to quantitatively locate and assess the level of damage.

2.4.4 Vibration-Based SHM of Bolted Joints

There has been substantial work on vibration-based structural health monitoring over the last several decades. For a comprehensive review of the advances in vibration based SHM, the reader is directed to Doebling et al. (1996; 1998) and Carden and Fanning (2004). Research is still ongoing, because no single method has yet been found that could identify every type of damage in every type of system (Carden and Fanning, 2004). However, considering all the research accomplished in vibration based SHM, the work on bolted joints has been limited.

Yu et al. (1999) used modal frequencies and mode shapes to identify damage in a frame structure with bolted joints. They used a combination of an analytical model coupled with experimental data to successfully detect damage. In another study, one approach that Caccese et al. (2004) used to detect bolt load loss was a low frequency modal analysis. They also investigated high frequency transfer functions between the actuator and sensors and high frequency transmittance functions between pairs of sensors.

Todd et al. (2004) used a novel technique adapted from nonlinear time series prediction. Their approach was applied to the detection of preload loss in a bolted joint in an aluminum frame structure excited by an applied chaotic waveform. Todd et al. demonstrated that their method was able to distinguish among preload losses in the joint. Also employing a time series technique, Moniz et al. (2005) used a multivariate, attractor based approach for feature extraction from the time series information resulting from a system's vibration. This approach was used to detect loosened bolts at either end of a composite beam bolted to a plate.

In a change from previous experimental work, Coelho et al. (2007) focused on the fatigue crack growth of bolted joints of aging aircraft. To investigate the use of an unsupervised machine learning method, they conducted damage detection experiments on a bolted single-lap joint instrumented with piezoelectric sensors and actuators. The damage consisted of a crack growth from a notched bolt hole at various torque levels; their method was most successful with a completely loose bolt.

Continuing the work of Coelho et al. (2007), Chattopadhyay et al. (2007) used a kernel-based machine learning technique to detect and classify various forms of damage states in both metallic and composite structures. A bolted single lap joint representative of those commonly used in aerospace structures was chosen for the experimental testing. The type of damage addressed was as combination of bolt loosening and fatigue crack damage. The damage detection algorithm employed was able to distinguish between different torque states and associated changes in the crack length of the joint.

Using vibration modal analysis, Okugawa and Tanaka (2007) conducted experimental testing on a one-bolt system; sub-space state identification to detect changes in the natural frequencies which identified a loosening bolt. Okugawa and Tanaka used a smart washer, a cantilevered plate type washer with a bonded PZT patch for self-sensing and

actuation. It was determined that this method had a very low sensitivity for detection preload loss.

In recent years, there has been an increase in interest in methods that rely on the ambient structural vibrations. With this in mind, Milanese et al. (2008) explored several frequency and time domain signal processing techniques to detect progressive bolt loosening in a bolted composite structure. Milanese et al. only used the output vibration response data from the structure using fiber optic strain sensors to simulate a scenario where the ambient vibrations could be used.

2.5 HILBERT-HUANG TRANSFORM

As mentioned in the introduction, the limitations of the majority of the vibration based damage detection methods has prompted the emergence of a new category of time-history analyses; this includes damage detection methods using signal processing techniques such as the Hilbert-Huang Transform (HHT). Huang et al. (1998) developed the Hilbert-Huang transform (HHT) in an effort to create an improved analysis method of nonlinear and non-stationary signals and, according to Loutridis (2004), to create a method for accurate time and frequency localization.

The key component of the HHT is a method called the Empirical Mode Decomposition (EMD), which is used in conjunction with the Hilbert transform. The first step of the HHT process is the decomposition of a signal using EMD into components, called Intrinsic Mode Functions (IMF), which represent the intrinsic oscillating modes of the signal. The IMFs are associated with energy at different time scales and contain important characteristics of the data (Rezaei, 2010). The second step is to apply the Hilbert transform to the decomposed IMFs and construct an energy-frequency-time distribution, known as the Hilbert Spectrum, in order to ascertain the local energy and instantaneous frequency. A more detailed description of the decomposition of the IMFs from the original signal can be found in Chapter 4: section 4.3, and Chapter 5: section 5.4.

2.5.1 Application of HHT in Structural Damage Detection

Rezaei (2010) states that the capability of the HHT to reveal physical meaning of the data has only been empirically proven (Huang et al., 1998), and although the HHT has been successfully tested and validated empirically, it lacks a strong theoretical background and analytical formulation. In spite of this, since its introduction in 1998, the Hilbert-Huang transform has been used by researchers in many fields including ocean and seismic engineering, nuclear physics, biomedical diagnostics and image processing (Loutridis, 2004). Furthermore, it has also been applied to structural damage detection in the field of structural health monitoring.

The Hilbert-Huang transform has been determined to be a powerful tool in the Vibration Based Damage Testing (VBDT) field (Rezaei, 2010), due to its simplicity, ability to deal with non-stationary and nonlinear signals, and its capability of extracting details buried in signals. Features of the HHT used in damage identification include the intrinsic mode functions, instantaneous frequency, instantaneous phase, and the Hilbert spectrum.

An early example of the use of HHT for structural health monitoring was presented by Quek et al. (2003), who illustrated the use of HHT for anomaly detection in beams and plates. The suitability of HHT was explored through four different types of anomalies: an aluminum beam with a crack, a sandwiched aluminum beam with an internal delamination, a reinforced concrete slab with different degrees of damage and a plate with distorted input signal. Quek et al. determined that the HHT is able to represent a localized event well and is sensitive to even slight distortions in the signal caused by damage.

The applicability of EMD for structural damage identification was experimentally investigated by Xu and Chen (2004). Their experimental set-up consisted of a three-story shear building model installed on a shaking table. Free vibration, random vibration and earthquake simulation tests were performed which all included damage in the form of a sudden stiffness change. Varying degrees of damage were induced using springs horizontally connected to the first floor; releasing the connecting springs decreased the structural stiffness. The EMD was applied to the dynamic response measurements of the

structure to identify the damage time instant and damage location for various test cases. Xu and Chen were successfully able to determine the damage time instant using the first IMF of the acceleration response, and concluded that the EMD was a promising tool for damage detection in real structures.

Similarly, Lin et al. (2005) used the HHT technique to analyze the data of an IASC-ASCE benchmark problem (Johnson et al., 2004) for the purposes of structural health monitoring. The data in question is from a benchmark structure consisting of an analytical structural model of a four-story two-bay steel frame structure. Lin et al. was able to successfully identify the natural frequencies, damping ratios, mode-shapes, and the stiffness and damping matrix of the structure with reasonable accuracy. Furthermore, Lin et al. were able to accurately detect the damage locations and severity of the benchmark structure using the HHT technique. Using the same data set, Liu et al. (2006) also used the HHT to successfully detect and locate the structural damages as well as detecting the instant of impact of damage during monitoring.

Cheraghi et al. (2007) employed the HHT signal analysis method for the evaluation of the vibration characteristics of polyvinyl chloride (PVC) pipes using piezoelectric sensors. They studied the use of the HHT experimentally and computationally using Finite Element simulations to establish the natural frequency and damping ratio of the pipe.

2.6 EMD ENERGY DAMAGE INDEX

Cheraghi et al. (2005) introduced a novel structural health monitoring method based on the HHT called the Empirical Mode Decomposition Energy Damage Index (EMD-EDI). The EMD-EDI is based on the energy of certain IMFs of the vibration signals.

Once the dynamic characteristics of a healthy structure during free vibration are collected through sensors, the acquired signals are then passed through a band-pass filter to ensure the existence of the first natural frequency within the data. This is followed by extraction of a specific IMF though the Empirical Mode Decomposition. Subsequently, the energy of the IMF, for each sensor, is established by:

$$E = \int_0^{t_0} (IMF)^2 \, dt \tag{2-1}$$

The above procedure is repeated for the same structure at its damaged state to determine the energy of each signal's first IMF. The last step is the application of the EMD-EDI to each sensor:

$$EMD - EDI = \left| \frac{E_{Healthy} - E_{Damaged}}{E_{Healthy}} \right| \times 100 \tag{2-2}$$

Once the EMD-EDI is calculated for each sensor, the existence and severity of damage may be determined by associating the index values with the existence of damage close to the respective sensors. The index values having the greatest amplitudes coupled with a progression of increasing index values translates to good results.

In summary, the methodology followed in the experiments documented herein is illustrated in Figure 2-7: Step 1: Monitor the vibration of a system in its healthy state using the response of sensors within the system. Step 2: Once again, monitor the vibration of the system in its damaged state using the responses of sensors within the system. Step 3: Analyze the signals and evaluate the EMD-EDI which is based on the

variation of IMF energy between the healthy and damage system states. Step 4: Establish whether damage exists based on the comparison of the EMD-EDIs evaluated in the last step.
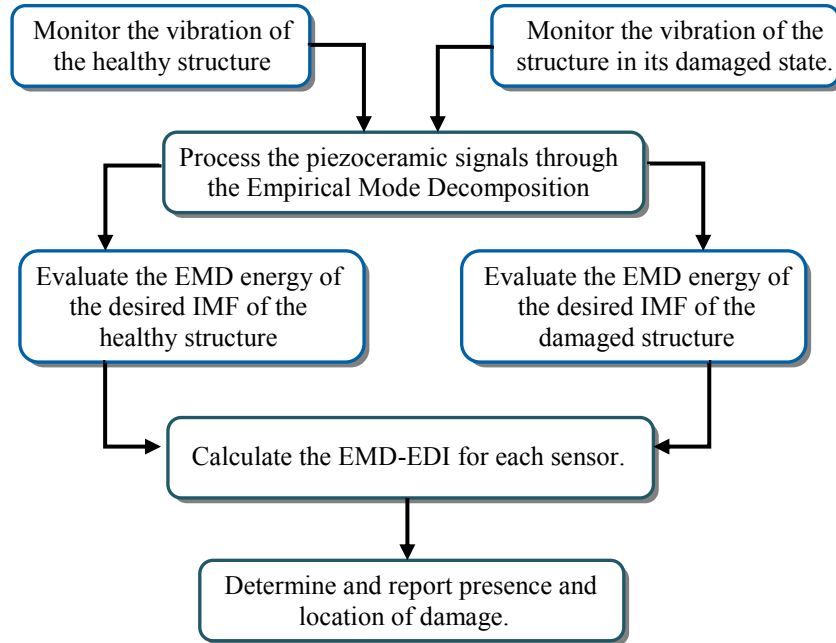
Figure 2-7 Damage detection methodology (adapted from Rezaei and Taheri, 2009).

2.6.1 Application of the EMD Energy Damage Index to SHM

Several researchers have performed experimental and numerical investigations in an effort to validate the effectiveness of the EMD-EDI method for structural health monitoring purposes. The majority of such works has concentrated on pipelines since they are such an integral part of today's residential and industrial infrastructure. Today's infrastructure relies on pipelines for conveying natural gas, oil, water, and communication and power cables.

The stability and reliability of pipelines may be affected by ground movement, environmental conditions, and damage caused by excavation equipment at any time throughout their service life, making pipeline maintenance of prime importance. Moreover, damage assessment of pipelines is especially critical for economic and community recovery after natural disasters (Park and Inman, 2005). Pipelines can be severely damaged by shaking, liquefaction, and landslides during earthquakes (Kitaura

and Miyajima, 1996). An immediate damage assessment may aid in preventing fires, explosions, and pollutions from broken gas and sewage lines (Park and Inman, 2005). For these reasons, the development of safe and reliable structural health monitoring techniques for pipelines is vital.

Mentioned earlier, Cheraghi et al. (2005) investigated the integrity of the EMD-EDI by performing a set of experiments on simply supported plastic pipes with adhesively bonded joints. The vibration response of the healthy and damaged pipes was monitored using piezoelectric patches bonded at the joint location. Joint damage was in the form of a quarter and half circumferential debond. They compared the results of the EMD method against two other damage indices based on the Fast Fourier and Wavelet signal analysis methods and concluded that EMD method could effectively detect the damage.

To further study and verify the EMD-EDI, Cheraghi and Taheri (2007) numerically evaluated the integrity of the method using Finite Element simulations. The subject of the investigation was a cantilevered aluminium pipe with various forms of defects, represented by the removal of elements in the pipe wall, simulating corrosion damage. The vibration response of the healthy and damaged pipes was monitored using piezoelectric patches spaced along the top of the pipe. The dynamic response of the pipe was analyzed using both the EMD-based procedure as well as methods based on Fourier transform, Wavelet transform, and Wavelet packet transform. Cheraghi and Taheri concluded that EMD and wavelet transform methods were the most sensitive and effective methods for detecting the damage location. Furthermore, the EMD-based method was the best method for identifying damage severity.

Rezaei and Taheri (2009) employed the EMD-EDI for damage detection of cantilevered steel pipes, instrumented with piezoceramic sensors. Various degrees of corrosion damage were simulated by partial and full circumferential reductions in wall thickness. The influence of several variables on the results was considered. Different test cases altering the support stiffness and the type of impact hammer head used to excite the pipe were completed. Rezaei and Taheri determined that the EMD-EDI is effective in detecting and localizing single and multiple areas of damage as well as qualitatively assessing the damage severity.

Subsequently, Rezaei and Taheri (2010) extended the use of the EMD-EDI to pipeline girth welds. A steel pipe with a mid-span girth weld was experimentally and numerically tested in both pressurized and non-pressurized conditions. In contrast to the earlier investigations, Rezaei and Taheri used both piezoceramic sensors and a laser Doppler vibrometer to monitor the free vibration of the pipe. Multiple damage cases were completed involving cracks, simulated by notches of various locations and depths, at the girth weld. The damage evaluation using the EMD-EDI was compared with the evaluation of the lag in instantaneous phase, a quantity derived from the HHT and proposed as another damage feature. Rezaei and Taheri concluded that their results were encouraging and promise the effectiveness of the proposed approaches as inexpensive systems for structural health monitoring purposes.

This thesis explores the integrity of the EMD-EDI for detecting damage in bolted joints, due to the limitations of the other vibration-based damage detection methods as outlined in Chapter 1. These studies serve to further expand the previous work accomplished on this method by focusing on a different type of structural damage than has been studied to date.

CHAPTER 3

DAMAGE DETECTION OF A STEEL PIPELINE BOLTED JOINT

The following chapter details the experimental tests performed on a simply supported steel pipe jointed at the mid-section using an 8-bolt flanged joint. An overview of the experimental set-up is shown in Figure 3-1. The objective of this study was to validate the effectiveness of using the EMD-EDI to detect various degrees of joint damage. Varying degrees of joint damage were simulated by reducing the torque load on the bolts and/or removing them completely. Three different combinations of piezoceramic sensors and/or impact locations were explored in total. As a result, this chapter is divided into three different sections, each detailing an experimental session.

Figure 3-1 Overview of experimental set-up.

3.1 GENERAL EXPERIMENTAL SET-UP

The test specimen used in this study was an ASTM compliant standard steel pipe (ASTM International, 2007) commonly used in oil and gas pipelines. Table 3-1 lists the specifications of the schedule 40 Grade B pipe having a nominal pipe size of 6. A total pipe length of 4.27 m was chosen so as to fit on the press bed in the steel laboratory. Furthermore, the length was kept as long as possible so that the set-up would reflect, as much as possible, a real case scenario and so that the boundary conditions would not have an overbearing effect on the results.

Table 3-1 Session 1-3 ASTM pipe dimensions and material properties.

Length	4.27	m	Density	7850	kg/m^3
Outer Diameter	168.3	mm	E	200	GPa
Wall Thickness	6.35	mm	v	0.3	

For sessions one through three, the mechanical joint utilized in the experiments was consistent. The ASTM and ASME/ANSI compliant forged steel flanges chosen were of the following type: Nominal Pipe Size (NPS) 6, class: 150, raised face, slip on, and material type: A105N. Accordingly, the red rubber gaskets used were NPS: 6, class: 150, 1/8 inch, and full face. SAE Grade 5 UNC hex head bolts were used (3/4 inch by 4 in) with corresponding sized nuts, and flat and lock washers. To create the mechanical joint in the pipe, the pipe was cut in two equal pieces, and the two flanges were welded onto the pipe. The flanges were continuously welded to the pipe on the inside of the joint with a small overlap over the pipe edge of approximately 23 mm, and tack welded on the outside of the joint.

Illustrated in Figure 3-2, the pipe and joint system was supported at either end using simple supports, bolted to the press bed. For this specific joint configuration, the maximum bolt torque was determined to be 124.7 N-m by the gasket manufacturer. The procedure to tighten the bolts was the industry standard which follows a criss-cross pattern across the face of the flange following the bolt numbering in Figure 3-3. Multiple passes should be completed at increments of 30%, 60% and then 100% of the maximum torque for the joint. For this joint, the magnitudes of these increments are listed in Table

3-2. The last step to tightening the joint is to go around the joint in a clockwise pattern and verify that every bolt is at the maximum torque. The joint was tightened using a torque wrench.

Figure 3-2 Boundary conditions.
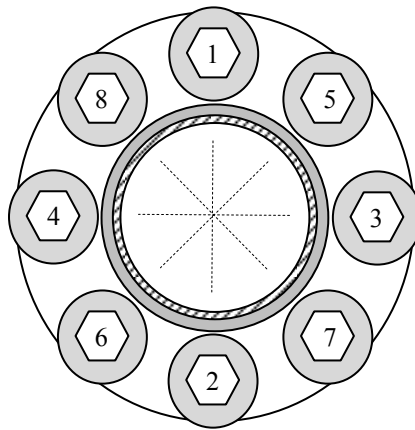
Figure 3-3 Session 1-3 bolt numbering.

Table 3-2 Session 1-3 bolt torque increments.

30% of Maximum	37.4	N-m
60% of Maximum	74.8	N-m
100% of Maximum	124.7	N-m

It may also be of some importance, considering the symmetry of the joint, that the bolts were always fastened so that the bolt heads lay on the same side as impact location C and D (Figure 3-4), which remained consistent for all three sessions.

To monitor the dynamic response of the system, piezoceramic sensors were bonded to the pipe and joint in several different arrangements. The piezoceramic sensors used for the entirety of the experimental testing were of type PZT-5H, extracted from 72.4 × 72.4 mm sheets available from Piezo Systems Inc. (Cambridge, MA). The dimensions of the sensors are listed in Table 3-3.

Table 3-3 Piezoceramic sensor dimensions.

Length	24.0 mm
Width	10.0 mm
Thickness	1.0 mm

Due to the small width of the sensors, fitting them to the curvature of the pipe's surface did not pose a problem. The material properties of the sensors (obtained from the manufacturer) are described using the following matrices. The density of PZT-5H is 7500 kg/m³.

$$s^E \left[\frac{m^2}{N}\right] = (10^{-12}) \begin{bmatrix} 16.5 & -4.78 & -8.45 & 0 & 0 & 0 \\ -4.78 & 16.5 & -8.45 & 0 & 0 & 0 \\ -8.45 & -8.45 & 20.7 & 0 & 0 & 0 \\ 0 & 0 & 0 & 43.5 & 0 & 0 \\ 0 & 0 & 0 & 0 & 43.5 & 0 \\ 0 & 0 & 0 & 0 & 0 & 42.6 \end{bmatrix}$$

$$d\left[\frac{C}{N}\right] = (10^{-12}) \begin{bmatrix} 0 & 0 & 0 & 0 & 741 & 0 \\ 0 & 0 & 0 & 741 & 0 & 0 \\ -274 & -274 & 593 & 0 & 0 & 0 \end{bmatrix} ;$$

$$\varepsilon^T [F/m] = (10^{-9}) \begin{bmatrix} 27.7 & 0 & 0 \\ 0 & 27.7 & 0 \\ 0 & 0 & 30.1 \end{bmatrix}$$

where S_E is the compliance matrix, d is the piezoelectric coupling matrix, and ε^S is the permittivity of the piezoceramic. The piezoceramic sheets were polarized through the

thickness allowing the sensors to be created by soldering two electrodes to the top and bottom surfaces of each piece cut from the piezoceramic sheet. However, soldering caused each sensor to have an uneven surface which prevented complete contact between the pipe surface and the sensor. Consequently, a steel plate of size $25.0 \times 10.0 \times 0.5$ mm was used as an adapter. Each adapter plate had a small semi-circular hole cut at the edge to fit around the solder. Placing the adapter plate between the sensor and the pipe surface allowed for increased contact.

Before a sensor was attached, the surface of the pipe was scoured using silicon-carbide paper. The pipe surface, sensor and adapter plate were then wiped clean of dust and oil with isopropyl alcohol. The preparation, resulting in clean and rough surfaces, permitted a stronger bond to be created. The piezoceramic sensors and the adapter plates were subsequently adhered to the pipe using a two part epoxy, Araldite 2011 (Huntsman Advanced Materials Americas Inc., Los Angeles, CA). The sensors were secured to the pipe, taped down using masking tape, and left to cure for twelve hours to create a strong bond.

3.2 SESSION 1

The following section includes a description of the experimental set-up for the initial combination of sensors/impact locations used, the testing procedure, the data analysis, and a presentation of the results followed by a discussion.

3.2.1 Experimental Set-Up

The set-up for the completion of damage detection was accomplished as follows and may be seen in Figure 3-4. Four impact locations were chosen for testing, Location A, B, C and D situated on either side of the joint. In order to maintain consistency between impacts, a steel ball measuring 12.7 mm in diameter was placed at each of the impact locations to provide a consistent impact target. The impact balls were attached to the pipe using the same epoxy as used for the sensors. An example impact location is shown in Figure 3-5.
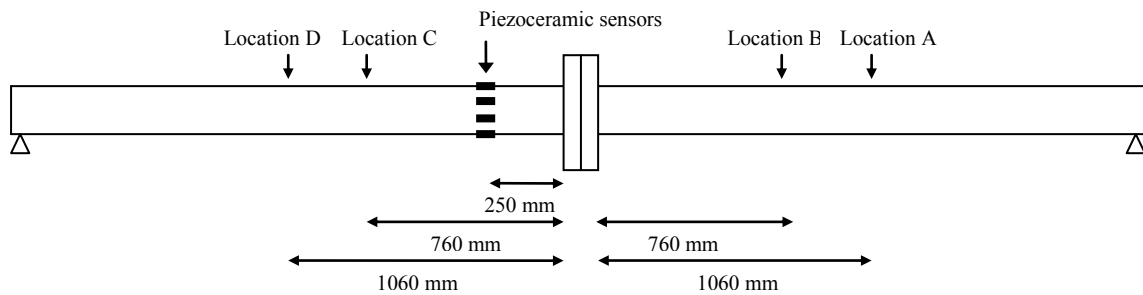
Figure 3-4 Session 1 experimental set-up.

Figure 3-5 Example impact location.

To monitor the system vibrations, six piezoceramic sensors were placed on the pipe at a distance of 250 mm from the outside of the closest flange measured to the center of the

sensors. The placement of these sensors along the pipe are shown in Figure 3-4 and the placement and numbering of the sensors is illustrated in a cross-section of the pipe in Figure 3-6, and in a photograph of the experimental set-up in Figure 3-7.
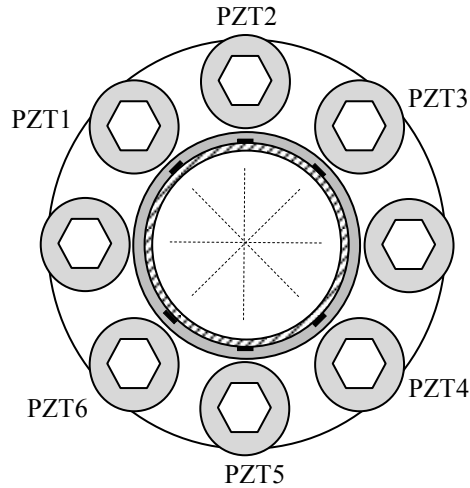
Figure 3-6 Session 1 PZT sensor placement and numbering.
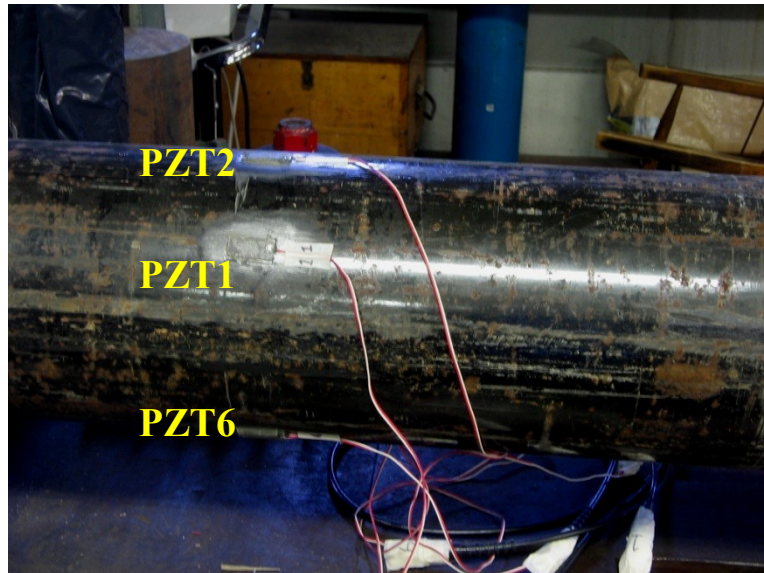
Figure 3-7 Session 1 sensor placement.

The sensor locations were chosen so that a comparison could be made between the results from the sensors at the top and bottom of the pipe as well as with the sensors situated at 45 degrees. Concerning the distance to the flange, it was thought that the sensors should be placed at a distance so that work on the joint would not have the chance of inadvertently damaging the sensors.

Since the sensors were only placed on one side of the pipe (thought to be sufficient since the set-up is symmetrical), the impact locations were chosen so that they would not be too close to the sensors (thereby interfering with the signals). Furthermore, the impact locations were placed on both sides of the joint in order to study the difference between the vibration-induced wave propagation through the joint, to reach the sensor. Moreover, having two impact locations per side permitted the exploration of whether impacts closer to the joint could have improved the results.

3.2.2 Testing

To create free vibration in the system, the pipe was excited using a piezoelectric impulse hammer (model 5800B5, Dytran Instrument Inc., Chatsworth, CA) outfitted with an aluminum tip which could excite frequencies up to 5 kHz. The hammer outputs an analog voltage which is representative of the input impulse. A typical hammer impulse signal is depicted in Figure 3-8 (a).

a)   b)
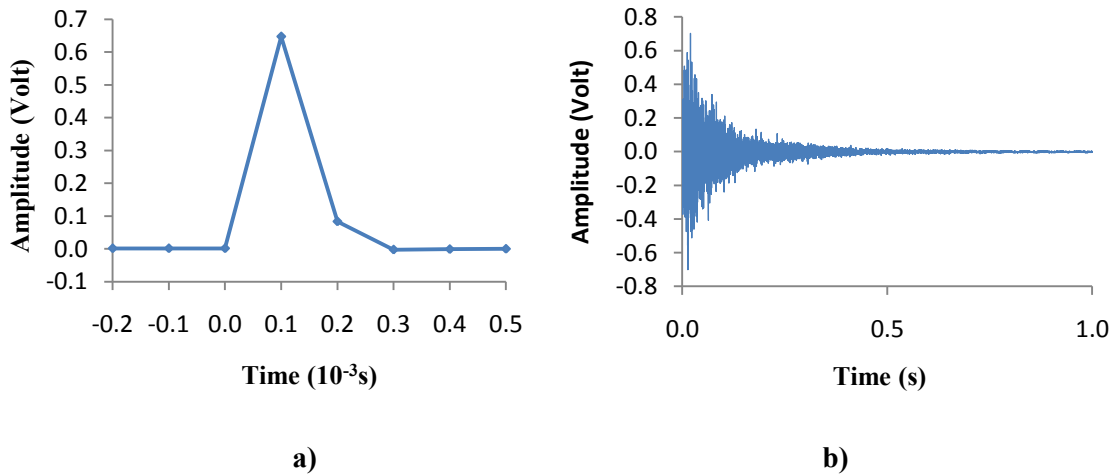
Figure 3-8 a) Typical impulse hammer signal **b)** Typical sensor response.

In order to collect the response of the PZT sensors and the impulse hammer, they were connected by BMC cables to a multifunction PCI 6220 data acquisition card manufactured by National Instruments Inc., Austin, Texas). The data acquisition (DAQ) system, shown in Figure 3-9, provided a limitation to the experiments in that the board can only hold up to 8 inputs, which meant that data from only seven sensors could be

concurrently read and recorded. Furthermore, the same gasket was used for all testing. A typical sensor response is depicted in Figure 3-8 (b).
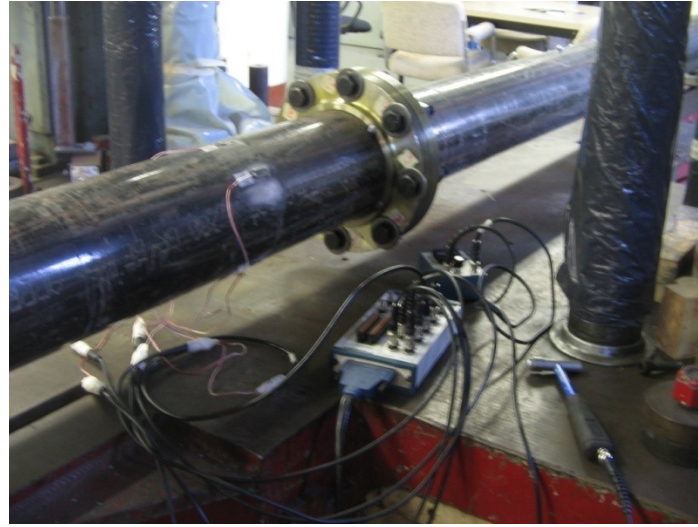
Figure 3-9 The data acquisition hardware.

For session 1, two healthy cases were completed, as well as four damage cases. A list of all the test cases considered for session 1 is shown in Table 3-4. Each healthy case and each damage case consisted of five impacts at each of the four impact locations in an effort to achieve consistent results. Two healthy cases were completed for comparison purposes so that the consistency between healthy states could be investigated. For each healthy state that was completed, the joint was fully loosened and re-torqued using the procedure outlined earlier.

Table 3-4 Session 1 healthy cases and damage cases.

State	Bolts Loosened	Damage Case
Healthy Case 1-1		HC 1-1
Healthy Case 1-2		HC 1-2
Damage Case 1-1	Bolt #1: Damaged 80%	DC 1-1
Damage Case 1-2	Bolt #1: Damaged 50%	DC 1-2
Damage Case 1-3	Bolt #1 and Bolt #5: Damaged 50%	DC 1-3
Damage Case 1-4	Bolt #1, #5 and #8: Damaged 50%	DC 1-4

For the damage cases, the percent of damage listed in the table is the percentage of the maximum torque to which the bolts were loosed. For example, the 80% for damage case

1-1 signifies that Bolt #1was loosened to 100 N-m (80% of 124.7 N-m).

Figure 3-10 is a schematic depicting the bolts included in the damage cases. The method used to loosen the bolt was as follows: with the aid of a torque wrench set to the value that the bolt should be loosened to, the bolt was loosened using an adjustable wrench a slight amount, then tested using the torque wrench for its current torque, and subsequently adjusted until the desired torque was reached.

For damage case 1-4, it was discovered that when the third bolt was loosened, Bolt #1 retightened and therefore each bolt had to be rechecked for the correct bolt torque.
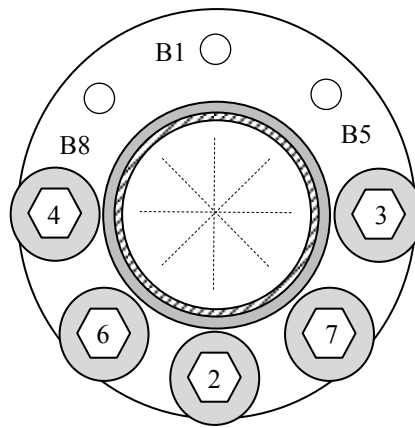
Figure 3-10 Session 1 damage overview.

3.2.3 Data Analysis

After monitoring and recording the free vibration of the pipe in its healthy state using the six piezoceramic sensors, damage was introduced in the joint by loosening the bolt(s) and the free vibration of the pipe was recorded in its damaged state. For all damages, the second healthy state was the comparison healthy state used in the calculation of the EMD-EDI. As mentioned in the previous section, four damage sessions were studied, which included the loosening of one bolt, two bolts, and three bolts to a lower torque.

All of the data for the experimental testing was recorded using a sampling frequency of 10 kHz. Once the data was collected using LabView software, the data for each impact was stored in an ASCII text file which included the responses of all the sensors and the impulse hammer. Subsequently, the recorded signals from the healthy and damaged pipe joints were processed using a Matlab code, developed in house by another member of the

research group, which performed the Empirical Mode Decomposition. This code was programmed to read the text file produced by the DAQ system and then process the response of all six sensors simultaneously. The code removes unwanted data before impact, filters signal noise, compensates for any offset, normalizes the response of any sensor with respect to the hammer input force, applies a low-pass filter in order to have the first natural frequency in the filtered data, decomposes the signals based on the EMD method, derives the IMFs, and finally calculates the energy of the desired IMF for each sensor (Rezaei and Taheri, 2009). A typical voltage signal of a sensor and its decomposition based on the EMD sifting process is illustrated in Figure 3-11.
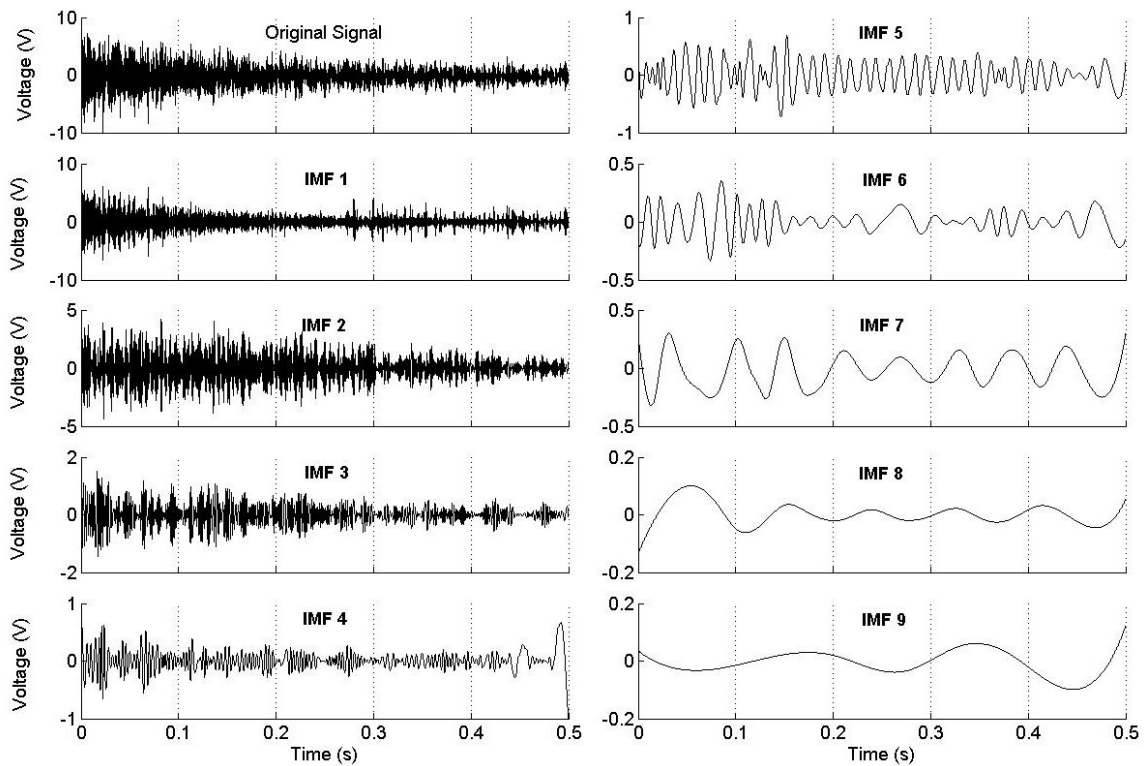
Figure 3-11 Typical signal decomposition from EMD (Rezaei and Taheri, 2010).

For each excitation, the vibration lasted for seconds before decaying to zero (see a typical vibration signal in Figure 3-8 (b)). Because the EMD-EDI is based on the comparison of special features in the vibration signals before and after damage creation, there is no limitation for the choice of signal duration, as long as the same duration is used to evaluate both the healthy and damaged state signals (Rezaei and Taheri, 2009). With this in mind, an interval of 0.5 seconds was chosen for the signal processing.

Furthermore, each of the acquired signals from the sensors was normalized based on the input (hammer) signal. The difference between the signals after normalization was considered to be a good measure of the repeatability of the impact procedure (Rezaei and Taheri, 2009).

To normalize the signals, the following procedure was followed (Rezaei and Taheri, 2009): The fast Fourier transform (FFT) of each sensor response was divided by the FFT of the hammer signal. Afterwards, the result was transferred to the time domain by the inverse fast Fourier Transform. Three impacts for each test case were processed and the IMF energies attained, and their average used for the EMD energy. Once the EMD energy of both the healthy and damages cases was calculated, the EMD-EDI was calculated for each damage case.

3.2.4 Results

In an effort to more fully understand the system dynamics, the first three natural frequencies of the pipe joint system were calculated analytically using the following equation for a simply supported beam (Chopra, 2001):

$$\omega_n = \frac{\beta_n}{L^2} \sqrt{\frac{EI}{m/L}} \; ; \; \beta_n = 3.1416, 6.2832, 9.4248 \; for \; n = 1,2,3 \tag{3-1}$$

where $\omega_n (rad/s)$ is the angular frequency of the nth mode, E is the modulus of elasticity, I is the second area moment of inertia, L is the beam length, and m is the mass of the beam. The mass of the joint itself was calculated separately and distributed along the length of the beam for the sake of calculation. The natural frequencies are listed in Table 3-5.

Table 3-5 Natural frequencies calculated analytically.

Natural frequency ($f = \omega/2\pi$)	
1	23 Hz
2	92 Hz
3	207 Hz

These were compared with the natural frequencies calculated using the Fast Fourier transform of the piezoceramic sensor's typical output signal shown in Figure 3-12. The

first two natural frequencies compare well while the third frequency does not, possibly due to the assumptions made for the calculation (i.e. distribution of the joint mass and stiffness).
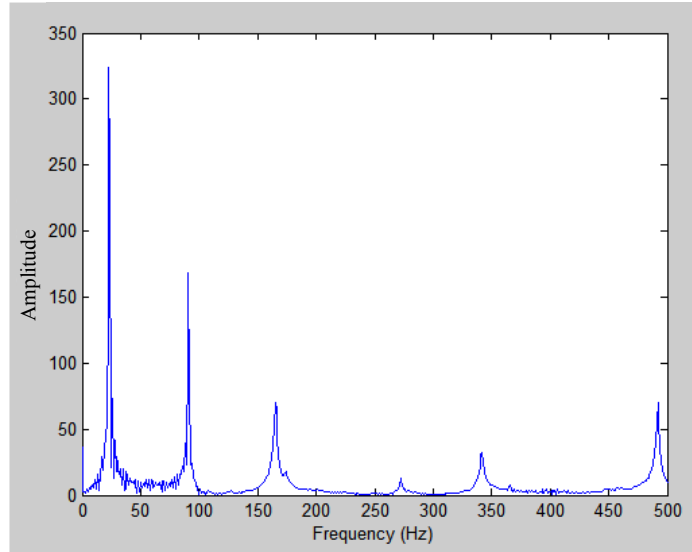
Figure 3-12 Natural frequencies of pipe-joint system from FFT of PZT7 data
(signal from session 2, HC 1-4, Location C, aluminium tip).

As part of the EMD-EDI procedure, the data should be filtered before it is decomposed (Cheraghi et al., 2005; Cheraghi and Taheri, 2007). Cheraghi et al. (2005) initially suggested that the band-pass filter should be of a magnitude to only retain the first frequency. However, it was later discovered through more research (Rezaei and Taheri, 2010) that the higher frequency components may need to be retained in the case of small localized damages. By analyzing the data using different frequency bands, it was found that a low-pass filter with a pass-band frequency of 2000 Hz provided the best resolution for identification of damage. This pass-band was chosen based on exhibition of damage progression as well as consideration of energy amplitude.

Figure 3-13 through Figure 3-16 illustrate the EMD-EDI calculated respectively for each impact location. Each graph illustrates the indices of all damage cases for each sensor. For example, the results for PZT2 were as follows: DC 1-1: index of 58; DC 1-2: index of 48; DC 1-3: index of 80; DC 1-4: index of 53. The results shown in these figures are based on the frequency band of 0-2000 Hz, and the energy of the first IMF.
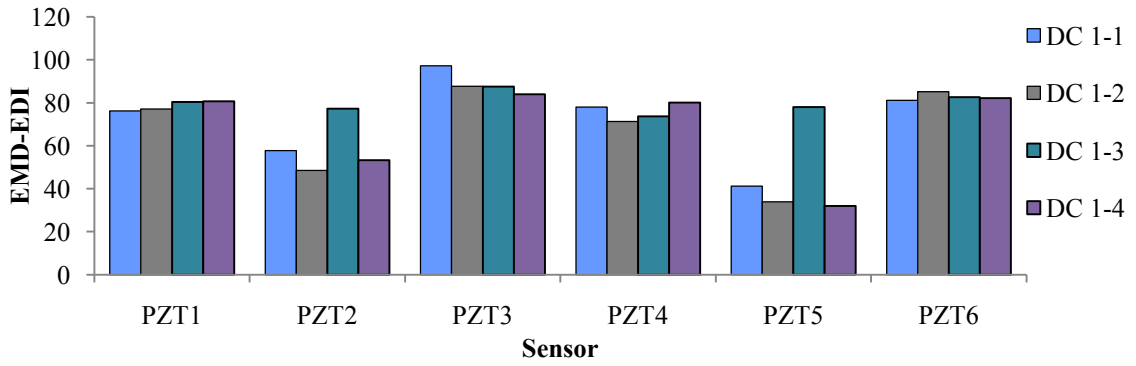
Figure 3-13 EMD-EDI, session 1, location A, IMF1.
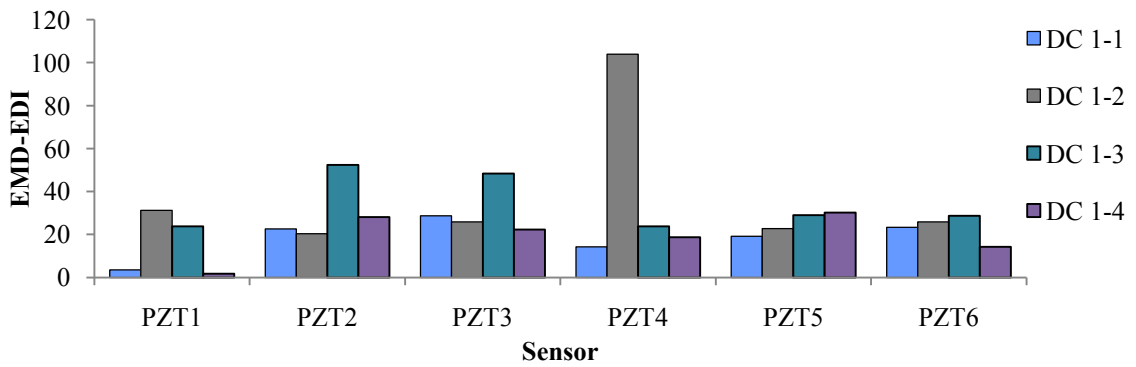
Figure 3-14 EMD-EDI, session 1, location B, IMF1.
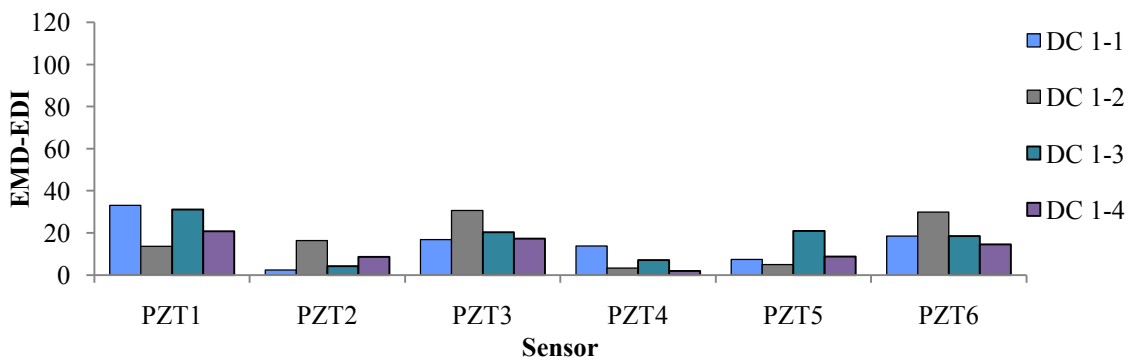
Figure 3-15 EMD-EDI, session 1, location C, IMF1.
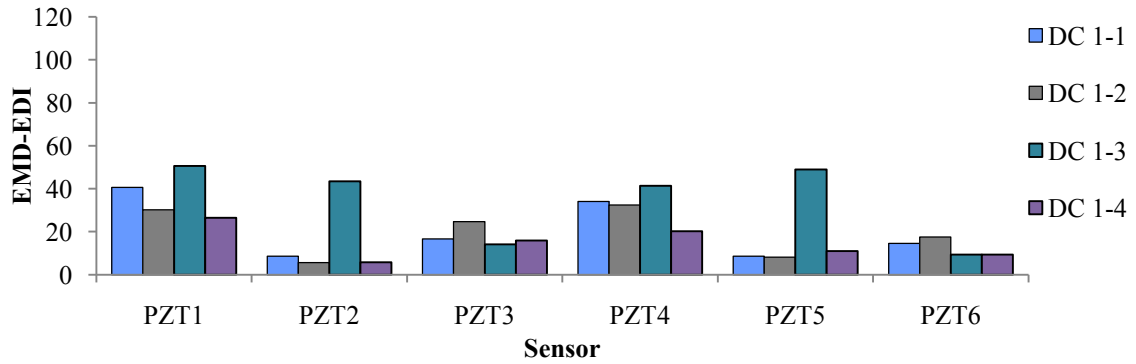
Figure 3-16 EMD-EDI, session 1, location D, IMF1.

From comparing Figure 3-13 through Figure 3-16, it is clear that impact locations A and B provided better damage progression overall. PZT1 and PZT5 respectively show damage progression for the two locations. Impact locations C and D did not produce any damage progression and the damage index amplitudes were in the same range as that of impact location B. It can therefore be postulated that the EMD based method can better detect damage progressions when the vibration signal travels through the joint to reach the sensors (see Figure 3-4).

One can also observe that the damage index amplitudes obtained through the signals excited by impacting the pipe at location A are much greater than those obtained by excitation at other locations. There is a great deal of similarity among the damage index amplitudes and the relationship among each damage index for impact locations C and D, which one would expect, considering the fact that the two impact locations are 0.3 m apart. Nevertheless, impact locations A and B do not show this similarity, which might suggest errors in some signal with respect to impact location A and B.

3.2.5 Consistency

As mentioned in section 3.2.3, once the five impacts for each test case were processed and the IMF energies obtained, only the three closest energies of the signals of each sensor were retained and their average used. When reducing the number of energies from five to three, it was desired to maintain the variation between the resulting EMD energy averages below 20% for each sensor. If the variation in the energies was above 20%, there was too much scatter in the impact data. Therefore, five additional tests were

conducted for the particular impact location. The variation of each impact induced EMD damage energy of a given sensor was calculated from the average using the following equation:

$$Variation = greater\ of\ \left|\frac{(E_{max} - E_{avg}) * 100}{E_{avg}}\right|, \left|\frac{(E_{min} - E_{avg}) * 100}{E_{avg}}\right| \qquad (3\text{-}2)$$

Tables A-1 and Table A-2 (Appendix A) report the calculated variation for each healthy and damage case state. Table A-1 lists the values for the pass-band frequency of 0-2000 Hz, IMF1 and Table A-2 lists the values for the pass-band frequency of 0-2000 Hz, IMF2 for the sake of examining whether energies calculated based on the second IMF could provide more conclusive results.

3.2.6 Result Repeatability

In order to address the question of result repeatability, the EMD energy of two healthy states was calculated as mentioned earlier. It was assumed that the difference between the average EMD energy for each sensor was a sufficient gauge with which to measure the repeatability of the impact procedure. The following equation was used to calculate the variability between the EMD energy of the healthy states.

$$Variation = greater\ of\ \left|\frac{(E_{avg,i} - E_{avg,i,j}) * 100}{E_{avg,i,j}}\right|, \left|\frac{(E_{avg,j} - E_{avg,i,j}) * 100}{E_{avg,i,j}}\right| \qquad (3\text{-}3)$$

where: i and j represent the two states being compared and

$E_{avg,i}$ = the average energy based on the vibration signals of the first state

$E_{avg,j}$ = the average energy based on the vibration signals of the second state

$E_{avg,i,j}$ = the average of the average energies of the two states

The range of comparison values are listed in Table A-3 in Appendix A. The EMD energies tabulated for impact location A do not compare well, having differences of at least 30%, which may explain the high magnitudes of the index for that location.

3.2.7 Discussion and Conclusions

Due to the poor consistency of the results concerning the progression of damage, as well as the high variability in the values of the EMD energies obtained at the healthy state, the decision was made to remove the gasket and repeat the tests to see if the results would improve with less damping in the joint. Furthermore, to improve the damage progression results, it was decided that new sensors would be placed in a closer proximity to the joint. Without consistent results demonstrating damage progression, the decision was made to maintain all four impact locations until better results could suggest the elimination of the less useful locations. Moreover, the same reasoning applies for the continued use of both IMFs to analyze the data until better results allow a good comparison.

3.3 SESSION 2

The following section includes a description of the experimental set-up for the second combination of sensors/impact locations used, the testing procedure, the data analysis, and a presentation of the results followed by a discussion.

3.3.1 Experimental Set-Up

The experimental set-up for session 2 was the same as for session 1, except for the lack of gasket and a different sensor arrangement. The gasket was removed in order to see if the lack of damping could improve the results. The experimental set-up for session 2 is illustrated in Figure 3-17. The sensor locations were chosen with the thought that sensors closer to the joint may provide better results.
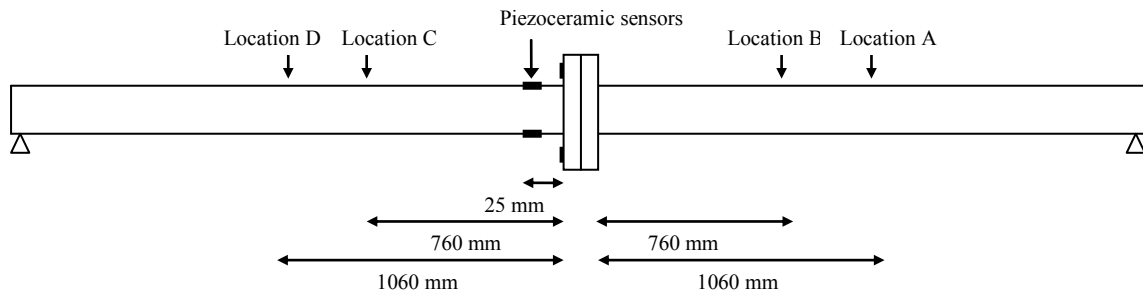
Figure 3-17 Session 2 experimental set-up.

Six new piezoceramic sensors were attached to the pipe and flange. To monitor the pipe vibrations, two piezoceramic sensors, PZT7 and PZT8, were placed on the pipe at a distance of 25.0 mm from the outside of the closest flange to the center of the sensors. To monitor the flange vibrations, four piezoceramic sensors were placed on the flange on the same side as the previous sensors. PZT9 and PZT10 were place on either side of Bolt 1 and PZT11 and PZT12 were placed on either side of Bolt 2 (refer to Figure 3-3).

The placement of these sensors along the pipe is shown in Figure 3-17 and the placement and numbering of the sensors is illustrated in a cross-section of the pipe in Figure 3-18, and in a photograph in Figure 3-19. The sensor locations were chosen so that a comparison could be made between those results from on the pipe and on the flange, as well between the results obtained from the sensors placed on the bottom and top of the pipe/flange.

59
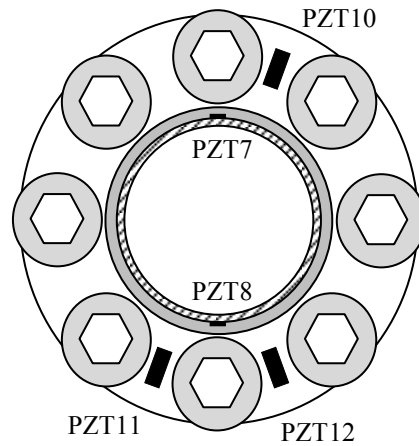
Figure 3-18 Session 2 PZT sensor placement and numbering.
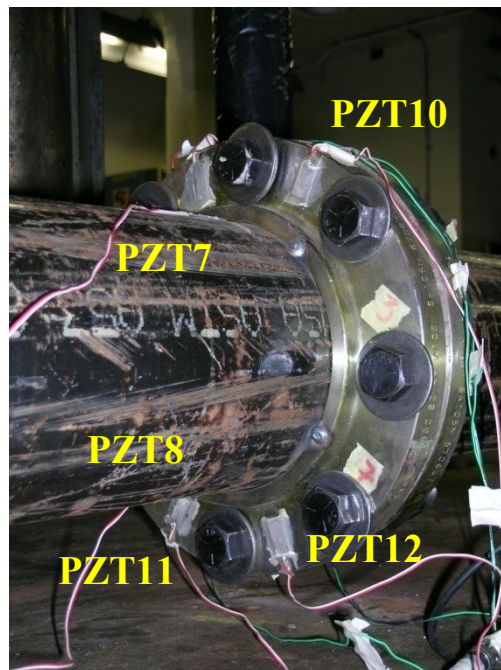
Figure 3-19 Session 2 sensor placement.

3.3.2 Testing

In contrast to session 1, two hammer tips, aluminium and plastic, were employed in order to determine which might yield better results. Unlike the aluminium tip, the hard plastic tip is only capable of exciting frequencies below 2 kHz. For session 2, ten impacts were completed for each impact location for all cases to ensure that impact errors were

60

not contributing to the lack of damage progression. A list of all test cases considered for session 2 is shown below in Table 3-6.

Table 3-6 Session 2 cases.

State	Bolts Loosened	Damage Case
Healthy Case 2-1		HC 2-1
Healthy Case 2-2		HC 2-2
Healthy Case 2-3		HC 2-3
Healthy Case 2-4		HC 2-4
Damage Case 2-1	Bolt #1: Damaged 80%	DC 2-1
Damage Case 2-2	Bolt #1: Damaged 66%	DC 2-2
Damage Case 2-3	Bolt #1 and Bolt #5: Damaged 66%	DC 2-3
Damage Case 2-4	Bolt #1 and Bolt #5: Damaged 50%	DC 2-4
Damage Case 2-5	Bolts #1, #5 and #8: Damaged 50%	DC 2-5
Damage Case 2-6	Bolt #1: Completely Loose Bolts #5 and #8: Damaged 50%	DC 2-6
Damage Case 2-7	Bolts #1 and #5: Completely Loose Bolt #8: Damaged 50%	DC 2-7
Damage Case 2-8	Bolts #1, #5 and #8: Completely Loose	DC 2-8
Damage Case 2-9	Bolts #1, #5, #8 and #4: Completely Loose	DC 2-9

Figure 3-20 is a schematic depicting the bolts included in the damage scenario listed above. Four healthy cases were completed for comparison purposes so that the consistency between healthy states could be investigated. For each healthy state that was completed, the joint was fully loosened and re-torqued using the procedure outlined in the experimental set-up discussed earlier. The four healthy states listed in Table 3-6 were performed again due to the poor results obtained for session 1. For the damage cases for which a bolt was completely loose, the bolt was completely removed from the joint.
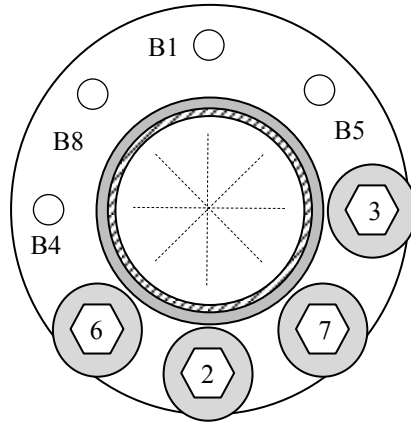
Figure 3-20 Session 2 damage overview.

3.3.3 Data Analysis

The data analysis for session 2 was completed in the same manner as for session 1, except that for session 2, five impact signals were chosen for the calculation of EMD average energy.

3.3.4 Results

For session 2, it was decided that in order to fully explore the range of bandwidth frequencies that might be suitable for this joint configuration, the full range of frequencies from 0-4000 Hz would be processed. Thirty-six pass-bands were explored using increments of 500 Hz. This range was chosen because the plastic tip excites frequencies up to 2 kHz and the aluminum hammer tip is capable of exciting frequencies of 5 kHz.

By analyzing the data using the different frequency bands, it was determined that a low-pass filter with a pass-band frequency of 2500 Hz provided the best resolution for identification of damage. This pass-band was chosen based on exhibition of damage progression as well as consideration of the index amplitude. Figure 3-21 through Figure 3-24 illustrate the aluminum tip results calculated for each sensor for each respective impact location. The results shown in these figures are based on the first IMF.

62
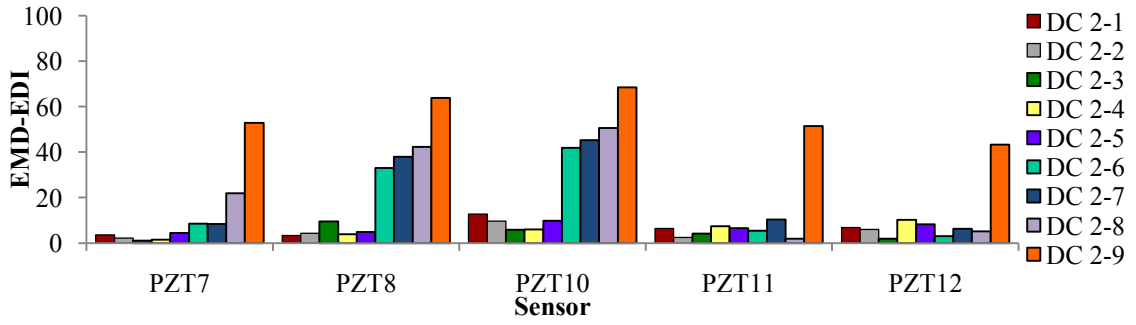
Figure 3-21 EMD-EDI, session 2, location A, 0-2500 Hz, IMF1, aluminium tip.
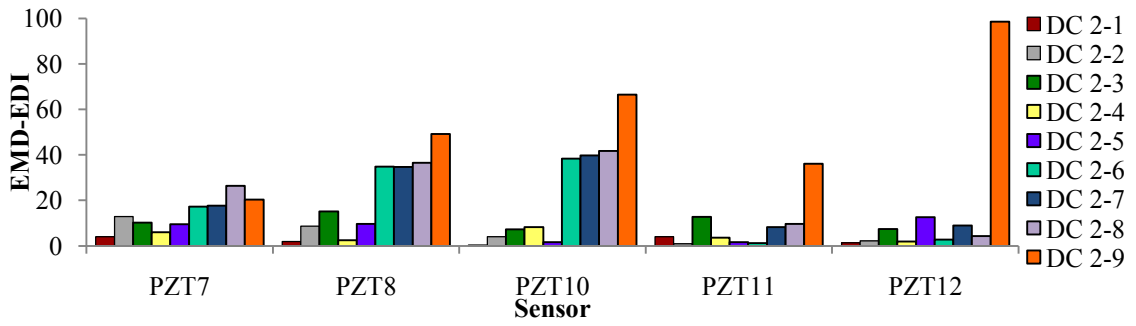
Figure 3-22 EMD-EDI, session 2, location B, 0-2500 Hz, IMF1, aluminium tip.
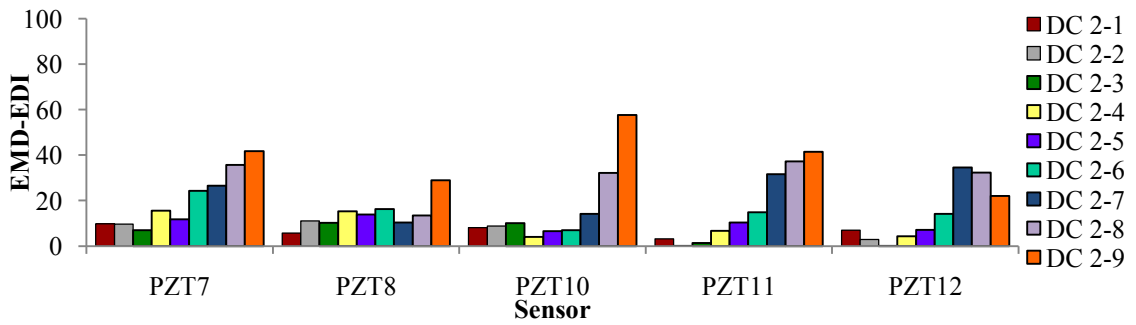
Figure 3-23 EMD-EDI, session 2, location C, 0-2500 Hz, IMF1, aluminium tip.
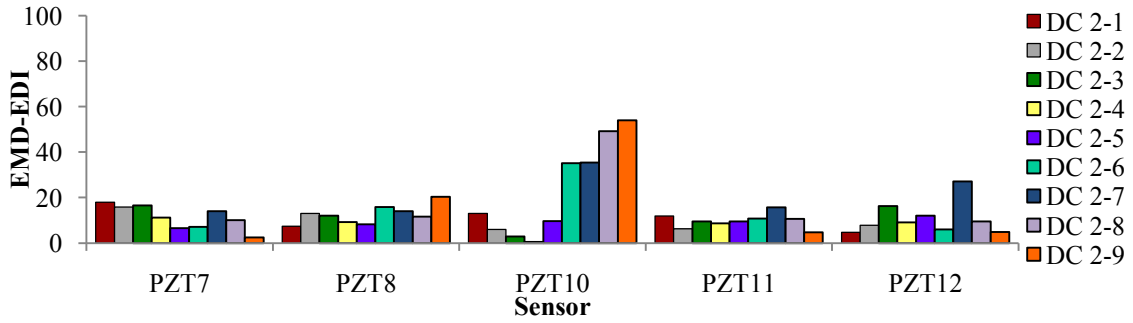
Figure 3-24 EMD-EDI, session 2, location D, 0-2500 Hz,
IMF1, aluminium tip.

Only one impact location graph is shown for the plastic tip as the results for the other impact locations are very similar in variability.
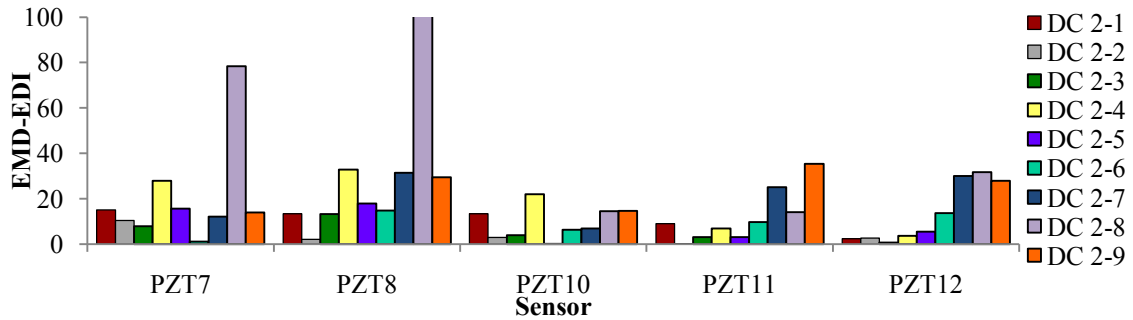
Figure 3-25 EMD-EDI, session 2, location C, 0-2500 Hz,
IMF1, plastic tip.

3.3.5 Consistency

The same process was used for session 2 as for session 1 to measure result consistency. In order to document the range of variability, Tables A-4 and A-5 (Appendix A) list the variations for each healthy and damage case. Table A-4 lists the values for the aluminum tip data and Table A-5 lists the values for the plastic tip data.

However, it must be noted that the signals were initially analyzed and accepted /rejected using the pass-band frequency of 0-2000 Hz since this was the best pass-band frequency for session 1. Therefore, it was the variability of the EMD energies using the pass-band of 0-2000 Hz that were verified as being below 20%. This is why a few high errors exist in Table A-5, which lists the values for the plastic tip data for the pass-band

64

frequency of 0-2500 Hz. This stands to reason because the plastic tip only excites reliable frequencies up to 2000 Hz.

3.3.6 Result Repeatability

In order to re-address the question of result repeatability, four healthy cases were completed as mentioned earlier. It was assumed that the difference between the average EMD energies of the healthy cases was a sufficient gauge with which to measure the repeatability of the impact procedure. Eqn. 3-3 was used to calculate the variability between healthy states.

The range of comparison values are listed in Table A-6 (aluminium tip) and Table A-7 (plastic tip) in Appendix A. The results are much improved from those of session 1, with values over 20% occurring only for PZT10 and PZT12 for the plastic tip. Once again, this high values may be due to the fact that the plastic tip only excites reliable frequencies up to 2000 Hz.

3.3.7 Discussion and Conclusions

Considering the above data, the frequency range of 0-2500 Hz yielded the best results in terms of damage index amplitude and damage progression with the aluminium tip yielding better results than the plastic tip.

From the comparison of impact locations (Figure 3-21 through Figure 3-24), impact location C produced the best results when all sensors were considered, yet it was out performed by impact location A for PZT7, PZT8 and PZT10 considering both index amplitude and damage progression. Impact location D produced the least clear results in terms of damage progression. It is interesting to note that the results for impact location B, although closer to the joint, were similar yet smaller in amplitude than those of impact location A. This trend is reversed considering the opposite side of the joint (C and D), for which the impact location closest to the joint, location C, provided the most useful results.

PZT10 demonstrated the best amplitude among all the sensors and showed damage progression for at least the last five damage cases for all impact locations (for the aluminum tip only). It is also clear from Figures 3-21 to 3-25 that PZT11 and PZT12 only

demonstrated good damage progression and amplitude for impact location C, the impact location closest to the sensors, (see Figure 3-17). Regarding whether the best location for the sensors is on the pipe itself or on the flange, the results are as of yet inconclusive.

Based on these results, it was decided that the next session would once again include both hammer tips to give further evidence substantiating the conclusion that the aluminum tip yields better results than the plastic tip. Furthermore, because of the variance in results between the four impact locations, the next session would include sensors on either side of the flange in an effort to discover which side of the pipe is better for impact with respect to the side that the sensors are on. The next session would also include two new impact locations closer to the joint on either side, and not consider the impact locations A and D.

It is also worthy of note that during this session, the introduced damage occurred only on top of the pipe, with bolts that are side by side. Therefore, in an effort to have a wider range of results, the next session will include loosened bolts that are not side by side, and that are located on either side of the pipe. Moreover, because the majority of the results from session 2 did not show damage progression for the first 5 damage progressions, only fully loosened bolts will be considered for the next session.

Finally, the decision to perform testing without a gasket yielded improved results overall. A possible inference would be that the damping caused by the presence of the gasket, and the type of gasket, may play a large role in the usefulness of this method.

3.4 SESSION 3

The following section includes a description of the experimental set-up for the third combination of sensors/impact locations used, the testing procedure, the data analysis, and a presentation of the results, followed by a discussion.

3.4.1 Experimental Set-Up

The experimental set-up for session 3 was the same as for session 2, except for a modified sensor arrangement. Similarly to session 2, no gasket was used for the tests. The experimental set-up for session 3 is illustrated in Figure 3-26.
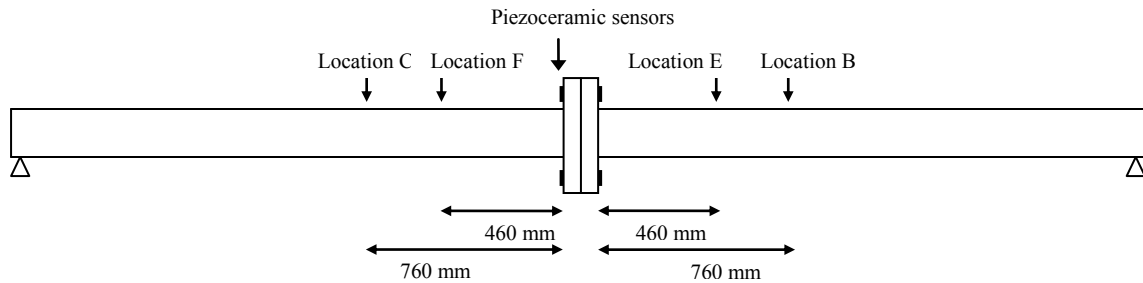
Figure 3-26 Session 3 experimental set-up.

Four new piezoceramic sensors, PZT13 through PZT16, were created and attached to the opposite side of the flange, mirroring the positions of PZT9 through PZT12 from session 2 that were also retained for this session. The placement of these sensors along the pipe is shown in Figure 3-26 and the placement and numbering of the sensors are also illustrated in a cross-section of the pipe in Figure 3-27, and in a photograph in Figure 3-28.

The sensor locations were chosen so that a comparison could be made between the results from either side of the flange to determine if one side would yield better results. The tightening procedure for session 3 was the same as for session 2.

67
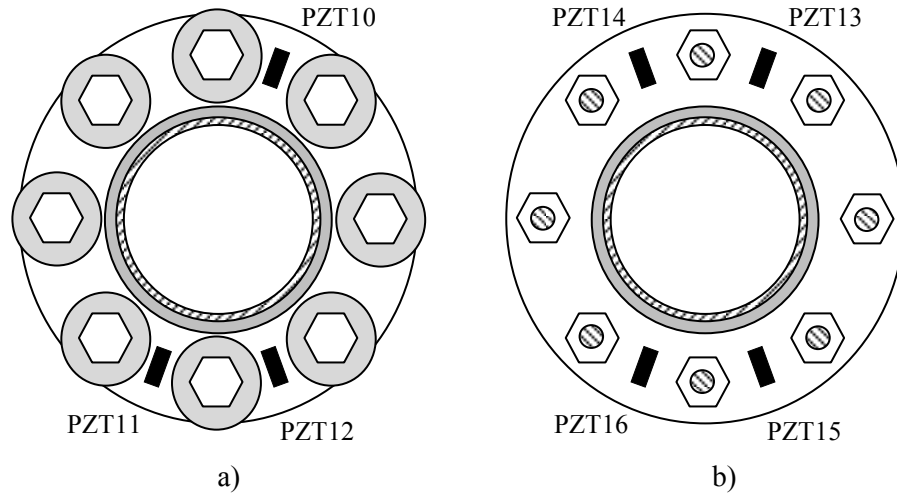
Figure 3-27 Session 3 PZT sensor placement and numbering **a)** Face of left flange **b)** Face of right flange.
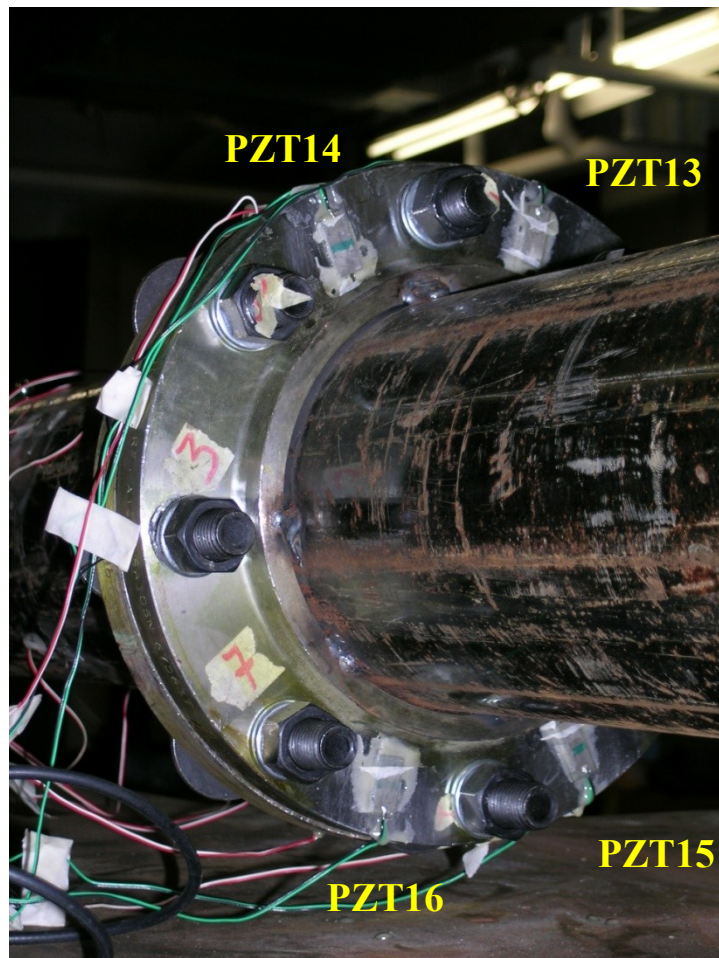
Figure 3-28 Session 3 sensor placement.

3.4.2 Testing

For session 3, seven impacts were completed for each impact location for the healthy state, and five impacts were completed for each impact location for each of the three damage states. The number of impacts was reduced from the number used in session 2 (i.e. 10) due to the consistency achieved in session 2. Similarly to session 2, both aluminium and plastics impact hammer tips were employed in order to help determine which might yield better results. A list of all test cases considered for session 3 is shown in Table 3-7. Figure 3-29 is a schematic depicting the bolts included in the damage cases listed in Table 3-7.

Table 3-7 Session 3 cases.

State	Bolts Loosened	Damage Case
Healthy Case 3-1		
Damage Case 3-1	Bolt #3: Removed from Joint	DC 3-1
Damage Case 3-2	Bolt #3 and Bolt #4: Removed from Joint	DC 3-2
Damage Case 3-3	Bolts #1, #3, #4: Removed from Joint	DC 3-3

For this session, only one healthy state was completed since it was felt that the issue of repeatability was dealt with sufficiently in session 2. Additionally, only complete removal of bolts was performed due to the difficulty in detecting a smaller amount of clamping force loss in the joint.
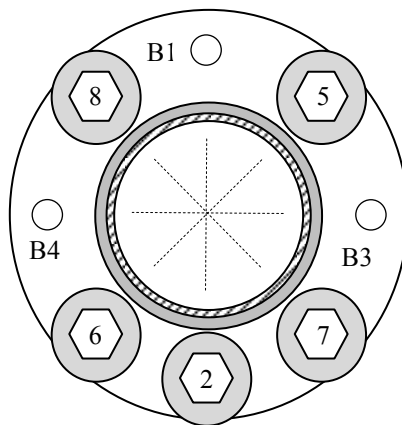
Figure 3-29 Session 3 damage overview.

3.4.3 Data Analysis

The data analysis for session 3 was completed in the same manner as for session 1 and 2 except that for session 3, five healthy case impact signals were chosen for the calculation of EMD average energy, and three of the damaged case signals.

3.4.4 Results

For session 3, the bandwidth frequencies in Table 3-8 were explored in an effort to determine which one would be the most suitable for this joint configuration. For each frequency range, both aluminum tip and plastic tip data was analyzed for both IMF 1 and IMF 2 as stated earlier. Until now, the experimental research performed for this method has concentrated on the first IMF (Cheraghi and Taheri, 2007; Rezaei and Taheri, 2009). It was therefore decided to explore the results from the second IMF.

Table 3-8 Session 3 frequencies ranges.

0-1000 Hz
0-2000 Hz
0-2500 Hz
1000-2000 Hz
1000-2500 Hz
1500-2000 Hz
0-500 Hz
500-2500 Hz

By analyzing the data according to the frequency ranges in Table 3-8, it was determined that a low-pass filter with a pass-band frequency of 2000 Hz provided the best resolution for identification of damage.

Figure 3-30 to Figure 3-33 illustrate the aluminum tip results for the first IMF. Likewise, Figure 3-34 through Figure 3-37 illustrates the plastic tip results for the first IMF. In each figure, the sensor results are illustrated and organized according to the sensors placed on the left side of the joint and those on the right (in reference to Figure 3-26).
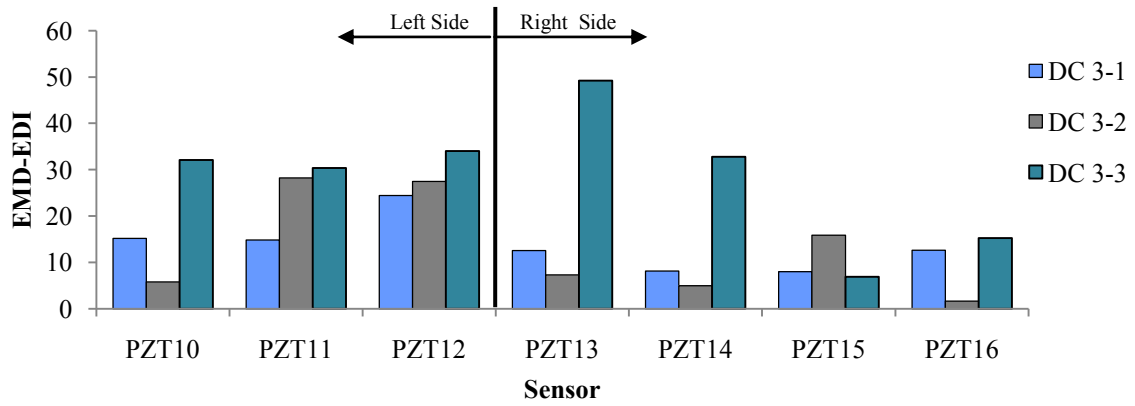
Figure 3-30 EMD-EDI, session 3, location B, 0-2000 Hz,
IMF1, aluminium tip.
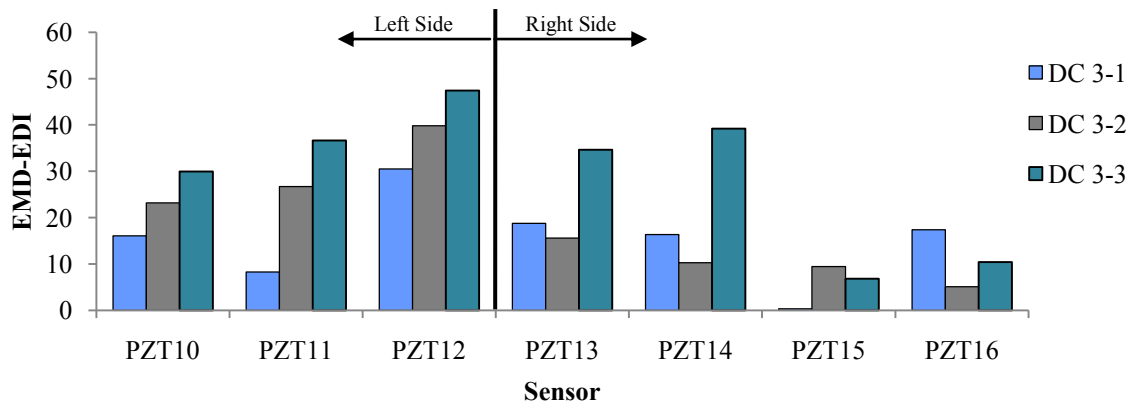
Figure 3-31 EMD-EDI, session 3, location C, 0-2000 Hz,
IMF1, aluminium tip.
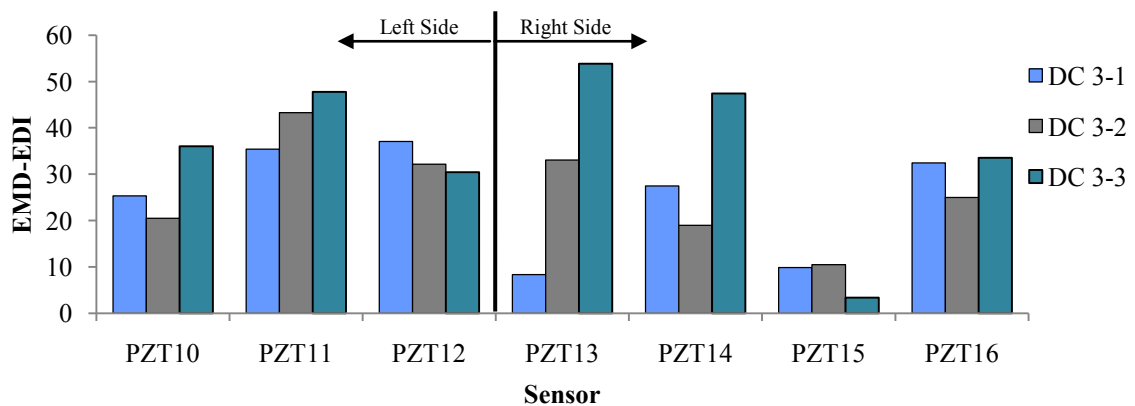
Figure 3-32 EMD-EDI, session 3, location E, 0-2000 Hz,
IMF1, aluminium tip.
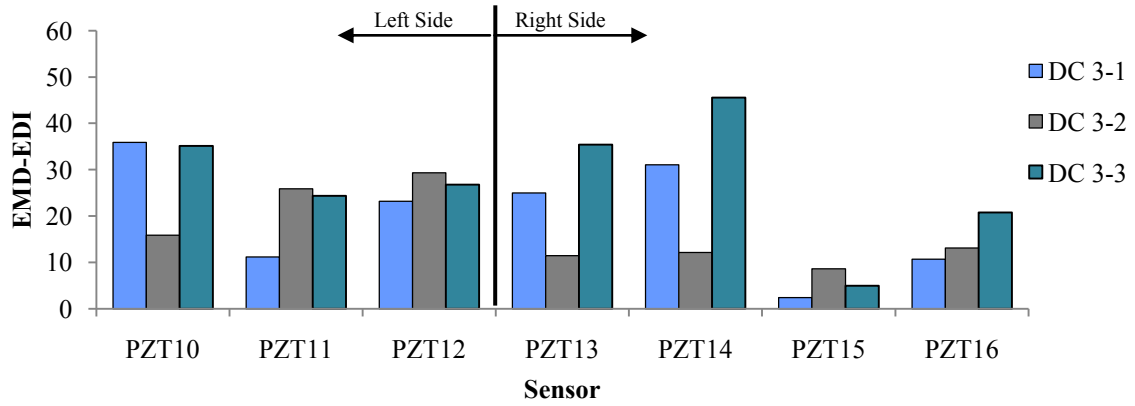
Figure 3-33 EMD-EDI, session 3, location F, 0-2000 Hz, IMF1, aluminium tip.
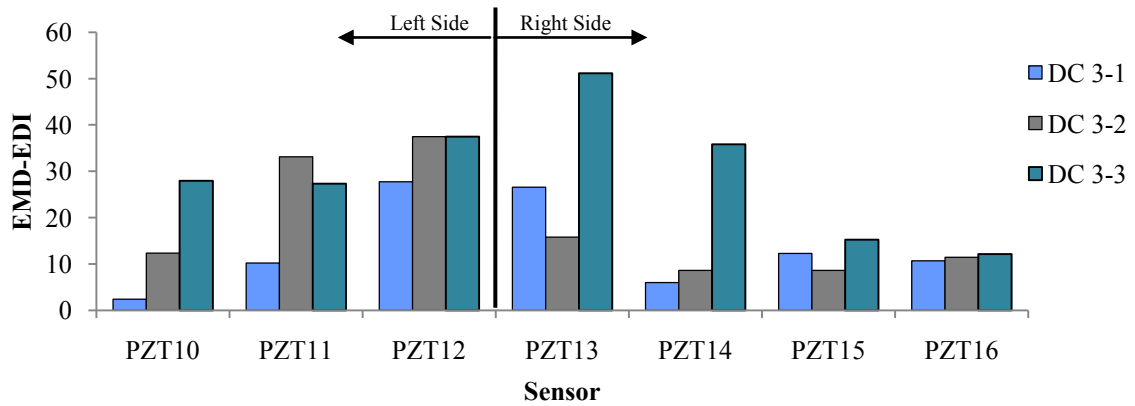
Figure 3-34 EMD-EDI, session 3, location B, 0-2000 Hz, IMF1, plastic tip.
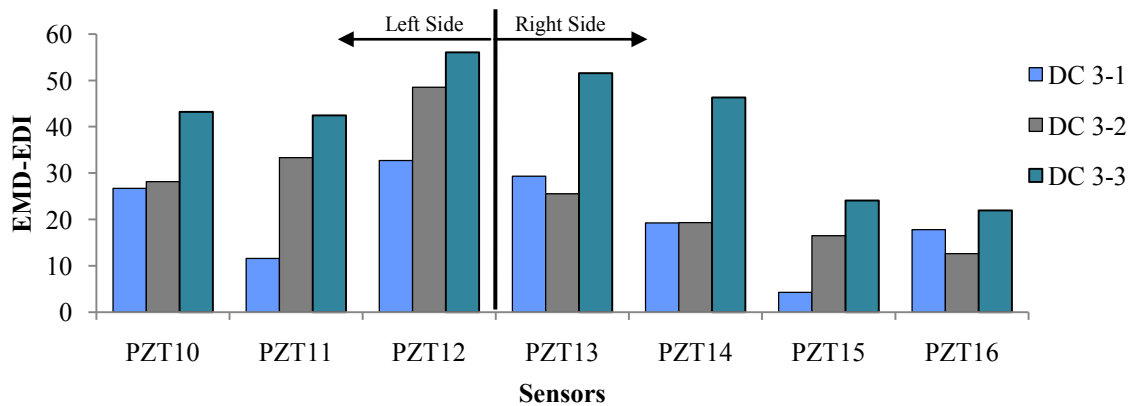
Figure 3-35 EMD-EDI, session 3, location C, 0-2000 Hz, IMF1, plastic tip.

72
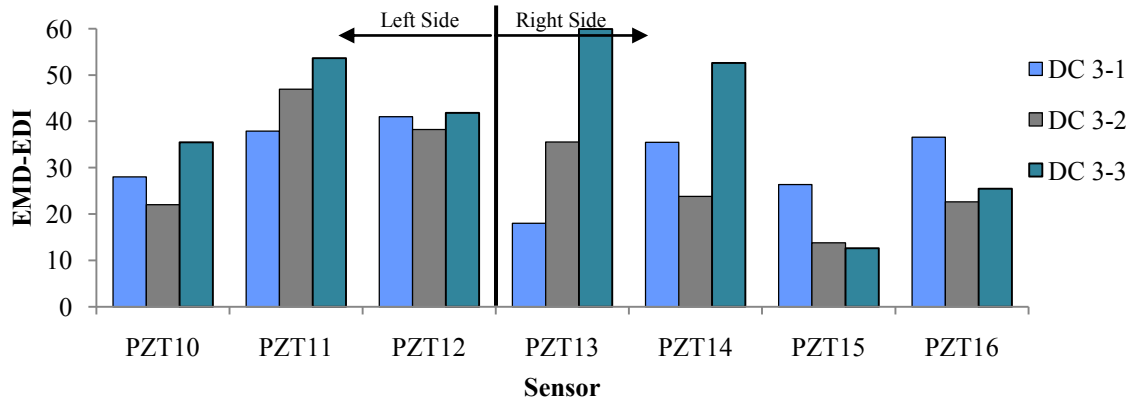
Figure 3-36 EMD-EDI, session 3, location E, 0-2000 Hz,
IMF1, plastic tip.
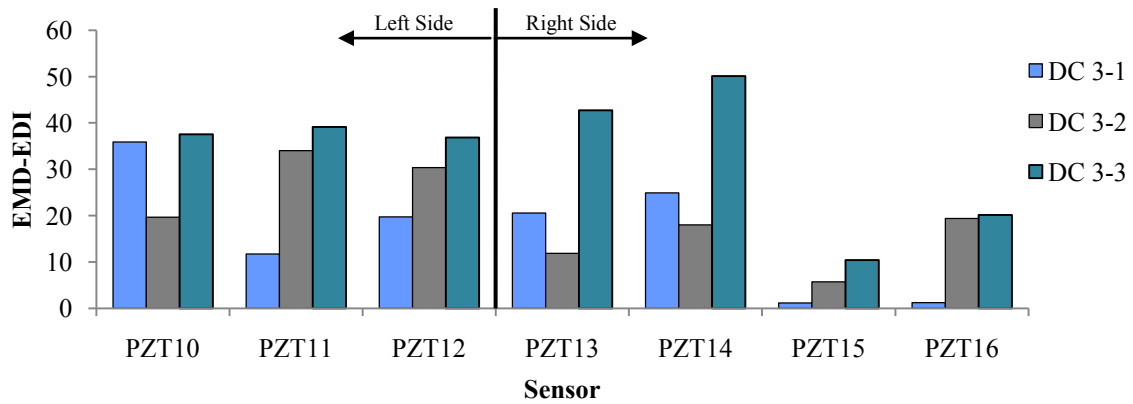
Figure 3-37 EMD-EDI, session 3, location F, 0-2000 Hz,
IMF1, plastic tip.

The results for the second IMF are shown as Figures A-1 through A-8 in Appendix A. A comparison of the results obtained based on the two IMFs demonstrate considerable similarity, although each IMF may show better progression for specific sensors for specific locations differently than the other IMF. It was therefore decided to add the IMFs to see if a better resolution of damage could be achieved. The results for the combined IMFs are shown as Figures A-9 through A-16 in Appendix A. The addition of the IMFs yields very similar results overall but slightly improved compared to the either the first or second IMF.

3.4.5 Consistency

The same process was used for session 3 as for sessions 1 and 2 to measure result consistency. Tables A-8 through A-11 in Appendix A list the variations in the EMD energy for each healthy and damage case. The values were all below 20%.

3.4.6 Discussion and Conclusions

The filtering frequency range of 0-2000 Hz yielded the best results in terms of damage index amplitude and damage progression. Moreover, the combined IMFs demonstrated the best resolution for damage detection.

From the comparison of data obtained for the impact locations for IMF1, IMF2 and the combined IMFs, it was observed that impact location B and C produced the best results concerning damage progression. Furthermore, the side of the flange that hosted the sensors relative to the impact location did not seem to have any significant influence on the results.

Concerning the influence of hammer tips, the two impulse hammer tips yielded approximately similar results overall, with the plastic tip producing more consistent results when considering the variability in EMD energies (Table A-8 through Table A-11). However, taking into account the results from session 2 that indicated that a frequency bandwidth that surpasses 2 kHz could produce improved damage resolution, it was concluded that the aluminum tip would be used for the subsequent testing.

It is interesting to note that for the results produced by combining the IMFs (A-9 through A-16), PZT10, PZT10, PZT12, and PZT14 yielded the most consistent damage indicators.

Last but not least, the pass-band frequency of 0-2000 Hz appears to be the most useful and applicable filtering frequency across all three sessions; it will therefore be used as the first pass-band frequency for the future analyses.

CHAPTER 4

DAMAGE DETECTION OF AN IN-SERVICE CONDENSATION PIPELINE JOINT

Julie Briand, Davood Rezaei and Farid Taheri

4.1 ABSTRACT

The early detection of damage in structural or mechanical systems is of vital importance. With early detection, the damage may be repaired before the integrity of the system is jeopardized, resulting in monetary losses, loss of life or limb, and environmental impacts. Among the various types of structural health monitoring techniques, vibration-based methods are of significant interest since the damage location does not need to be known beforehand, making it a more versatile approach. The non-destructive damage detection method used for the experiments herein is a novel vibration-based method which uses an index called the EMD Energy Damage Index, developed with the aim of providing improved qualitative results compared to those methods currently available. As part of an effort to establish the integrity and limitation of this novel damage detection method, field testing was completed on a mechanical pipe joint on a condensation line, located in the physical plant of Dalhousie University. Piezoceramic sensors, placed at various locations around the joint were used to monitor the free vibration of the pipe imposed through the use of an impulse hammer. Multiple damage progression scenarios were completed, each having a healthy state and multiple damage cases. Subsequently, the recorded signals from the healthy and damaged joint were processed through the EMD Energy Damage Index developed in-house in an effort to detect the inflicted damage. The proposed methodology successfully detected the inflicted damages. In this paper, the effects of impact location, sensor location, frequency bandwidth, intrinsic mode functions, and boundary conditions are discussed.

4.2 INTRODUCTION

Bolted joints are widely used in aerospace, mechanical and structural systems. Wherever bolted systems exist in environments which impose vibration, shocks or thermal cycling on the threaded fasteners, they are at risk of self-loosening caused by such dynamic loads (Hess, 1998), especially if proper joint assembly guidelines have not been followed. If the loosened bolts are not detected early, ignorance of the problem may lead to joint failure resulting in monetary losses, environmental impacts and possibly loss of life or limb. According to the Industrial Fasteners Institute (1995), self-loosening in conjunction with fatigue failure is the most frequent cause of failure of dynamically loaded bolted joints.

Structural health monitoring methods may be used for early detection of a joint's loss of integrity. In the field of structural health monitoring, Vibration Based Damage Detection (VBDD) is a non-destructive evaluation technique rapidly expanding in popularity. The basis for most VBDD methods is that the occurrence of damage in a system alters the dynamic properties of the system. Accordingly, system damage may be identified by measuring deviations in the structural dynamic characteristics associated with the changes in the physical system caused by the damage. For instance, Moniz et al. (2005) used a multivariate, attractor based approach for feature extraction from the time series information resulting from a system's vibration. This approach was used to detect loosened bolts at either end of a composite beam bolted to a plate. Furthermore, Ritdumrongkul et al. (2004) applied the electrical impedance method to two aluminum beams bolted together, modeled using the Spectral Element Method. By knowing that the electrical impedance is related to the mechanical impedance of the structure, Ritdumrongkul et al. (2004) were able to detect the loosened bolt through changes in the electrical impedance caused by changes in the structural dynamic properties.

A considerable amount of research in the field of VBDD has been concentrated on assessment of modal parameters as damage metrics. Concerning the loosening of threaded fasteners, Todd et al. (2004) conducted experiments on a beam with threaded

fasteners constraining the ends and used changes in the resonant frequencies and mode shapes to attempt to identify bolt loosening. In another study, one approach that Caccese et al. (2004) used to detect bolt load loss was using a low frequency modal analysis. However, in practical applications modal parameters are not always successful in identifying damage due to their sensitivity to boundary conditions, sensor location, sensor spacing, nonlinearities, and environmental effects such as temperature and humidity (Pines and Salvino, 2006).

To overcome the above mentioned drawbacks, another category of VBDD methods known as time series analysis techniques has evolved. The concept behind these methods is to extract damage metrics based on the analysis of the vibration signals acquired from the structure before and after damage. The Fourier transform and Wavelet Transform are the two well known techniques in this area that have been previously employed by researchers. For instance, Krawczuk (2002) introduced an optimization process based on a genetic algorithm for small crack detection in beams using the Fourier transform of the dynamic responses of the structure. Quek et al. (2001) examined the distribution of wavelet coefficients of a beam's deflection profiles through which sudden changes were proposed as a crack indicator.

Another time-series analysis, known as the Hilbert-Huang Transform (HHT), was introduced by Huang et al. (1998), which is an adaptive technique that decomposes the vibration signals in both time and frequency domains. This method has received significant attention for its use in structural health monitoring and has been successfully applied in the diagnosis of damage in building structures (Xu and Chen, 2004), (Lin et al., 2005). Additionally, Cheraghi et al. (2007) and Cheraghi and Taheri (2007) employed the decomposition part of the HHT known as Empirical Mode Decomposition (EMD) and proposed a damage index called the EMD Energy Damage Index (EMD-EDI) for structural health monitoring; subsequently verifying its applicability through numerical and experimental studies. The EMD-EDI utilizes an energy term obtained from EMD and compares the healthy and damaged states of a structure in order to identify the damage.

In the present paper, the integrity of the EMD-EDI (Cheraghi and Taheri, 2007; Cheraghi et al., 2007) has been further investigated through an experimental study performed on an in-service condensation pipeline with a 12-bolt mechanical joint. The

joint/pipe was excited with an impulse hammer and the resulting free vibration was captured via piezoceramic sensors bonded on the system in the vicinity of the joint. Damage was created by loosening successive bolts to a fully loose condition. The signals obtained from the piezoceramic sensors were processed through a MATLAB code developed in-house to carry out the signal processing, the Empirical Mode Decomposition and the calculation of the EMD energy term for each healthy and damage state. The effects of impact location, sensor location, frequency bandwidth, intrinsic mode functions, and boundary conditions are discussed in relation to the successful detection of damage.

4.3 METHODOLOGY

In 1998, Huang et al. (1998) introduced a new adaptive signal processing method called the Hilbert-Huang Transform (HHT), which nearly satisfies all the requirements for processing linear, non-linear, stationary, and non-stationary signals. The HHT consists of two main parts: EMD and the Hilbert transform. The EMD method decomposes a real signal into a collection of simpler modes (IMFs). The IMFs are unique intrinsic oscillating modes within the data and are associated with energy at different time scales and contain important data characteristics (Huang et al., 1998). The HHT applies the original Hilbert transform to the extracted IMFs and derives the local energy and instantaneous frequencies, thereby providing an energy-frequency-time distribution of the data.

The Empirical Mode Decomposition employs a sifting process to extract the IMFs. Each IMF satisfies two conditions. First, the number of extrema and the number of zero crossings are either equal or differ at most by one. Secondly, the average of the envelopes, defined by the local maxima and local minima, is zero. The first IMF component contains the shortest period component of the signal. To derive other IMFs, the first IMF is removed from the signal and the residue is considered as the new signal and the sifting process is performed to obtain the second IMF component. This procedure is repeated for all subsequent residues to derive the longer period components. After extracting all IMFs, the original signal is decomposed into n empirical modes, c_i, and a

residue, r_n, which can be either the mean trend or a constant. This process can be represented by the following mathematical relation:

$$X(t) = \sum_{i=1}^{n} c_i + r_n \qquad (4\text{-}1)$$

In the present work, the damage index introduced by Cheraghi et al. (2007), and Cheraghi and Taheri (2007) was used for damage identification. This damage index is based on the energy of the vibration signal's IMFs. According to this method, the dynamic response of the healthy structure during its free vibration is collected through sensors; the acquired signals are then passed through a band-pass filter to ensure the existence of the first natural frequency within the data. This is followed by extraction of the IMFs through EMD. Finally, the energy of the desired IMF for each sensor is established by:

$$E = \int_{0}^{t_0} (IMF)^2 \, dt \qquad (4\text{-}2)$$

The above procedure is subsequently repeated for the same structure during its damaged state to once again determine the energy of each signal's first IMF. The last step is the application of the EMD-EDI to the extracted IMF energy of each sensor's signal:

$$EMD - EDI = \left| \frac{E_{Healthy} - E_{Damaged}}{E_{Healthy}} \right| \times 100 \qquad (4\text{-}3)$$

Once the EMD-EDI is calculated for each sensor, the existence and severity of the damage may be determined by associating high index values with the existence of damage close to the respective sensors.

Cheraghi and Taheri (2007) suggested applying a band-pass filter to the data to keep only the first frequency component. However, in the experimental investigations carried out by Rezaei and Taheri (2009), it was concluded that this method only works well for systems where the first frequency is the dominant vibrating frequency of the structure. Otherwise, more frequency components should be included within the band-pass filter in order to avoid the elimination of damage sensitive frequency components.

In summary, the methodology followed in the experiment documented in this paper is as follows: Step 1: Monitor the vibration of a system in its healthy state using the

response of sensors within the system. Step 2: Once again, monitor the vibration of the system in its damaged state using the responses of sensors within the system. Step 3: Analyze the signals and evaluate the EMD-EDI which is based on the variation of IMF energy between the healthy and damage system states. Step 4: Establish whether damage exists based on the comparison of the EMD-EDIs evaluated in the last step.

4.4 EXPERIMENTAL STUDY

A 12-bolt mechanical joint (shown in Figure 4-1), located in the underground tunnels at the Central Services Building at Dalhousie University, NS, was chosen for the case studies due to ease of access. The joint was located on an insulated condensation line, 1.524 m to the right of an elbow and 1.092 m to the left of an anchor (support), respectively shown in Figure 4-2 (a) and (b). The pipe had a diameter of 203 mm and the bolts were 33.34 mm in diameter. To employ the first and third steps of the EMD damage detection methodology, the set-up for this experimental study, detailed in Figure 4-1, was accomplished as follows.

To capture the dynamic response of the joint, 8 piezoceramic (PZT) sensors were bonded to the flange and pipe in the vicinity of the joint. The sensors were labeled PZT1 through PZT8 and are denoted by the numbers 1 through 8 in Figure 4-1. The sensors were created from type PZT-5H sheets, 1.0 mm thick, available from Piezo Systems Inc. (Cambridge, MA, USA). The sensors were 24.0 mm long by 10.0 mm wide rectangles and polarized through the thickness. In order to monitor and compare the response of different locations on the pipe and flange, the sensors were bonded in the following locations: PZT1 was attached to the left vertical face of the flange between Bolt1 and Bolt12. PZT2 and PZT3 were respectively bonded to the top and bottom of the pipe at a distance of 82.6 mm from the joint centre to the edge of the PZT (see Figure 4-1 (c)). Mirroring the placement of PZT2, PZT4 was attached to the top of the pipe to the right of the joint at a distance of 82.6 mm from the joint centre to the edge of the PZT sensor (see Figure 4-1 (c)). Likewise, PZT5 was placed on the vertical face of the right flange to mirror the placement of PZT1. In order to obtain data for the side of the pipe, PZT7 and PZT8 were respectively placed to the right and left sides of the joint on the side of the pipe at a distance of 82.6 mm from the joint centre to the edge of the PZT sensors.

To induce free vibration in the system, the pipe was impacted at two locations on the pipe with a piezoelectric impulse hammer (model 5800B5) manufactured by Dytran Instrument Inc. (Chatsworth, CA, USA). An aluminum hammer tip was utilized for all testing. The two impact locations chosen for testing were Impact Locations B and D, shown in Figure 4-1 (c), directly opposite to one another. A 12.7 mm chrome alloy steel ball was bonded to the pipe at each impact location as a target in order to maintain consistency during testing. Impact locations B and D were respectively located on the right and left sides of the joint at a distance of 298.5 mm from the joint centre. The two locations were placed on either side of the joint in an attempt to determine what effect the different boundary conditions would have on the results.
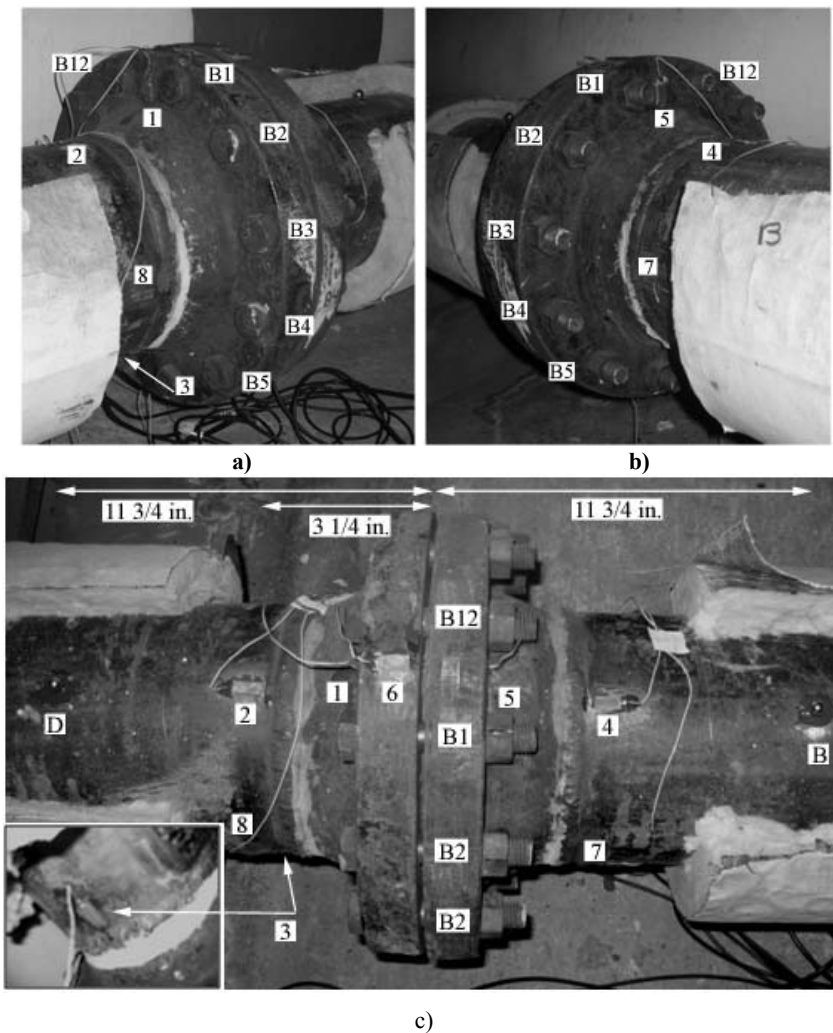
Figure 4-1 Piezoceramic sensor locations for part 2 **a)** Left side view of joint **b)** Right side view of joint **c)** Top view of joint.

<center>a)   b)</center>
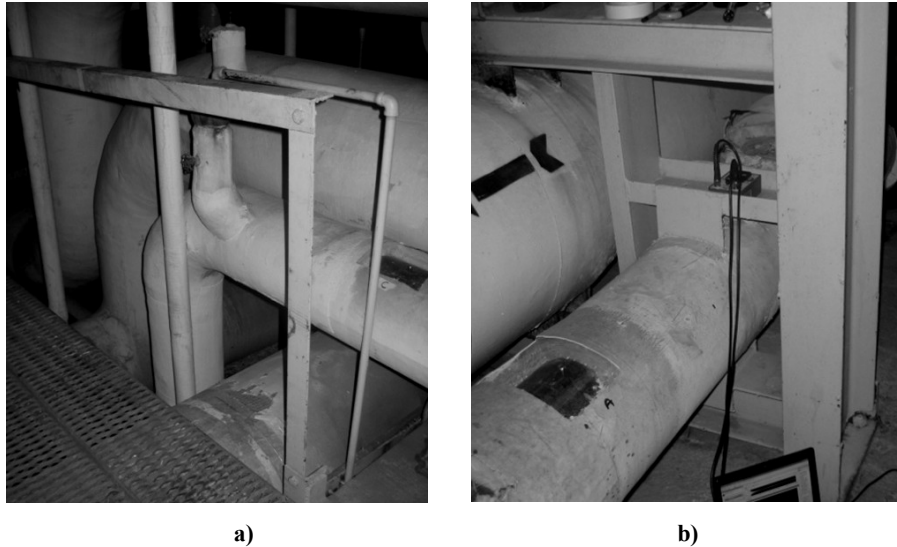
Figure 4-2 Pipeline boundary conditions **a)** Elbow at left side of joint **b)** Anchor at right side of joint.

Furthermore, the impact location's distance to the joint was chosen in an effort to compromise between the desire not to corrupt the sensor signal (from PZT2, PZT3, PZT4, PZT7 and PZT8) by an impact in close proximity to the sensors and the knowledge, gained from prior testing, which indicated that impacts further from the joint yielded less accurate results. As the condensation pipe originally was covered in approximately 44.5 mm of insulation, the insulation in the vicinity of the impact locations and sensor placement was removed. The PZT sensors and impact targets were attached to the pipe using Araldite 2014, after the surface area had been scoured using sandpaper and wiped free of dust and other residue.

During vibration, the response of the impulse hammer and the sensors were simultaneously collected through two NI 9215 modules inserted in an NI cDAQ-9172 data acquisition chassis manufactured by National Instruments Inc. (Austin, Texas, USA) and saved as an ASCII text file. With only eight data acquisition channels available, it was only possible to monitor the response of seven sensors concurrently, since the hammer signal was also required for analysis and required the eighth connector. Consequently, the results for scenarios 2 and 3 only give data for PZT2 through PZT8. It may be noted in the results section that scenario 1 only has three sensors whereas scenarios 2 and 3 have seven. This is due to scenario 1 occurring prior to the other

<center>82</center>

scenarios at which time only three sensors had been placed. The remaining sensors were placed after this scenario in an effort to more fully capture the joint response.

The data collected for each healthy state and damage state, typically comprised of 10 or 5 text files per state, was subsequently analyzed using a MATLAB code developed in-house which served to: (a) normalize the data with respect to the hammer signal, (b) process the data using Empirical Mode Decomposition, and (c) calculate the EMD-EDI for each damage case. The onsite experimental set-up detailed above is depicted in Figure 4-3.
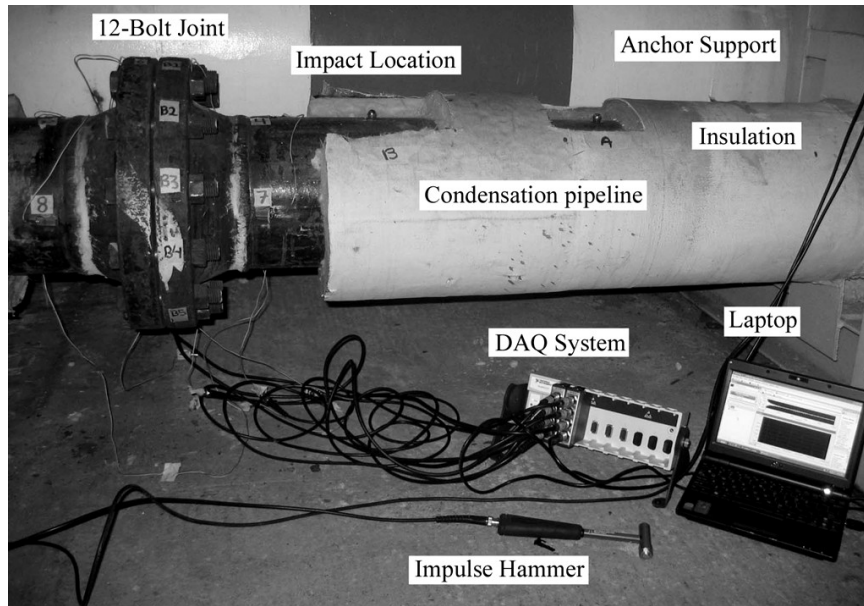
Figure 4-3 Experimental set-up.

To accomplish step 2 of the damage detection methodology, listed in Table 4-1 are the three damage scenarios that were completed during testing. In order to preserve the joint's functionality during the experiment, a state of damage was created by having a professional steamfitter loosen bolt(s). Of the twelve bolts on the joint, only six were accessible, therefore damage in the form of loosened bolts was applied to these six bolts, labeled B12 through B5 as illustrated in Figure 4-1. For each damage scenario, each bolt was fully loosened, past the stage of finger-tight. After each scenario was completed, the loosened bolts were retightened based on the steamfitter's judgment; a torque wrench was purposely not used, in order to follow actual practice in the real situation. Therefore, testing for a new healthy state had to be completed after each scenario.

To obtain an accurate average energy for each sensor and for each damage case, multiple impacts were required for each state. For all scenarios, 10 impact scenarios were completed for each healthy case, whereas only 5 impact scenarios were completed for each damage case. The reasoning for the greater number of impacts for the healthy case was to ensure a solid base for the index evaluation. Also of note is that for scenario 1, only impact location B was used, whereas for scenarios 2 and 3 both impact locations B and D were used; the change in the number of impact locations is due to scenario 1 occurring prior to the other scenarios when impact location D had not yet been placed.

Table 4-1 Damaged joint scenarios.

Scenario	State	Bolts Loosened	Damage Case
Scenario 1	Healthy Pipe 1		
	Damage Case 1-1	Bolt #1	DC 1-1
	Damage Case 1-2	Bolt #1 and #2	DC 1-2
Scenario 2	Healthy Pipe 2		
	Damage Case 2-3	Bolt #12	DC 2-3
	Damage Case 2-4	Bolt #12 and #1	DC 2-4
	Damage Case 2-5	Bolt #12, #1and #2	DC 2-5
Scenario 3	Healthy Pipe 3		
	Damage Case 3-6	Bolt #5	DC 3-6
	Damage Case 3-7	Bolt #5 and #3	DC 3-7

4.5 RESULTS AND DISCUSSION

After monitoring and recording the free vibration of the pipe in its healthy state through the piezoceramic sensors, damage was introduced in the joint by loosening subsequent bolts and the free vibration of the pipe was recorded for each damaged state. As mentioned in the previous section, three damage scenarios were studied which included one bolt, two bolts, and in one scenario, three bolts completely loosened. Subsequently, in order to complete step 4 and 5 of the damage detection process, the recorded signals from the healthy and damaged pipe joint were processed and the EMD-EDI were evaluated in an effort to establish the presence of the inflicted damage.

4.5.1 Result Analysis

For the healthy state of scenario 1, five signals were chosen for each impact location and for the damage cases of scenario 1, three signals were used. As a part of the EMD-EDI procedure, the data should be filtered before decomposing. By analyzing the data using different frequency bands, it was found that a low-pass filter with a cutoff frequency of 2000 Hz provided the best resolution for identification of damage for scenario 1. Figure 4-4 and Figure 4-5 illustrate the EMD-EDI calculated for sensors PZT1, PZT2 and PZT3, for scenario 1. The results shown in Figure 4-4 and Figure 4-5 are respectively based on the energy of the first and second IMFs. The damage case labels used in all of the legends for the following graphs are explained in Table 4-1.
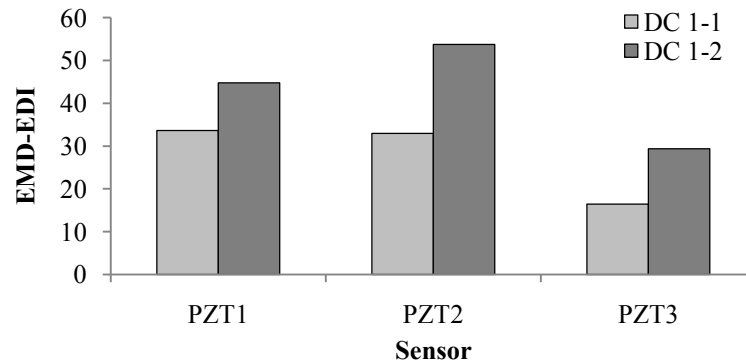
Figure 4-4 Scenario 1, impact location B, IMF 1.

As can be seen in Figure 4-4, of the three sensors used for scenario 1, all were successful in detecting the presence and progression of damage. Moreover, PZT1 and PZT2 provided the best damage identification in reference to index amplitude. The performance of PZT1 and PZT2 may be due to their close proximity to the damaged bolts, whereas PZT3 was located on the bottom surface of the pipe and far from the damaged area. After analyzing the results using the EMD-EDI based on the first IMF, the second IMF was also investigated as a case study. Figure 4-5 illustrates that the second IMF was also successful in damage identification of the joint.
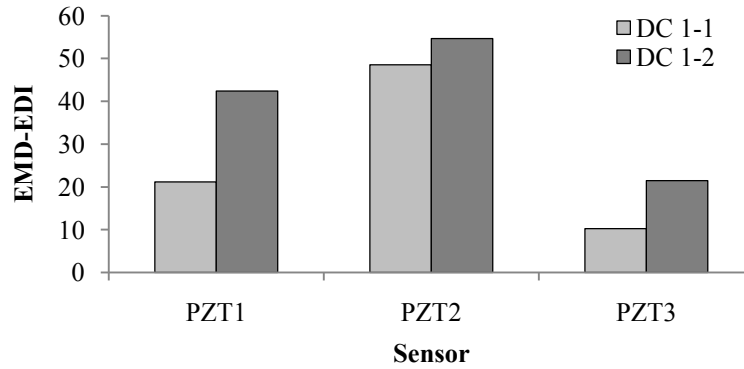
Figure 4-5 Scenario 1, impact location B, IMF 2.

The same signal selection scheme used in scenario 1 was followed for the second scenario. However, for scenario 3, three signals were chosen for each impact location for both the healthy and damaged cases. By analyzing the data for scenario 2 and 3 using different frequency bands, it was found that frequency bands of 0-2000 Hz, and 1000-2000 Hz both provided the best resolution for identification of the damage when both IMFs were taken into consideration. However, for the purposes of this paper, only the results from the frequency band of 0-2000 Hz will be shown.

The bandwidth of 0-2000 Hz was chosen based on the exhibition of damage progression and damage index amplitude observed for the first scenario. Accordingly, a bandwidth of 0-2000 Hz was used to process all the data for scenarios 2 and 3. Figure 4-6 and Figure 4-7 respectively illustrate the EMD-EDI calculated for impact locations B and D for sensors 2 through 8. The results shown in these figures are based on the energy of the first IMF.
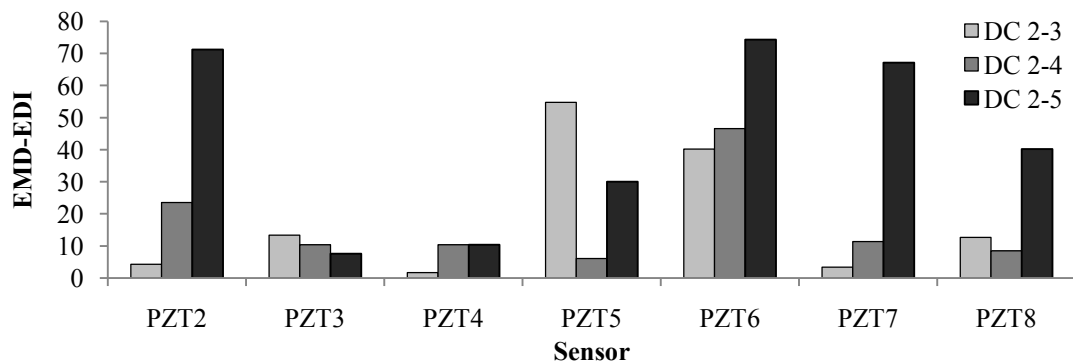
Figure 4-6 Scenario 2, impact location B, IMF 1.

86

A comparison of Figure 4-6 and Figure **4-7** with Figure 4-4 reveals an interesting phenomenon, in that PZT2, the sensor giving the most consistent results for scenario 2, was also the sensor that gave the most promising results for scenario 1. Also, impact location D provided relatively better damage progression overall with four out of seven PZTs (PZT2, PZT4, PZT5, PZT8) showing full damage progression, whereas impact location B only showed full progression with three PZTs (PZT2, PZT6, PZT7). Furthermore, the amplitude of the damage indices was greater overall for impact location D. Both locations showed a damage progression for PZT2 with impact location B also illustrating relatively high amplitude and clear damage progression for PZT6 and PZT7, whereas location D also demonstrated comparable results for PZTs 4, 5 and 8. Once again, PZT3, the sensor furthest from the damage, did not give a clear indication of the inflicted damage for either impact location.

Figure 4-7 Scenario 2, impact location D, IMF 1.
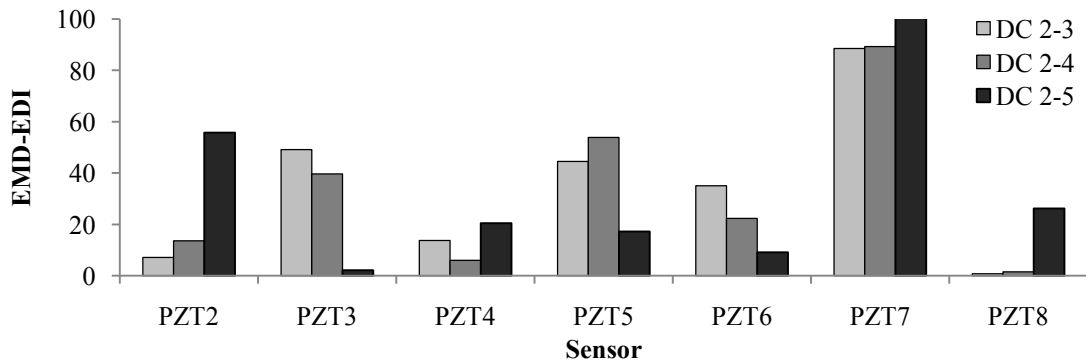
Figure 4-8 Scenario 2, impact location B, IMF 2.

After analyzing the results using the EMD-EDI based on the first IMF, the second IMF was also investigated as a case study. Figure 4-8 and Figure 4-9 illustrate that the

second IMF was also successful in damage identification, if not damage progression. However, a high damage index is the damage criterion with more significance because in most cases, the damage would be fixed before it progresses to a more dangerous condition.
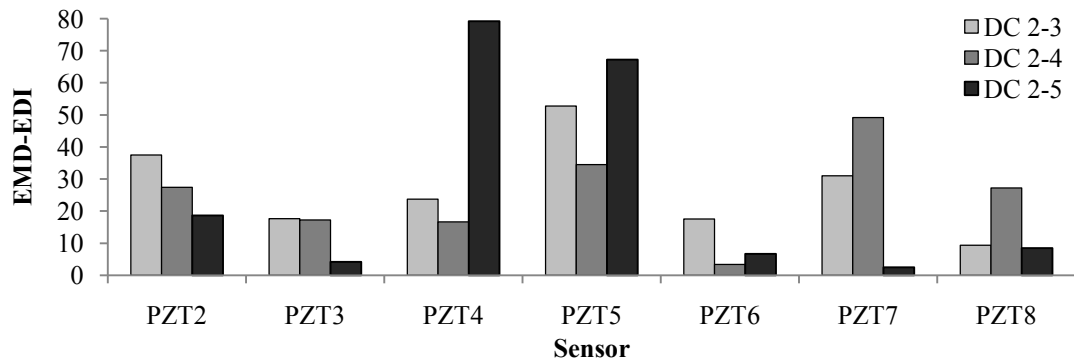
Figure 4-9 Scenario 2, impact location D, IMF 2.

Figure 4-10 Figure 4-11 respectively illustrate the EMD-EDI calculated for impact locations B and D for sensors 2 through 8 for scenario 3. The results shown in the following two figures are based on the frequency band of 0-2000 Hz, and the energy of the first IMF. As can be seen from comparing Figure 4-10 Figure 4-11, impact location B provided better damage progression with five out of seven PZTs (PZT3, PZT4, PZT5, PZT7, PZT8) showing damage progression, whereas location D only showed progression with PZT8. However, similarly to scenario 2, the damage index amplitude for location D is significantly higher overall with each sensor clearly giving an indication of the inflicted damage. Both locations showed a damage progression for PZT 8 with location B showing additional damage progression for PZTs 3, 4, 5 and 7.
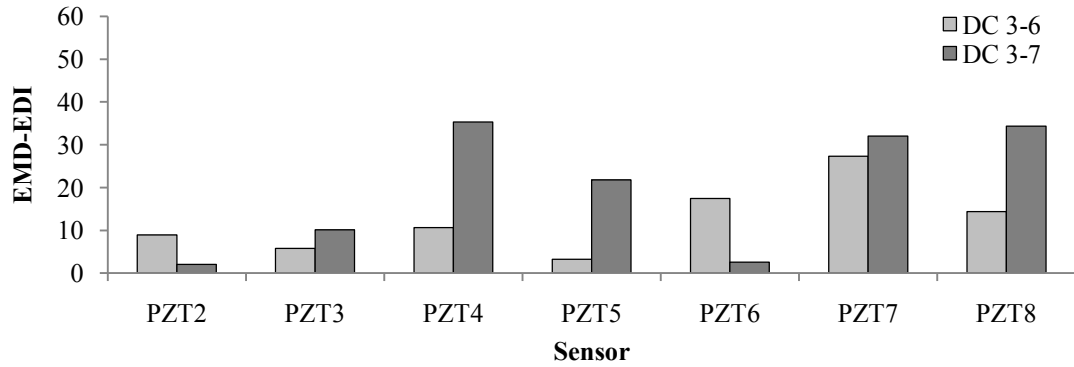
Figure 4-10 Scenario 3, impact location B, IMF 1.
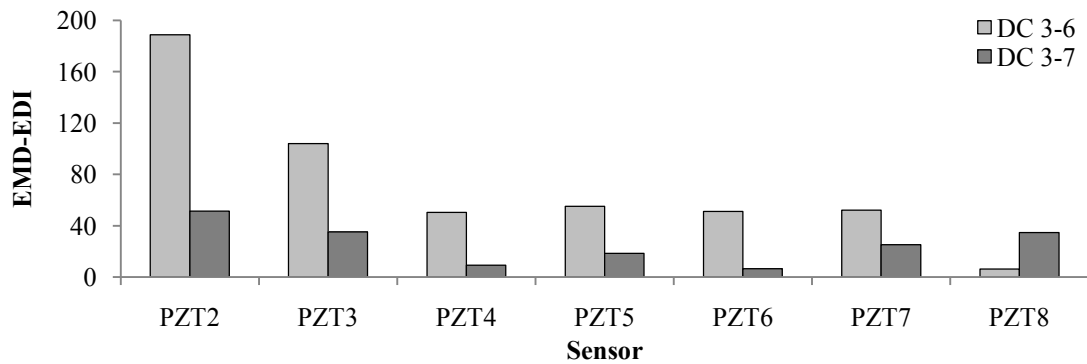
Figure 4-11 Scenario 3, impact location D, IMF 1.

After analyzing the results using the EMD-EDI based on the first IMF, the second IMF was also investigated as a case study. Figure 4-12 and Figure 4-13 illustrate that the second IMF was also successful in damage identification, if not damage progression.
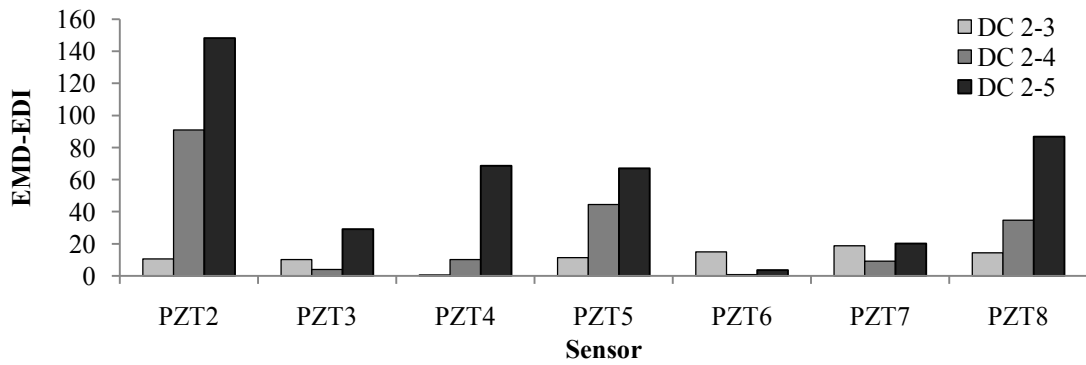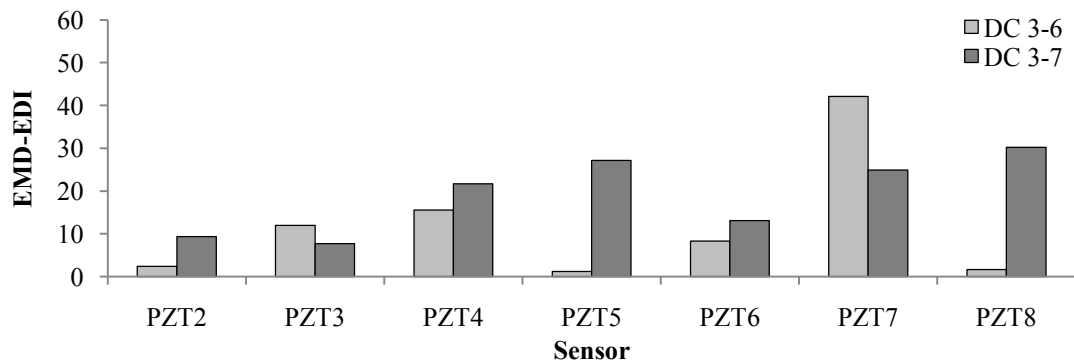

Figure 4-12 Scenario 3, impact location B, IMF 2.
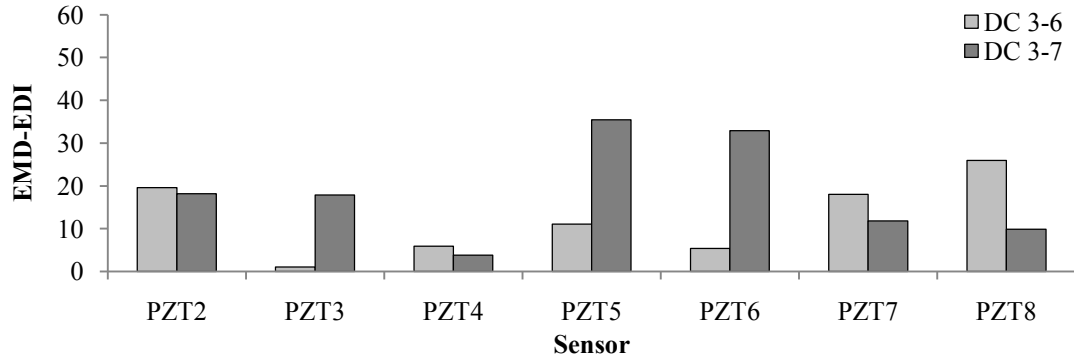
Figure 4-13 Scenario 3, impact location D, IMF 2.

It is interesting to note that the sensors closest to the damage, namely PZT7 and PZT8, yielded among the best results for scenario 3 except in the case of impact location D, IMF1. Even though the pipe is impacted at its apex, the impact excites many modes of vibration, not necessarily in the vertical direction, thereby producing strain in various sensors around the circumference of the pipe. It may be theorized from the results of the three scenarios that the sensors located closest to the damage have the highest probability of detecting the presence of damage.

4.5.2 Discussion

From Figure 4-4 through Figure **4-13**, it can be observed that the EMD-EDI amplitude for several of the sensors (PZT2, PZT7 and PZT8) in the vicinity of their respective damages is in general more consistent with varying impact locations and IMFs and clearly demonstrates the capability of the proposed damage index in identifying and localizing the damage. Taking each damage index individually, each sensor was able to detect each damage state as compared to the healthy state. Furthermore, at varying times, several sensors were able to detect not only the damage, but the damage progression of the successively loosened bolts. From an analysis of the above results, it is clear that the placement of the sensors on and around the flanges has an effect on the resulting EMD-EDI amplitude and progression. However, no clear pattern is as yet discernable regarding why certain sensors demonstrate a greater sensitivity to the damage under certain conditions.

Additionally, a comparison of the above results between IMF1 and IMF2 illustrate that an analysis based on IMF1 for impact location D yields greater index amplitudes than for impact location B. It is hypothesized that the higher index magnitudes were due to the left end of the pipe (see Figure 4-1) not being constrained, but instead with more freedom to vibrate than the anchor support allowed the pipe on the other side of the joint. It is worth noting that this greater index amplitude does not appear for the analysis based on the second IMF. These results serve to indicate that while the second IMF may indeed demonstrate good qualitative results in some cases, in other cases the results are much less useful than those of IMF1 and are therefore not helpful in damage identification for this experimental set-up. In real situations of damage detection for health monitoring, once an indication of damage at a joint is noted, one would not wait to see damage progression; therefore, a high EMD-EDI amplitude is the most favorable indicator which would serve to indicate based on the previous results, that when testing, impacting the side of the joint with a less restrained boundary condition will give relatively better results than the more constrained side.

Several items should be taken as variables in this experiment that possibly had an untoward influence on the results. First, no method was available to monitor the fluid flow and therefore it is unknown how much flow variation occurred during the tests, and what affect it may have had on the results. Second, due to corrosion on the pipe, the bond of PZT3, PZT7 and PZT8 to the pipe may not have been able to transmit the appropriate strains from the pipe to the sensors. Finally, without a torque wrench available, the bolts were retightened after each scenario relying only on the steamfitter's experience. Moreover, as it was impossible to access the entire joint with the tools available, it was not possible to verify the torque of each bolt in the joint for the healthy condition which could introduce more uncertainty in the results.

4.6 CONCLUSIONS

The objective of this study was to experimentally confirm the use of the EMD-EDI for the evaluation of the damaged condition of an in service 12-bolt joint mechanical joint located on a condensation pipeline. The EMD-EDI is based on the variation of the IMF energy, decomposed from the vibration signals using EMD, prior to and following the

occurrence of damage in a system. Three damage scenarios were analyzed, with each damage scenario progressing from a healthy state, to having one bolt completely loosened, then two and then in the second scenario, three.

This experimental study documented and herein demonstrated that the EMD-EDI can successfully detect the presence of damage. However, it is important to note that sensor placement, boundary conditions and therefore the impact locations have a significant influence on the results which should be carefully considered when choosing sensor and impact location placement. Moreover, additional work is required to determine if the proximity of a sensor to a loosened bolt increases the ability of the sensor to detect damage. Furthermore, the band-pass filter used for signal filtering should be applied carefully to avoid filtering out frequency components that contain meaningful information required for the proposed damage detection method.

4.7 ACKNOWLEDGEMENTS

4.8 REFERENCES

Caccese, V., Mewer, R., & Vel, S. (2004). Detection of bolt load loss in hybrid composite/metal bolted connections. Engineering Structures, 26(7), 895.

Cheraghi, N., & Taheri, F. (2007). A damage index for structural health monitoring based on the empirical mode decomposition. *J. of Mechanics of Materials and Structures, 2*(1), 43-62.

Cheraghi, N., Riley, M. J., & Taheri, F. (2007). Application of Hilbert-Huang transform for evaluation of vibration characteristics of plastic pipes using piezoelectric sensors. *Structural Engineering Mechanics, 25*(6), 653-674.

Hess, D. P. (1998). Vibration and shock induced loosening. In *Handbook of bolts and bolted joints,* J. H. Bickford, & S. Nassar (Eds.), (pp. 757). Marcel Dekker, Inc.: New York.

Huang, N. E., Shen, Z., Long, S. R., Wu, M. C., Shih, H. H., Zheng, Q., Nai-Chyuan, Y., Tung, C. C., & Liu, H. H. (1998). The empirical mode decomposition and the Hilbert spectrum for nonlinear and non-stationary time series analysis. *Philosophical Transactions of the Royal Society A: Mathematical, Physical and Engineering Sciences, 454*(1971), 903-995.

Industrial Fasteners Institute: Division VI Aerospace Fasteners. (1995). *Test application handbook relating to mechanical fasteners*. Industrial Fasteners Institute: Cleveland, Ohio.

Krawczuk, M. (2002). Application of spectral beam finite element with a crack and iterative search technique for damage detection. *Finite Elements in Analysis and Design, 38*(6), 537-548.

Lin, S., Yang, J. N., & Zhou, L. (2005). Damage identification of a benchmark building for structural health monitoring. *Smart Materials & Structures, 14*(3), S162-S169.

Moniz, L., Nichols, J., Nichols, C., Seaver, M., Trickey, S., & Todd, M. (2005). A multivariate, attractor-based approach to structural health monitoring. *Journal of Sound and Vibration, 283*(1-2), 295-310.

Pines, D., & Salvino, L. (2006). Structural health monitoring using empirical mode decomposition and the hilbert phase. *Journal of Sound and Vibration, 294*(1-2), 97-124.

Quek, S. T., Wang, Q., Zhang, L., & Ang, K. K. (2001). Sensitivity analysis of notch detection in beams by wavelet technique. *International J. of Mechanical Sciences, 43*, 2899-2910.

Rezaei, D., & Taheri, F. (2009). Experimental validation of a novel structural damage detection method based on empirical mode decomposition. *Smart Materials and Structures, 18*(4).

Ritdumrongkul, S., Abe, M., Fujino, Y., & Miyashita, T. (2004). Quantitative health monitoring of bolted joints using a piezoceramic actuator-sensor. *Smart Materials and Structures, 13*(1), 20-29.

Todd, M. D., Nichols, J. M., Nichols, C. J., & Virgin, L. N. (2004). An assessment of modal property effectiveness in detecting bolted joint degradation: Theory and experiment. *Journal of Sound and Vibration, 275*(3-5), 1113-1126. Retrieved from http://dx.doi.org/10.1016/j.jsv.2003.10.037

Xu, Y. L., & Chen, J. (2004). Structural damage detection using empirical mode decomposition: Experimental investigation. *Journal of Engineering Mechanics, 130*(11), 1279-1288.

CHAPTER 5

DAMAGE DETECTION OF A PRESSURIZED STEEL PIPELINE JOINT USING AN EMPIRICAL MODE DECOMPOSITION-BASED ENERGY DAMAGE INDEX

Julie Briand and Farid Taheri
Prepared Article Ready for Submission

5.1 ABSTRACT

The development of safe and reliable structural health monitoring techniques for pipelines is vital due to their importance for the safe and reliable transportation of fluids necessary for our infrastructure. The non-destructive damage detection method used for the experiments herein is a novel vibration-based method which uses an index called the Empirical Mode Decomposition Energy Damage Index, developed with the aim of providing improved qualitative results compared to those methods currently available. As part of an effort to establish the integrity and limitation of this novel damage detection method, experiments were conducted on a pressurized steel pipeline with a bolted joint. Piezoceramic sensors, placed at various locations around the joint were used to monitor the free vibration of the pipe imposed through the use of an impulse hammer. Multiple damage progression scenarios were completed, each consisting of a healthy state and multiple damage cases. Subsequently, the recorded signals from the healthy and damaged joint were processed using the Empirical Mode Decomposition Energy Damage Index in an effort to detect the inflicted damage. The methodology was used with varying degrees of success to detect the inflicted damages. In this paper, the effects of impact location, sensor location, frequency bandwidth, and the influence of the order of the intrinsic mode functions on the results are discussed.

Keywords: Vibration-based damage detection; piezoelectric sensors; structural health monitoring; bolted pipeline joint; empirical mode decomposition.

5.2 INTRODUCTION

Pipelines are an integral part of today's residential and industrial infrastructure. They are essential for the safe and effective transportation of natural gas, oil, water, waste products, and communication/power cables. The stability and reliability of pipelines may be affected by ground movement, environmental conditions, the interaction with the fluids they carry, and damage caused by external hazards at any time throughout their service life. These factors make regular pipeline inspection and maintenance especially important.

Moreover, damage assessment of pipelines is critical for economic and community recovery after natural disasters (Park and Inman, 2005). An immediate damage assessment may aid in preventing fires, explosions, and pollution from broken gas and sewage lines (Park and Inman, 2005). Dependent on the contents and pressure of the pipeline system, leakage or failure may have potentially catastrophic consequences. As one of the critical components of a pressurized system, the failure of bolted joints may result in disastrous outcomes (Energy Institute (Great Britain), 2007).

One of the most common causes of bolted joint failure is vibration induced bolt loosening, if the joint is exposed to environments which impose dynamic loading such as vibration or shocks on the threaded fasteners (Hess, 1998; Industrial Fasteners Institute, 1995; Pai and Hess, 2002). This failure mode is exacerbated by the incorrect and uncontrolled assembly practices of the majority of bolted joints (Corbett, 1998) leading to an insufficient clamping force which contributes to joint failure.

To date, traditional non-destructive methods used to assess damaged joints include visual inspection, the cylindrical guided wave technique (CGWT), phased array ultrasonics, and time-of-flight ultrasonics (Energy Institute (Great Britain), 2007). However, quick and effective prioritization of actions after a disaster is infeasible with manual inspection (Johnson et al., 2004). For this reason and those mentioned above, the development of safe and reliable structural health monitoring techniques for pipelines is vital for operational reliability, reduction in maintenance costs, and operator/public safety. However, the amount of research performed on the structural health monitoring of bolted joints has been somewhat limited.

One of the widely studied qualitative SHM techniques currently under development to assess bolted joint damage is the electromechanical impedance-based method (Yan et al., 2007) which takes advantage of the direct relation between the electrical impedance of a bonded PZT patch to the mechanical impedance of the host structure. The damage location is ascertained due to the known localized detection area surrounding each sensor and the damage severity is qualitatively assessed using a damage index which measures the change in the impedance before and after damage (Ritdumrongkul and Fujino, 2006).

For example, Park et al. (2003) used this local diagnostic method and performed preliminary experimental testing on a single bolt lap-joint in an effort to monitor bolt preload loss in real time. To improve upon the impedance method and make it more economically feasible, Peairs et al. (2004) experimentally investigated the use of a low cost impedance method on a model pipeline with bolted joints which uses a digital signal analyzer with an Fast Fourier Transform (FFT) function instead of the very expensive impedance analyzer.

Ritdumrongkul et al. (2004) also used the impedance method in conjunction with a spectral element method (SEM) model for damage characterization. Laboratory experiments were performed on a suspended two-joint and four-joint aluminum beam where damage was simulated by loosening bolts and the numerical models were used to quantitatively locate and assess the level of damage.

However, even though it has been successfully illustrated that the impedance method is successful in damage detection of bolted joints, the equipment required to perform this testing is expensive (Peairs et al., 2004) and therefore unfeasible in situations with lower budgets.

Vibration Based Damage Detection (VBDD) is another category of non-destructive evaluation techniques that has been rapidly growing in popularity over the past several decades. Damage detection using VBDT methods is based on the fact that modal properties such as frequencies, mode shapes, and the modal damping of a structure are functions of physical properties like mass, stiffness, and damping. When defects or damage occur in a structure, some or all of these physical properties may change and lead to alterations in the dynamic properties of the system. For a comprehensive review of the

advances in vibration based SHM, the reader is directed to Doebling et al. (1996; 1998) and Carden and Fanning (2004).

In recent years, structural health monitoring via modal characteristics has emerged as one category of vibration damage detection that has received attention by many researchers. Modal based damage detection methods rely on alterations in the modal parameters of a structure such as natural frequencies/mode shapes, modal strain energy etc. for an indication of damage.

Modal parameters have been studied as damage sensitive features with different degrees of success. For example, Shi (2000) employed modal strain energy for the localization and quantification of damage numerically and experimentally on a single-bay, two-story portal frame structure. Damage was created in the structure by loosening the joints. In another work, Todd et al. (2004) experimentally and theoretically assessed modal property effectiveness to detect bolted joint degradation in the supports of a beam.

However, the use of modal methods is limited due to their sensitivity to boundary conditions, sensor spacing, environmental effects such as temperature and moisture and nonlinearities (Pines and Salvino, 2006). Additionally, most modal based damage identification methods require numerical simulations of the specified structure which decreases the practicality and effectiveness of the approach (Rezaei and Taheri, 2009). Furthermore, Todd et al. (2004) also stated that only significant preload losses are typically detectable when vibration-based techniques such as modal analysis are employed (Fasel et al., 2009), since the resulting frequencies are too low to identify small changes in preload loss, and localized damage (Doebling et al., 1998).

Non-modal based methods include autoregressive approaches, neural networks, time series analyses and various other pattern recognition approaches (Nichols, 2003). Research using auto-regressive modeling was conducted by Fasel et al. (2009). Experiments and numerical analyses were performed to detect bolt preload reduction using a chaotic structural excitation with a damage detection algorithm based on auto-regressive modeling. Signals were applied to the structure using macro fiber composite (MFC) patches.

For instance, Michaelides et al. (2008) used a statistical time series model called the Statistical Power Spectral Density-based method to a thin plate with joints. Nichols

(2003) explored the use of the steady-state dynamic analysis for damage detection instead of the traditional transient or stochastic vibration analysis. Experimental testing was performed on a scaled three story frame for which damage was created by bolt removal. Continuing on with the research into steady-state dynamics analysis, Todd et al. (2004) also used time series analysis to detect preload loss in a bolted joint in an aluminium frame structure.

Another time-series technique, the Hilbert-Huang transform (HHT), was developed by Huang et al. (1998) and has been successfully applied to structural health monitoring techniques in mechanical and civil systems (Loutridis, 2004; Pines and Salvino, 2006). The HHT is an adaptive signal processing technique that is able to produce signal decomposition in time and frequency domains, thus providing valuable information for damage detection purposes (Rezaei and Taheri, 2010).

Empirical Mode Decomposition (EMD), the key component in the HHT, was used by Loutridis (2004) to detect and monitor the growth of a tooth root crack in a gear system. Loutridis illustrated that the defect evolution can be monitored by computing the energy of the intrinsic mode that has the greatest damage sensitivity, manifested through an increase in its envelope amplitude. Pines and Salvino (2006) experimentally investigated the capability of HHT by applying it to the damage detection of a three story building model. It was concluded that the results on the laboratory experimental structure were promising; they could determine the presence and location, and severity of damage with respect to a baseline. Cheraghi and Taheri (2008) completed a theoretical investigation of the vibration characteristics of a six degree of freedom mechanical system to ascertain the capability and integrity of EMD with respect to assessing performance in structures.

Cheraghi et al. (2005) introduced a novel structural health monitoring method based on the HHT, called the Empirical Mode Decomposition Energy Damage Index (EMD-EDI). This method combines a time-series analysis technique with a local diagnosis approach through the use of piezoceramic sensors. Cheraghi et al. investigated the integrity of the EMD-EDI by performing a set of experiments on simply supported plastic pipes with adhesively bonded joints. The vibration response of the healthy and damaged pipes was monitored using piezoelectric patches bonded at the joint location. It was concluded that the index could effectively detect the joint damage.

99

The EMD-EDI was further investigated by Cheraghi and Taheri (2007) who numerically evaluated the integrity of the method using Finite Element simulations. The subject of the investigation was a cantilevered aluminium pipe with various forms of corrosion damage represented by the removal of material (elements) in the pipe wall. Subsequently, Rezaei and Taheri (2009) experimentally employed the EMD-EDI for damage detection of cantilevered steel pipes with various degrees of simulated corrosion damage. Rezaei and Taheri (2010) then extended the use of the EMD-EDI to detect a flaw in pipeline girth welds in both pressurized and non-pressurized conditions.

Rezaei and Taheri (2010; 2009) determined that the EMD-EDI was effective in detecting and localizing single and multiple areas of damage as well as qualitatively assessing the damage severity. As such, this method holds promise for an effective an inexpensive system for structural health monitoring.

5.3 MOTIVATIONS AND OBJECTIVES

The objective of the research summarized in this paper was to further examine the effectiveness and integrity of the EMD-EDI method applied to bolted joints. With the limited amount of structural health monitoring research performed on bolted joints, it was thought to be an ideal topic to extend the research previously conducted concerning the evaluation of the integrity of the EMD-EDI method. In an effort to determine the optimal parameters for damage detection, the effects of two different impact locations and six different sensor locations were investigated. Furthermore, the effect of frequency bandwidth, used for signal filtering, and the influence of the order of the intrinsic mode functions on the results were investigated.

5.4 EMPIRICAL MODE DECOMPOSITION

In 1998, Huang et al. (1998) developed the Hilbert-Huang transform (HHT) in an effort to create an improved analysis method of nonlinear and non-stationary signals and, according to Loutridis (2004), to create a method for accurate time and frequency localization. The key component of the HHT is a method called the Empirical Mode Decomposition (EMD), which is used in conjunction with the Hilbert transform.

The first step of the HHT process is the decomposition of a signal using EMD into components. EMD assumes that every signal is composed of a number of unique intrinsic oscillating modes called Intrinsic Mode Functions (IMFs). The IMFs are associated with energy at different time scales and contain important characteristics of the data (Huang et al., 1998). The second step is to apply the Hilbert transform to the decomposed IMFs and construct an energy-frequency-time distribution, known as the Hilbert Spectrum, in order to ascertain the local energy and instantaneous frequency.

The Empirical Mode Decomposition employs a sifting process to extract the IMFs, thereby providing a description of the frequency contents of a signal. The procedure of the sifting process is schematically illustrated in Figure 5-1. To extract the IMFs for a given time signal $x(t)$, two cubic splines are fitted through the local maxima and minima to produce the upper and lower envelopes, respectively. The upper and lower envelopes should cover all the data. Then the mean of these two splines or envelopes (m_1) is subtracted from the original signal. The difference between the signal and the mean is called the first component (h_1):

$$h_1 = x(t) - m_1 \qquad (5\text{-}1)$$

At this stage h_1 is treated as the original time signal and the sifting process is repeated to get the next component by:

$$h_{1k} = h_{1(k-1)} - m_{1k} \qquad (5\text{-}2)$$

where k is the operation (sifting) cycle number. At each step the sifting process produces a more symmetric signal with respect to zero mean. The above procedure is schematically illustrated in Figure 5-2. If the sifting process continues to the extreme, it will remove the physically meaningful amplitudes and fluctuations. So, Huang et al. (1998) proposed a criterion based on limiting the size of the standard deviation, SD, computed from two successive sifting results. This stoppage criterion can be expressed as:

$$SD = \sum_{t=0}^{T} \left[\frac{\left| h_{1(k-1)}(t) - h_{1k}(t) \right|^2}{h_{1(k-1)}^2(t)} \right] \qquad (5\text{-}3)$$

If the SD is smaller than a predetermined value (usually between 0.2 and 0.3), the sifting process is stopped and h_{1k} is called the first IMF component (c_1) of the signal:

$$c_1 = h_{1k} \qquad\qquad (5\text{-}4)$$
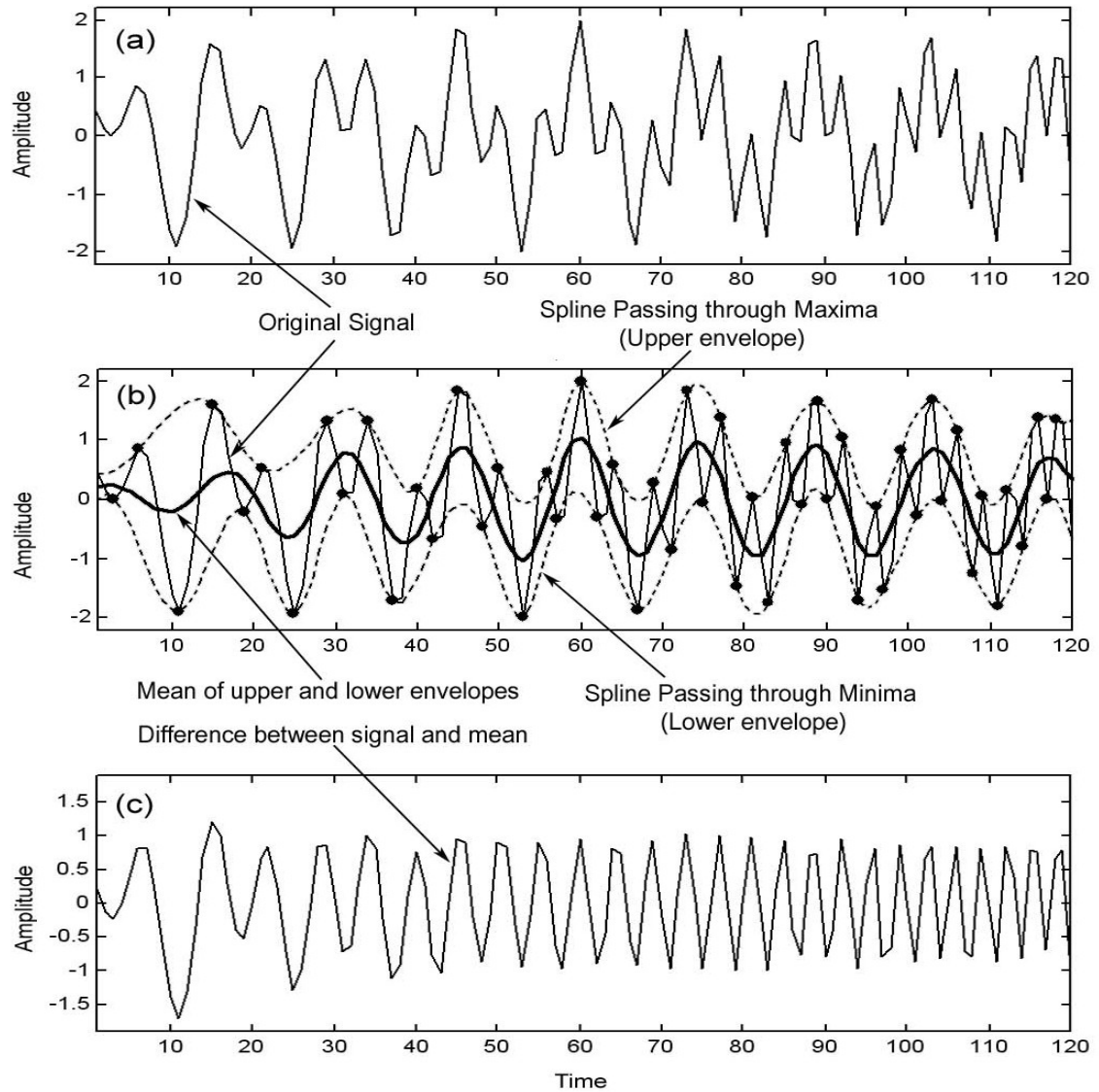
Figure 5-1 A schematic representation of one sifting cycle **a)** The original signal **b)** The signal in thin solid line; the upper and lower envelopes in dot-dashed lines; the mean in thick solid line **c)** The difference between the signal and mean (adapted from Rezaei and Taheri, 2009).

The first IMF component, c_1, contains the finest scale or the shortest period component of the signal. To derive other IMFs, the first component is removed from the signal:

$$r_1 = x(t) - c_1 \qquad\qquad (5\text{-}5)$$

The residual, r_1, contains the larger scales or longer period components. Then, the residual is considered as the new signal and the sifting process is performed on it to obtain the second IMF component. This procedure is repeated for all subsequent residuals to derive the longer period components. At each repetition the signal is modified with respect to the obtained IMF as following:

$$r_n = r_{n-1} - c_n \qquad (5\text{-}6)$$

After extracting all IMFs, the original signal is decomposed into n empirical modes and a residue, r_n, which can be either the mean trend or a constant, as mathematically represented by:

$$X(t) = \sum_{i=1}^{n} c_i + r_n \qquad (5\text{-}7)$$

5.5 EMD ENERGY DAMAGE INDEX

The research documented in the following paper used the novel structural health monitoring method introduced in 2005 by Cheraghi et al. (2005). This method is based on the HHT and is called the Empirical Mode Decomposition Energy Damage Index (EMD-EDI). The EMD-EDI is based on the energy of certain IMFs of the vibration signals.

In this method, once the dynamic characteristics of a healthy structure during free vibration are collected through sensors, the acquired signals are then passed through a band-pass filter to ensure the existence of the first natural frequency within the data. This is followed by the extraction of a specific IMF though Empirical Mode Decomposition. Subsequently, the energy of the IMF, for each sensor, is established by:

$$E = \int_{0}^{t_0} (IMF)^2 dt \qquad (5\text{-}8)$$

The above procedure is then repeated for the same structure during its damaged state to once again determine the energy of each signal's first IMF. The last step is the application of the EMD-EDI is to the extracted IMF energy of each sensor's signal:

$$EME - EDI = \left| \frac{E_{Healthy} - E_{Damaged}}{E_{Healthy}} \right| x100 \tag{5-9}$$

The above damage index provides the percentage difference in the structure's energy in its healthy and damage states. Once the EMD-EDI is calculated for each sensor, the existence and severity of the damage may be determined by relative comparison of the indices: high index values reveal the existence of damage close to the respective sensors.

In summary, the methodology followed in the experiment documented herein is as follows which is also illustrated in the following flow chart (Figure 5-2):

Step 1: Monitor the vibration of a system in its healthy state using the response of sensors within the system.

Step 2: Once again, monitor the vibration of the system in its damaged state using the responses of sensors within the system.

Step 3: Analyze the signals and evaluate the EMD-EDI; which is based on the variation of IMF energy between the healthy and damage system states.

Step 4: Establish whether damage exists based on the comparison of the EMD-EDIs evaluated in the last step.
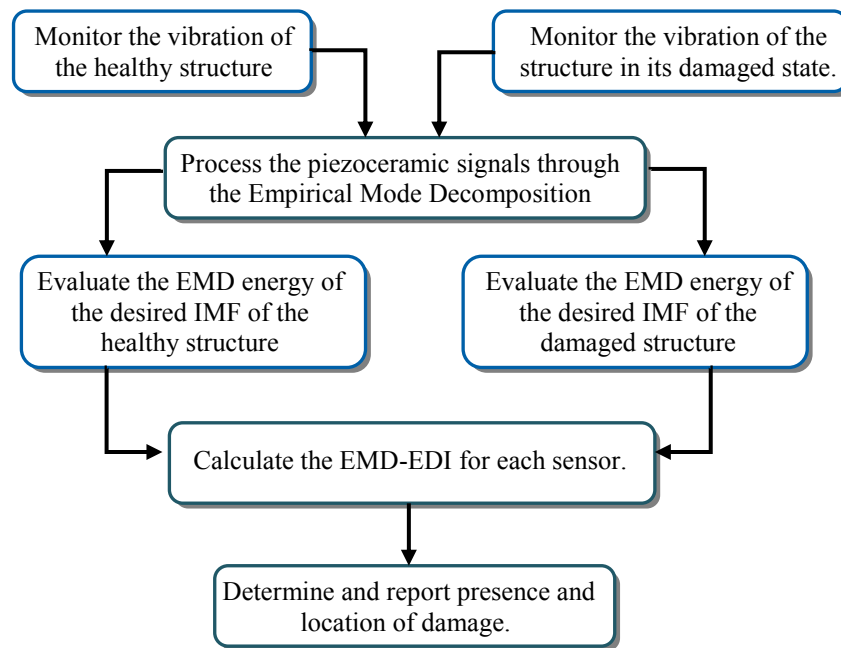
Figure 5-2 Damage detection methodology (adapted from Rezaei and Taheri, 2009).

5.6 EXPERIMENTAL SET-UP

The test specimen used in this study was an ANSI/ASME compliant (1985) standard steel pipe commonly used in oil and gas pipelines. The specifications of the schedule 40 SA106 Grade B pipe, with a nominal pipe size of six, are listed in Table 5-1. An overview of the experimental set-up is illustrated in Figure 5-3. As shown, the jointed pipe is suspended from either end with nylon rope from two steel saw horses. To comply with normal operating pressures in oil and gas pipelines, the pipe joint system was loaded with an internal water pressure of 10 MPa during all testing. The internal pressure of 10 MPa was attained through use of a GDS Instruments Limited 125 MPa High Pressure Controller, depicted in Figure 5-3.

Table 5-1 ANSI/ASME pipe dimensions and material properties.

Length	4.036	m	Density	7850	kg/m^3
Outer Diameter	168.3	mm	E	200	GPa
Wall Thickness	7.10	mm	v	0.3	

For the bolted joint, ASTM and ASME/ANSI compliant forged steel flanges were chosen of the following type: NPS: 6, class: 600, raised face, slip on, and material type A105N. The spiral wound metallic gaskets used were NPS: 6, class: 300, and style WRI 304-GRI 304 IR. SAE Grade 8 UNC hex head bolts were used (25.4 mm by 152.4 mm) with corresponding sized nuts, and grade 8 flat washers as well as lock washers.

To create the mechanical joint in the pipe, the pipe was cut in two approximately equal lengths, 2019 mm (left half) and 2016 mm (right half), and the two flanges were welded onto the pipe. The flanges were continuously welded to the pipe on the inside of the joint with a small overlap over the pipe edge of approximately 13 mm, and were also continuously welded to the pipe on the outside of the joint. The ends of the pipe were sealed using square steel plates shown in Figure 5-4. The plates (176 mm by 176 mm by 13 mm) were welded to the outside of the pipe.

For this specific joint configuration, the maximum bolt torque was determined to be 786 N-m. This value was calculated using the ASME - International Boiler and Pressure Vessel Code by the gasket manufacturer. Before bolting, the bolts and nut faces were

Figure 5-3 Experimental set-up overview.
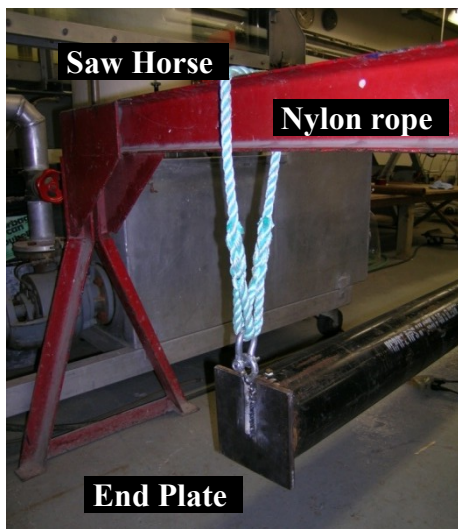
a)
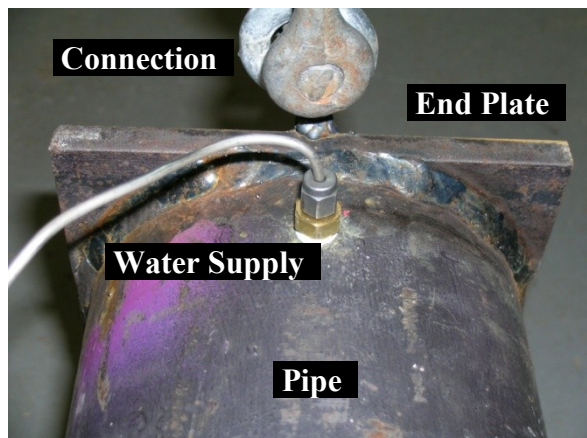
b)

Figure 5-4 a) Boundary condition **b)** Pressure connection.

lubricated using anti-seize lubricant manufactured by Permatex (Milton, Ontario). The procedure to tighten the bolts was the industry standard, which followed a criss-cross pattern across the face of the flange following the bolt numbering in Figure 5-5. Multiple passes had to be completed at increments of 30%, 60% and then 100% of the maximum torque for the joint.

For this joint, the magnitudes of these increments are listed in Table 5-2. The last step is tightening the bolts in a clockwise pattern to verify that every bolt is at the maximum torque. The joint was tightened using a torque wrench.
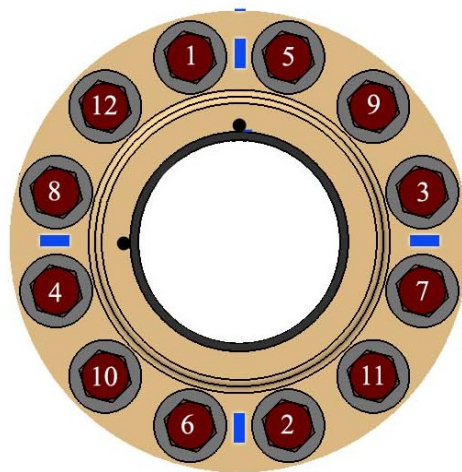
Figure 5-5 Bolt sequence.

Table 5-2 Torque increments.

30% of Maximum	236	N-m
60% of Maximum	472	N-m
100% of Maximum	786	N-m

In order to tighten the joint, the two halves were first bolted together to a hand-tight condition on the ground, with the pipes supported by blocks of wood. Subsequently, a forklift was used to set them on two sawhorses after which the joint was tightened using the procedure outlined above. It may also be of some importance, considering the symmetry of the joint, that the bolts were always fastened so that the bolt heads lay on the same side as the impact locations A and S, as shown in Figure 5-6.

The piezoceramic sensors used for the entirety of the experimental testing were of type PZT-5H, extracted from 72.4 × 72.4 mm sheets available from Piezo Systems Inc. (Cambridge, MA). The dimensions of the sensors are listed in Table 5-3.

Table 5-3 Piezoceramic sensor dimensions

Length	24.0	mm
Width	10.0	mm
Thickness	1.0	mm

Due to the small width of the sensors, fitting them to the curvature of the pipe's surface did not pose a problem. The material properties of the sensors (obtained from the manufacturer) are described using the following matrices. The density of PZT-5H is 7500 kg/m^3.

$$s^E \left[\frac{m^2}{N}\right] = (10^{-12}) \begin{bmatrix} 16.5 & -4.78 & -8.45 & 0 & 0 & 0 \\ -4.78 & 16.5 & -8.45 & 0 & 0 & 0 \\ -8.45 & -8.45 & 20.7 & 0 & 0 & 0 \\ 0 & 0 & 0 & 43.5 & 0 & 0 \\ 0 & 0 & 0 & 0 & 43.5 & 0 \\ 0 & 0 & 0 & 0 & 0 & 42.6 \end{bmatrix}$$

$$d \left[\frac{C}{N}\right] = (10^{-12}) \begin{bmatrix} 0 & 0 & 0 & 0 & 741 & 0 \\ 0 & 0 & 0 & 741 & 0 & 0 \\ -274 & -274 & 593 & 0 & 0 & 0 \end{bmatrix} ;$$

$$\varepsilon^T [F/m] = (10^{-9}) \begin{bmatrix} 27.7 & 0 & 0 \\ 0 & 27.7 & 0 \\ 0 & 0 & 30.1 \end{bmatrix}$$

where S_E is the compliance matrix, d is the piezoelectric coupling matrix, and ε^S is the permittivity of the piezoceramic. The piezoceramic sheets were polarized through the thickness allowing the sensors to be created by soldering two electrodes to the top and bottom surfaces of each piece cut from the piezoceramic sheet. However, soldering caused each sensor to have an uneven surface which prevented complete contact between the pipe surface and the sensor. Consequently, a steel shim of size 25.0 × 10.0 × 0.5 mm was used as an adapter. Each adapter plate had a small semi-circular hole cut at the edge

to fit around the solder. Placing the adapter plate between the sensor and the pipe surface allowed for increased contact.

Before a sensor was attached, the surface of the pipe was scoured using silicon-carbide paper and the pipe surface, sensor and adapter plate were wiped clean of dust and oil with isopropyl alcohol. The preparation, resulting in clean and rough surfaces, permitted the achievement of a stronger bond. The piezoceramic sensors were subsequently adhered to the adapters and the adapters to the pipe using a two part epoxy, Araldite 2011 (Huntsman Advanced Materials Americas Inc., Los Angeles, CA). The sensors were secured to the pipe by using masking tape, and left to cure for twelve hours to create a strong bond. Figure 5-6 (a) shows a typical sensor attached to the pipe.

a)   b)
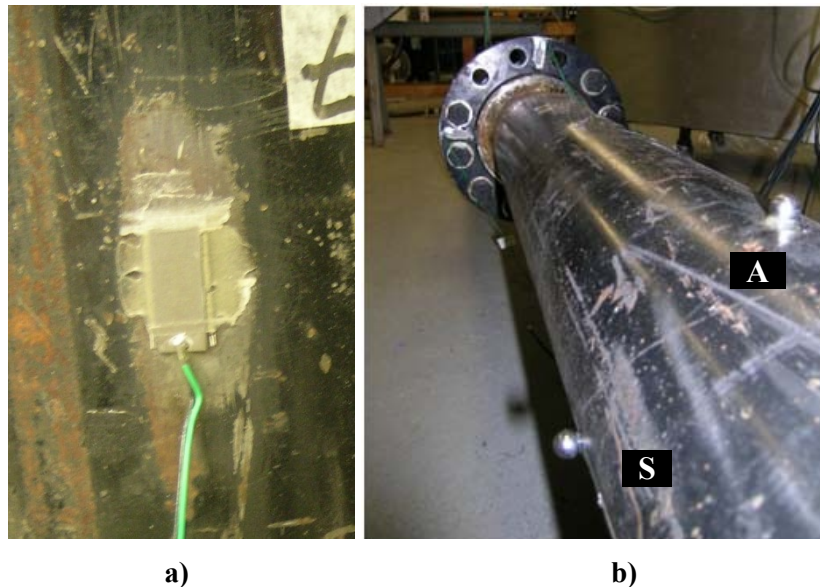
Figure 5-6 a) Typical bonded piezoceramic sensor **b)** Impact locations.

The set-up for the completion of the damage detection was accomplished as follows, as shown in Figure 5-7. Two impact locations were chosen for testing, Locations A and S, respectively situated on the apex of the pipe and the side of the pipe (see Figure 5-6 (b)). In order to ensure consistency of the impact location, a steel ball measuring 12.7 mm in diameter was attached at each of the impact locations to provide a target. The impact balls were attached to the pipe using the same epoxy as the sensors. These impact locations were chosen in an effort to determine the differences, if any, between impacts around the circumference of the pipe.

Six piezoceramic sensors were attached to the pipe and flange. The placement and numbering of the sensors is illustrated in a cross-section of the pipe in Figure 5-8.

All dimensions in millimeters
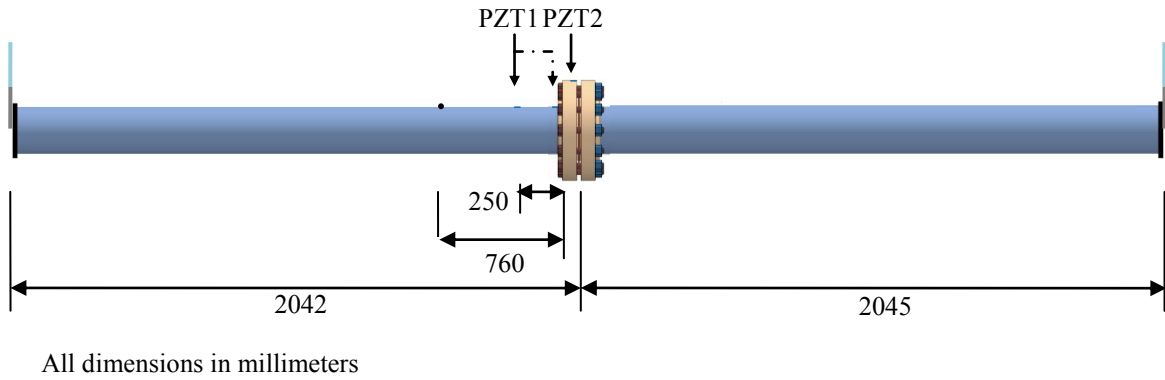
Figure 5-7 Experimental set-up.
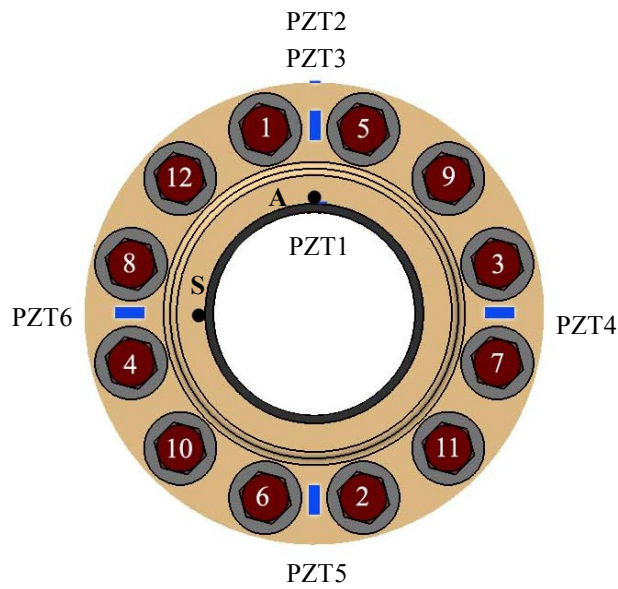
Figure 5-8 PZT arrangement.

To monitor the flange vibrations, four piezoceramic sensors, PZT3 through PZT6, were placed on one flange face at the locations of 12, 3, 6 and 9 o'clock. An additional sensor, PZT2, was placed on top of the flange, directly above PZT3. To monitor the pipe vibrations initially, the remaining piezoceramic sensor, PZT1, was placed on the pipe at a distance of 250 mm measured from the center of the sensor to the outside of the closest flange (Figure 5-7). This sensor set-up was utilized for only the first damage scenario as

110

described in Table 5-4. Due to the low amplitudes of the resulting EMD-EDI, the placement of PZT1 was altered for the remaining three damage scenarios. PZT1 was consequently placed directly at the base of the weld connecting the flange and pipe as illustrated in Figure 5-7 and Figure 5-9.

The placement and numbering of all the sensors is illustrated in Figure 5-9. The sensor locations were chosen so that a comparison might be made between those results from on the pipe and on the flange, as well as between the different sensors located on the flange face.
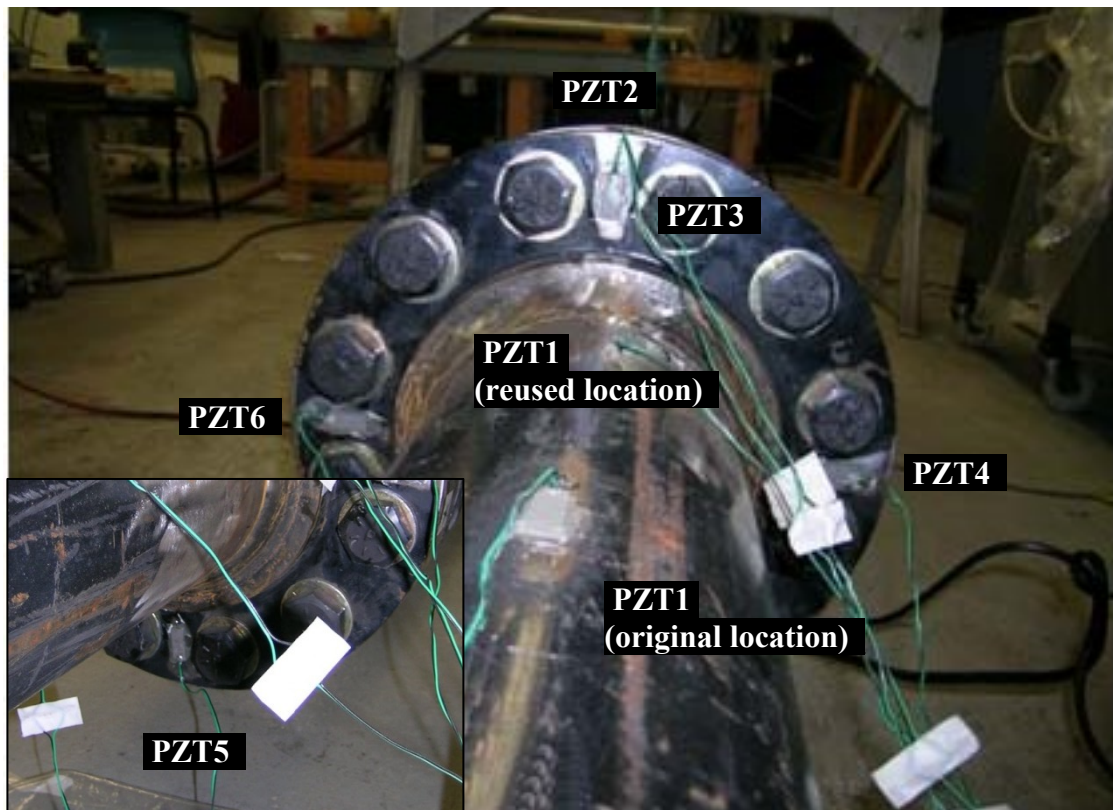
Figure 5-9 Piezoceramic arrangement.

5.7 EXPERIMENTAL TESTING & ANALYSIS

To create free vibration in the system, the pipe was excited using a piezoelectric impulse hammer (model 5800B5, Dytran Instrument Inc., Chatsworth, CA) outfitted with an aluminum tip, which can excite frequencies up to 5 kHz. The hammer outputs an

analog voltage which is representative of the input impulse. A typical hammer impulse signal is depicted in Figure 5-10 (a).
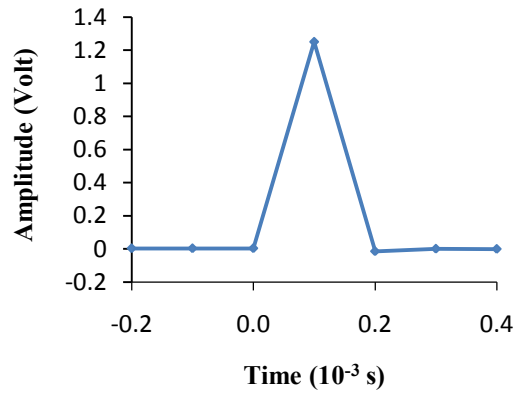
a)
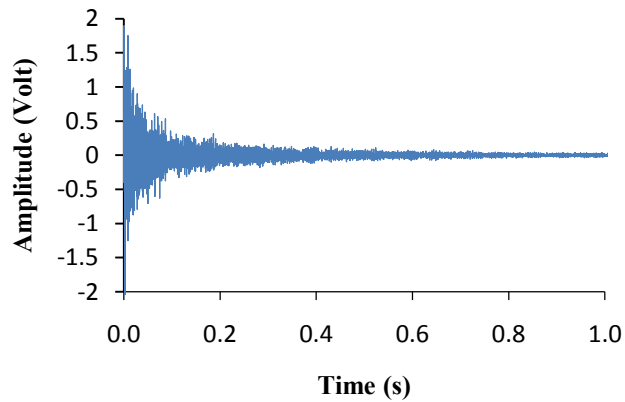
b)

Figure 5-10 a) Typical impulse hammer signal **b)** Typical sensor response.

During vibration, the response of the impulse hammer and the sensors were simultaneously collected through two NI 9215 modules mounted on an NI cDAQ-9172 data acquisition chassis, manufactured by National Instruments Inc. (Austin, Texas, USA). With only eight data acquisition channels available, it was only possible to monitor the response of seven sensors concurrently, since the hammer signal was also required for analysis and required the eighth connector. All of the data for the experimental testing was recorded using a sampling frequency of 10 kHz. A typical

sensor response is depicted in Figure 5-10 (b). The data acquisition system is illustrated in Figure 5-11.
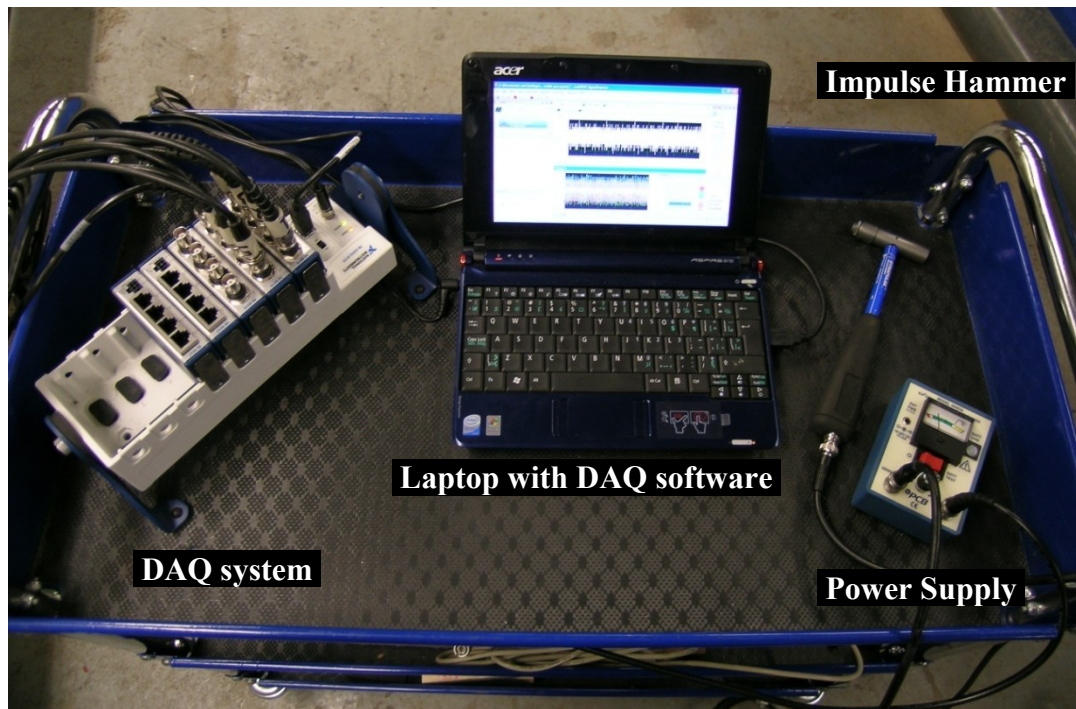
Figure 5-11 The data acquisition hardware**.**

Once the data was collected using the LABView software, the data for each impact was stored in an ASCII text file, which included the responses of all the sensors and the impulse hammer. Subsequently, the recorded signals from the healthy and damaged pipe joint were processed using a Matlab code, developed in house, which performed the Empirical Mode Decomposition.

This code was programmed to read the text file produced by the DAQ system and then process the response of all sensors simultaneously. The code removes unwanted data before impact, filters signal noise, compensates for any offset, normalizes the response of any sensor with respect to the hammer input force, applies a low-pass filter in order to have the first natural frequency in the filtered data, decomposes the signals based on the EMD method, derives the IMFs, and finally calculates the energy of the desired IMF for each sensor (EMD energy) (Rezaei and Taheri, 2009).

For each excitation, the vibration lasted for seconds before decaying to zero (see Figure 5-10 (b)). Because the EMD-EDI is based on the comparison of special features in the PZT signals before and after damage creation, there is no limitation for the choice of

113

signal duration as long as the same duration was used to evaluate both the healthy and damaged state signals (Rezaei and Taheri, 2009). With this in mind, an interval of 0.5 seconds was chosen for the signal processing.

The testing procedure used for the experiments followed the methodology outlined in Figure 5-2. Four different damage scenarios were completed, each having a healthy case and multiple damage cases. Table 5-4 lists the scenarios involving the healthy cases and damage cases investigated for each of the four scenarios.

Table 5-4 Damaged joint scenarios.

Scenario	State	Bolts Loosened	Damage Case
Scenario 1	Healthy Pipe		HC 1-1
	Damage Case 1-1	Bolt #5	DC 1-1
	Damage Case 1-2	Bolt #5 and Bolt #1	DC 1-2
	Damage Case 1-3	Bolts #5, #1 and #12	DC 1-3
	Damage Case 1-4	Bolts #5, #1, #12 and #9	DC 1-4
	Damage Case 1-5	Bolts #5, #1, #12, #9 and #8	DC 1-5
Scenario 2	Healthy Pipe		HC 2-1
	Damage Case 2-6	Bolt #2	DC 2-6
	Damage Case 2-7	Bolt #2 and Bolt #6	DC 2-7
	Damage Case 2-8	Bolts#2, #6 and #10	DC 2-8
Scenario 3	Healthy Pipe		HC 3-1
	Damage Case 3-9	Bolt #3	DC 3-9
	Damage Case 3-10	Bolt #3 and Bolt #7	DC 3-10
	Damage Case 3-11	Bolts#3, #7 and #9	DC 3-11
Scenario 4	Healthy Pipe		HC 4-1
	Damage Case 4-12	Bolt #11	DC 4-12
	Damage Case 4-13	Bolt #11 and Bolt #12	DC 4-13
	Damage Case 4-14	Bolts#11, #12 and #10	DC 4-14
	Damage Case 4-15	Bolts #11, #12, #10 and #9	DC 4-15
	Damage Case 4-16	Bolts #11, #12, #10, #9 and #6	DC 4-16
	Damage Case 4-17	Bolts #11, #12, #10, #9, #6 and #2	DC 4-17

For each scenario, once the vibration of the healthy system was collected and processed through the EMD, damage was introduced to the system and the vibration of the pipe was again monitored, collected and processed. Testing was halted when leakage occurred in the joint; therefore for each scenario, leakage occurred during the last damage case. Figure 5-12 is a schematic depicting the bolts included in the damage cases for each scenario.
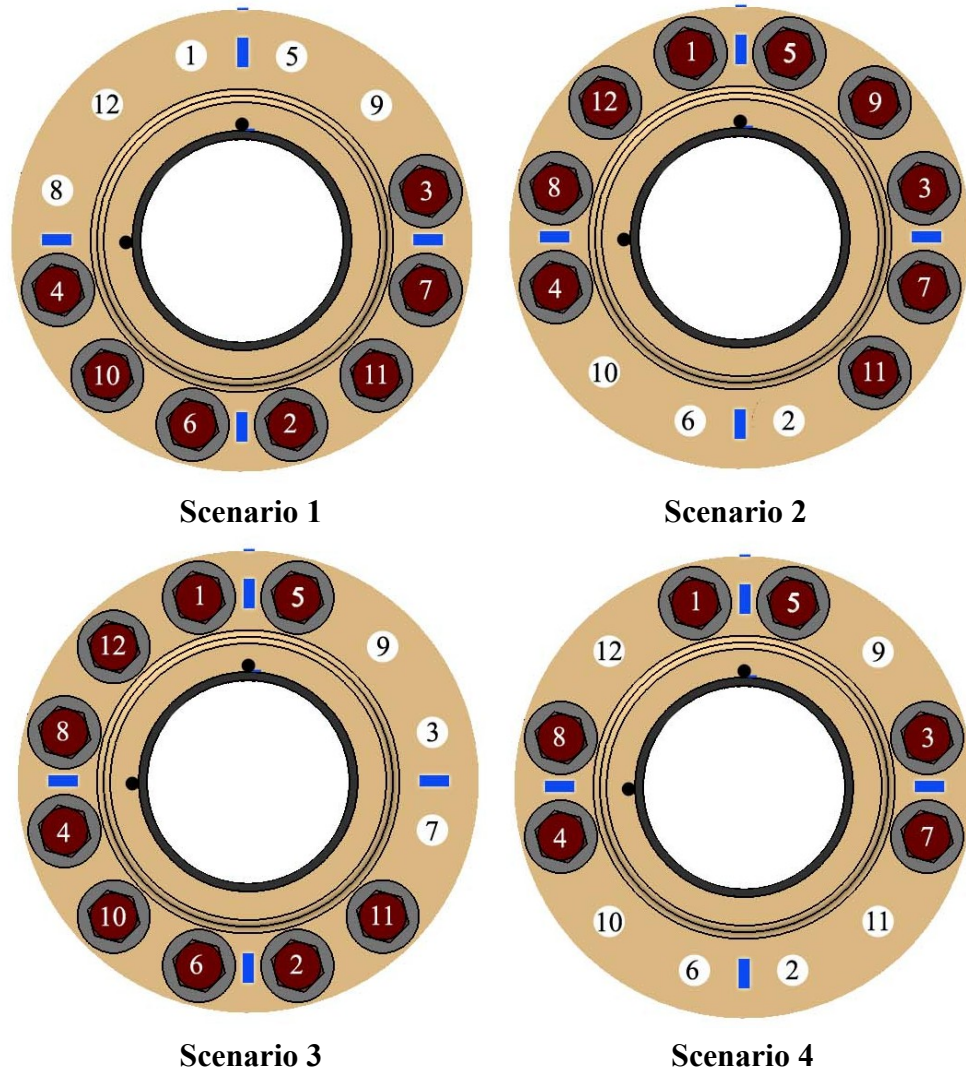
Figure 5-12 Damage scenarios.

In order to achieve consistent results, five impacts/data collections were completed for each of the two impact locations for each test case. Furthermore, each of the acquired

signals from the sensors was normalized based on the input (hammer) signal. The difference between the signals after normalization was considered to be a good measure of the repeatability of the impact procedure (Rezaei and Taheri, 2009).

To normalize the signals, the following procedure was followed (Rezaei and Taheri, 2009): The fast Fourier transform of each sensor response was divided by the fast Fourier transform of the hammer signal. Afterwards, the result was transferred to the time domain by the inverse fast Fourier Transform. Once the five impacts for each test case were processed and the IMF energies attained, their average was calculated to use for the EMD energy.

Once the EMD energy of both the healthy and damages cases was calculated, the EMD-EDI was calculated for each damage case.

5.8 RESULTS AND DISCUSSION

Cheraghi and Taheri (2007) suggested applying a band-pass filter to the data to keep only the first frequency component. However, in the experimental investigations carried out by Rezaei and Taheri (2009), it was concluded that this method only works well for systems where the first frequency is the dominant vibrating frequency of the structure. Otherwise, more frequency components should be included within the band-pass filter in order to avoid the elimination of damage sensitive frequency components.

By analyzing the data using different frequency bands, it was found that a low-pass filter with a pass-band frequency of 2000 Hz was one of the frequency ranges that provided the best resolution for identification of damage. The following graphs, (Figures 5-13 through 5-20) use the added EMD-EDI values of IMF1 and IMF2. The added IMFs gave better resolution than either IMF by itself. The other frequency ranges that yielded similar results are 0-1500 Hz and 500-2000 Hz for scenario 1, 0-1500 Hz and 500-2500 Hz for scenario 2, 0-1500 Hz and 1000-2500 Hz for scenario 3 and 0-2500 Hz and 500-2500 Hz for scenario 4. These pass-bands were chosen based on exhibition of damage progression as well as consideration of energy amplitude.

Scenario 1
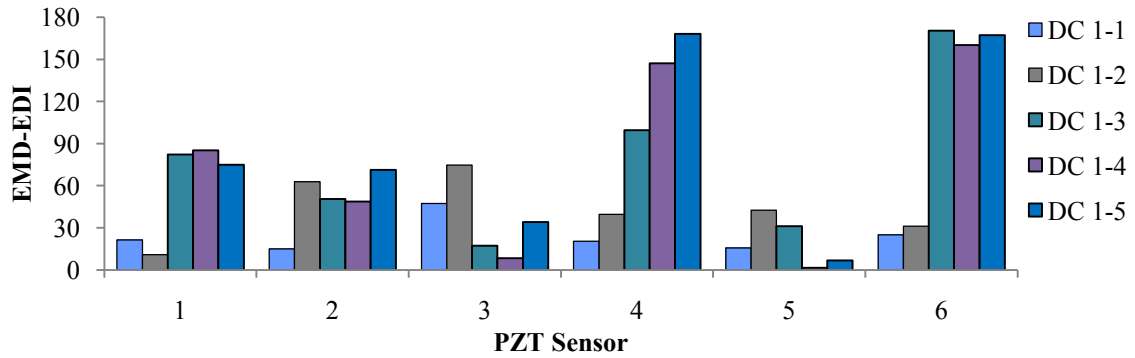
Figure 5-13 Damage scenario 1, 0-2000 Hz, impact location A, added IMFs.
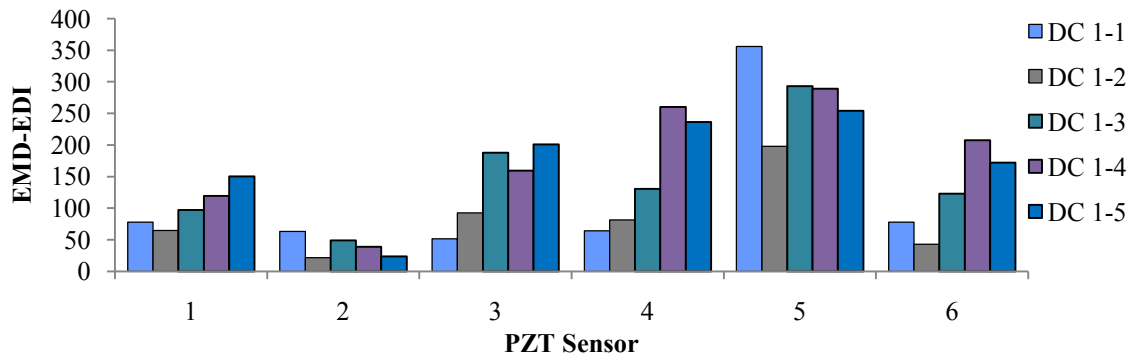
Figure 5-14 Damage scenario 1, 0-2000 Hz, impact location S, added IMFs.

Scenario 2
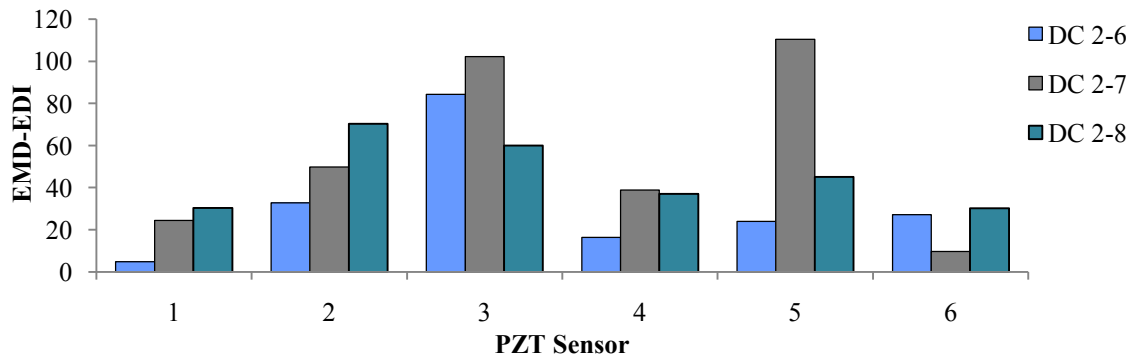
Figure 5-15 Damage scenario 2, 0-2000 Hz, impact location A, added IMFs.
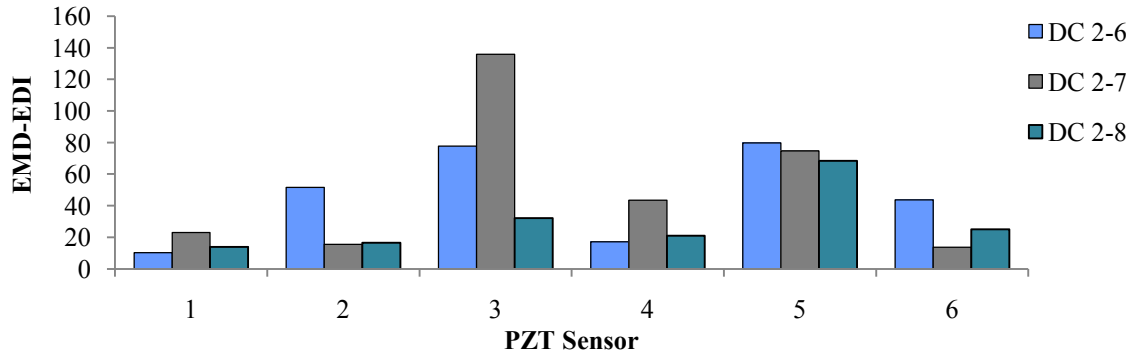
Figure 5-16 Damage scenario 2, 0-2000 Hz, impact location S, added IMFs.

Scenario 3
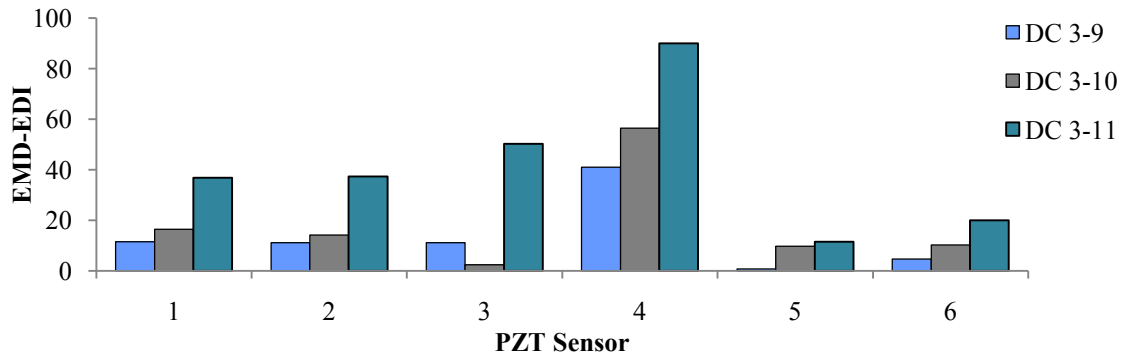
Figure 5-17 Damage scenario 3, 0-2000 Hz, impact location A, added IMFs.
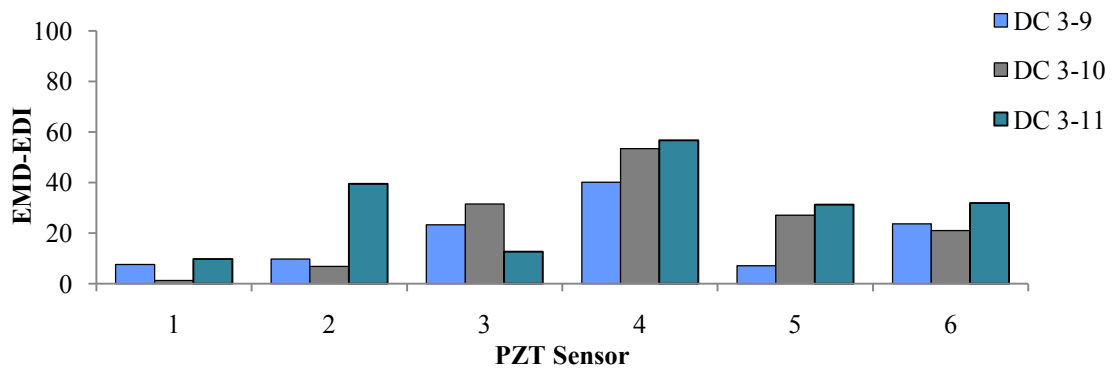
Figure 5-18 Damage scenario 3, 0-2000 Hz, impact location S, added IMFs.

Scenario 4
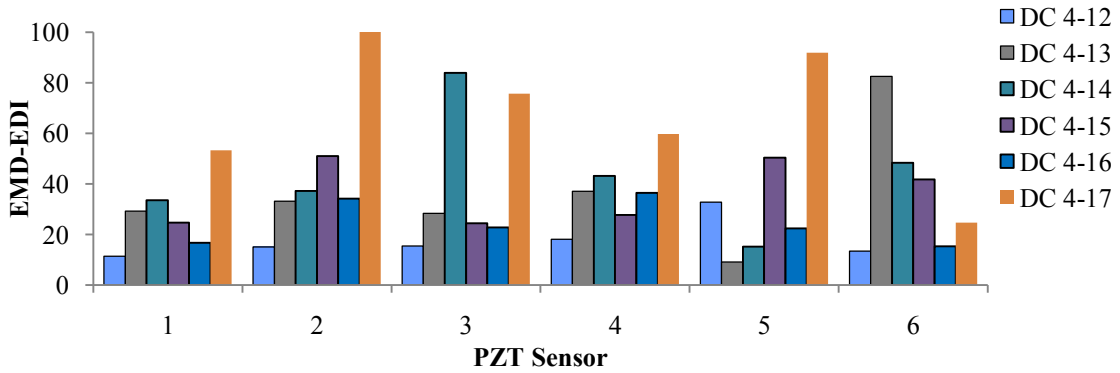
Figure 5-19 Damage scenario 4, 0-2000 Hz, impact location A, added IMFs.
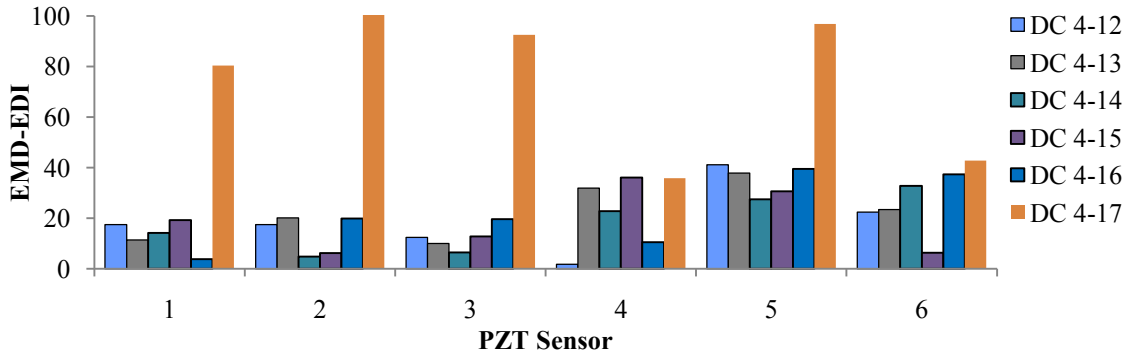
Figure 5-20 Damage scenario 4, 0-2000 Hz, impact location S, added IMFs.

From the above graphs, one can observe that the damage indices for impact location S, on the side of the pipe, are significantly greater for damage scenarios 1 and 2 which are located respectively on the top and bottom of the joint. Furthermore, for scenario 1 and 4, both impact locations demonstrate similar damage progression detection whereas for scenarios 2 and 3, the results from impacting the pipe at Location A deliver improved damage progression detection.

5.9 CONCLUSIONS

The objective of this study was to experimentally confirm the use of the EMD-EDI for the evaluation of the damaged condition of a pressurized steel pipeline with a 12-bolt flanged joint. The EMD-EDI is based on the theory that IMFs, decomposed from a vibration signal, contain damage sensitive features. The damage sensitive feature used by

the EMD-EDI is the variation in the EMD energy of an IMF prior to and following the occurrence of damage in a system. Four damage scenarios were analyzed, with each damage scenario progressing from a healthy state to having multiple bolts completely loose.

This experimental study demonstrated that the EMD-EDI can successfully detect the presence of damage in bolted pipeline joints. The results indicated inconsistency in the progression of damage detection. However, it is believed that at least some of this inconsistency is due to the variability inherent in using a hand held impulse hammer. Further work is currently being conducted using an electric hammer which provides consistent impacts. It is also important to note that sensor placement and impact locations have a significant influence on the results. As such, further work is required to understand the most efficient location choices. Furthermore, it is important to note that the band-pass filter used for signal filtering should be applied carefully to avoid filtering out frequency components that contain meaningful information.

5.10 ACKNOWLEDGEMENTS

5.11 REFERENCES

ANSI/ASME. (1985). *ANSI / ASME B36.19M-1985 - american national standard for welded and seamless wrought steel pipe* ANSI/ASME.

Carden, E., & Fanning, P. (2004). Vibration based condition monitoring: A review. *Structural Health Monitoring, 3*(4), 355-377.

Cheraghi, N., Riley, M. J., & & Taheri, F. (2005). A novel approach for detection of damage in adhesively bonded joints in plastic pipes based on vibration methods using piezoelectric sensors. In *Proceedings of the IEEE International Conference on Systems, Man and Cybernetics,* Hawaii, USA, 10-12 Oct., pp. 3472-3478.

Cheraghi, N., & Taheri, F. (2008). Application of the empirical mode decomposition for system identification and structural health monitoring. *International J. of Applied Mathematics and Engineering Sciences, 2*(1), 61-72.

Cheraghi, N., & Taheri, F. (2007). A damage index for structural health monitoring based on the empirical mode decomposition. *J. of Mechanics of Materials and Structures, 2*(1), 43-62.

Corbett, R. (1998). Stretch control. In *Handbook of bolts and bolted joints,* J. H. Bickford, & S. Nassar (Eds.), (pp. 571). Marcel Dekker, Inc.: New York.

Doebling, S. W., Farrar, C. R., Prime, M. B., & Shevitz, D. W. (1996). *Damage identification and health monitoring of structural and mechanical systems from changes in their vibration characteristics: A literature review.* Report No. LA-13070-MS, Los Alamos National Laboratory.

Doebling, S. W., Farrar, C. R., & Prime, M. B. (1998). A summary review of vibration-based damage identification methods. *The Shock and Vibration Digest, 30*(2), 91-105.

Energy Institute (Great Britain). (2007). *Guidelines for the management of the integrity of bolted joints for pressurised systems.* (2nd ed.). Energy Institute: London.

Fasel, T., Kennel, M., Todd, M., Clayton, E., & Park, G. (2009). Damage state evaluation of experimental and simulated bolted joints using chaotic ultrasonic waves. *Smart Structures and Systems, 5*(4), 329-344.

Hess, D. P. (1998). Vibration and shock induced loosening. In *Handbook of bolts and bolted joints,* J. H. Bickford, & S. Nassar (Eds.), (pp. 757). Marcel Dekker, Inc.: New York.

Huang, N. E., Shen, Z., Long, S. R., Wu, M. C., Shih, H. H., Zheng, Q., Nai-Chyuan, Y., Tung, C. C., & Liu, H. H. (1998). The empirical mode decomposition and the hilbert spectrum for nonlinear and non-stationary time series analysis. *Philosophical Transactions of the Royal Society A: Mathematical, Physical and Engineering Sciences, 454*(1971), 903-995.

Industrial Fasteners Institute: Division VI Aerospace Fasteners. (1995). *Test application handbook relating to mechanical fasteners*. Industrial Fasteners Institute: Cleveland, Ohio.

Johnson, E. A., Lam, H. F., Katafygiotis, L. S., & Beck, J. L. (2004). Phase I IASC-ASCE structural health monitoring benchmark problem using simulated data. *Journal of Engineering Mechanics, 130*(1), 3-15.

Loutridis, S. (2004). Damage detection in gear systems using empirical mode decomposition. *Engineering Structures, 26*(12), 1833-1841.

Michaelides, P. G., & Fassois, S. D. (2008). Damage detection and localization in the joints of a thin plate via a statistical power spectral density based method. In *Proceedings of the 4th European Workshop on Structural Health Monitoring,* Krakow, Poland, July, 937-944.

Nichols, J. M. (2003). Using state space predictive modeling with chaotic interrogation in detecting joint preload loss in a frame structure experiment. *Smart Materials Structures, 12*(4), 580-601.

Pai, N. G., & Hess, D. P. (2002). Three-dimensional finite element analysis of threaded fastener loosening due to dynamic shear load. *Engineering Failure Analysis, 9*(4), 383-402. Retrieved from http://dx.doi.org/10.1016/S1350-6307(01)00024-3

Park, G., & Inman, D. J. (2005). Impedance-based structural health monitoring. In *Damage prognosis for aerospace, civil and mechanical systems,* D. J. Inman, C. R. Farrar, V. Lopes Jr. & V. Steffen Jr. (Eds.), (pp. 275). John Wiley and Sons, Ltd.: Great Britain.

Park, G., Muntges, D. E., & Inman, D. J. (2003). Self-repairing joints employing shape-memory alloy actuators. *Journal of the Minerals, Metals and Materials Society, 55*(12), 33-37.

Peairs, D. M., Park, G., & Inman, D. J. (2004). Improving accessibility of the impedance-based structural health monitoring method. *Journal of Intelligent Material Systems and Structures, 15*(2), 129-140. Retrieved from http://dx.doi.org/10.1177/1045389X04039914

Pines, D., & Salvino, L. (2006). Structural health monitoring using empirical mode decomposition and the hilbert phase. *Journal of Sound and Vibration, 294*(1-2), 97-124.

Rezaei, D., & Taheri, F. (2010). Health monitoring of pipeline girth weld using empirical mode decomposition. *Smart Materials and Structures, 19*(5).

Rezaei, D., & Taheri, F. (2009). Experimental validation of a novel structural damage detection method based on empirical mode decomposition. *Smart Materials and Structures, 18*(4).

Ritdumrongkul, S., Abe, M., Fujino, Y., & Miyashita, T. (2004). Quantitative health monitoring of bolted joints using a piezoceramic actuator-sensor. *Smart Materials and Structures, 13*(1), 20-29.

Ritdumrongkul, S., & Fujino, Y. (2006). Identification of the location and level of damage in multiple-bolted-joint structures by PZT actuator-sensors. *Journal of Structural Engineering, 132*(2), 304-311.

Shi, Z. (2000). Structural damage detection from modal strain energy change. *Journal of Engineering Mechanics, 126*(12), 1216-1223.

Todd, M., Erickson, K., Chang, L., Lee, K., & Nichols, J. (2004). Using chaotic interrogation and attractor nonlinear cross-prediction error to detect fastener preload loss in an aluminum frame. *Chaos, 14*(2), 387-399. doi:10.1063/1.1688091

Todd, M. D., Nichols, J. M., Nichols, C. J., & Virgin, L. N. (2004). An assessment of modal property effectiveness in detecting bolted joint degradation: Theory and experiment. *Journal of Sound and Vibration, 275*(3-5), 1113-1126. Retrieved from http://dx.doi.org/10.1016/j.jsv.2003.10.037

Yan, Y., Cheng, L., Wu, Z., & Yam, L. (2007). Development in vibration-based structural damage detection technique. *Mechanical Systems and Signal Processing, 21*(5), 2198-2211.

CHAPTER 6

DAMAGE DETECTION OF A PVC PIPELINE JOINT

The following chapter details the experimental tests performed on two PVC pipes jointed together using an 8-bolt flanged joint. Two boundary conditions were investigated: free-free and cantilevered. An overview of the experimental set-up is shown in Figure 6-1. The objective of this study was to validate the effectiveness of using the EMD-EDI to detect various degrees of joint damage with a type of material able to provide a greater damping effect than steel. It was also decided to explore the effect of different boundary conditions on the results. Varying degrees of joint damage were simulated by removing bolts.

a)   b)

Figure 6-1 Overview of experimental set-up **a)** Free-free boundary condition **b)** Cantilevered boundary condition.

6.1 EXPERIMENTAL SET-UP

The test specimen used in this study was a PVC pipe manufactured by IPEX (Ipex Inc., 2010) commonly used for applications such as industrial and process piping, pulp and paper, food processing, water and sewage treatment, and irrigation. The specifications of the 150 mm nominal pipe are listed in Table 6-1. A total pipe length of 4.6 m was chosen so as to conform to the previous experimental research performed thus far.

Table 6-1 PVC pipe dimensions and material properties.

Length	4.6	m	Density	1420	kg/m^3
Outer Diameter	168.3	mm	E	2.758	GPa
Wall Thickness	7.1	mm	v	0.38	

Flat faced, schedule 80 IPEX Vanstone socket PVC flanges were chosen in conjunction with full faced neoprene gaskets. Correspondingly the gaskets had an NPS of 6 and were 1/8 inches thick. SAE Grade 5 UNC hex head bolts were used (19.0 mm by 102 mm) with corresponding sized nuts, and flat washers. The fasteners used were the same as the fasteners used for the experiments on the 8-bolt joint in Chapter 3 except that no spring washers were used. To create the mechanical joint in the pipe, the pipe was cut in two approximately equal pieces of 2315 mm (left half) and 2291 mm (right half) (depicted in Figure 6-5 and 6-6). Subsequently, the two flanges were attached to the pipe using solvent welding using IPEX primer (Xirtec 7) and PVC cement (Xirtec 11).

Concerning the boundary conditions, two different boundary conditions were tested for the two damage scenarios detailed in the testing section. First, the pipe was suspended from saw horses using a nylon rope at either end, as shown in Figure 6-2. The nylon ropes were positioned at the mid-point along the beam of the saw horse. The second boundary condition consisted of the pipe being cantilevered off the edge of a platform, shown in Figure 6-3.

Figure 6-2 Free-free boundary condition.

Figure 6-3 Cantilevered boundary condition.

For this specific joint configuration, the maximum bolt torque was determined to be 67.8 N-m. This value was given in the manual of the joint and pipe manufacturer (Ipex Inc., 2010). Before bolting, the bolts and nut faces were lubricated using the Anti-seize lubricant manufactured by Permatex (Milton, Ontario).

The procedure to tighten the bolts was the industry standard, which follows a criss-cross pattern across the face of the flange following the bolt numbering in Figure 6-4. Multiple passes should be completed at increments of 30%, 60% and then 100% of the

maximum torque for the joint. For this joint, the magnitudes of these increments are listed in Table 6-2. The last step to tightening the joint is to go around the joint clockwise and verify that every bolt is at the maximum torque. The joint was tightened using a torque wrench.
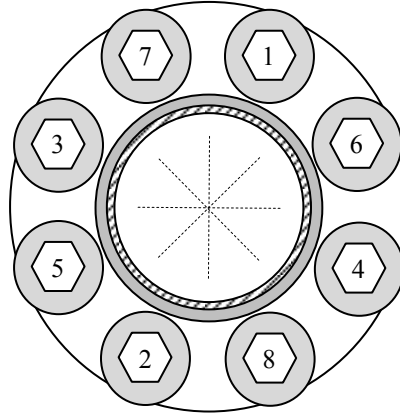
Figure 6-4 Bolt numbering.

Table 6-2 Torque increments.

30% of Maximum	20.3	N-m
60% of Maximum	40.7	N-m
100% of Maximum	67.8	N-m

It may also be of some importance, considering the symmetry of the joint, that the bolts were always fastened so that the bolt heads lay on the same side as the impact location.

The piezoceramic sensors used to monitor the dynamic response of the systems were of the same type and dimensions as used in the previous experiments. The dimensions of the sensors are listed in Table 3-3.

The set-up for the completion of the damage detection was accomplished as follows and may be seen in Figure 6-5 and Figure 6-6. Only one impact location was chosen for testing, located 280 mm from the edge of the flange socket. In order to maintain consistency between impacts, a steel ball measuring 12.7 mm in diameter was placed at the impact location to provide a consistent impact target. The impact ball, illustrated in Figure 6-7, was attached to the pipe using the same epoxy as for the sensors.
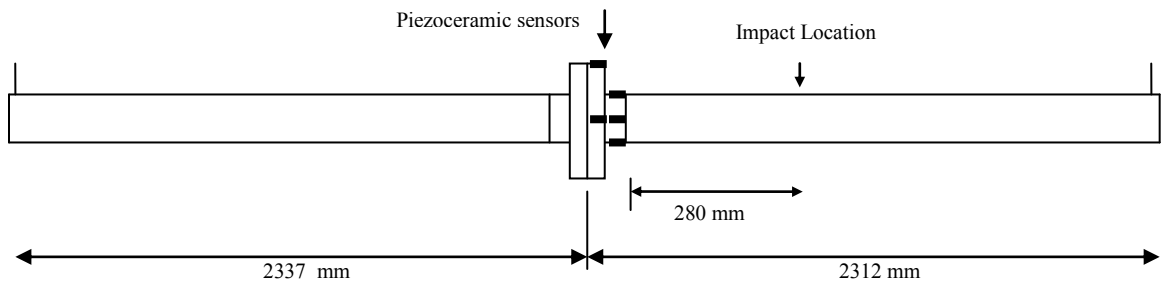
Figure 6-5 Free-free experimental set-up.
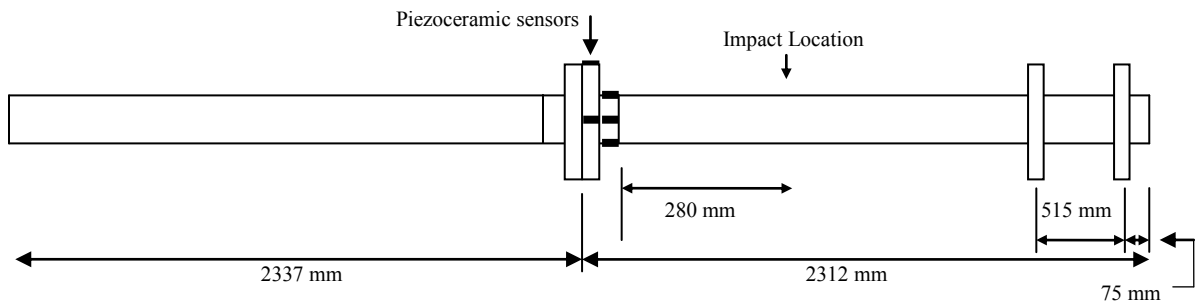
Figure 6-6 Cantilevered experimental set-up.

Figure 6-7 Impact location.

To monitor the system vibrations, seven new piezoceramic sensors were created and attached to the pipe and flange. Four piezoceramic sensors, PZT1 through PZT4, were placed on the flange socket at 0°, 90°, 180° and 270°. The sensors were placed at a

distance of 12.7 mm from the socket edge to the edge of the sensor. The three remaining sensors were placed on top of the flange, directly above PZT1, PZT2 and PZT4. The placement of the sensors along the pipe is shown in Figure 6-5 Figure 6-6. The placement and numbering of the sensors is illustrated in a cross-section of the pipe in Figure 6-8, and in a photograph in Figure 6-9. The sensor locations were chosen so that a comparison might be made between those results from on the pipe and on the flange, as well between the results from different areas around the flange edge.
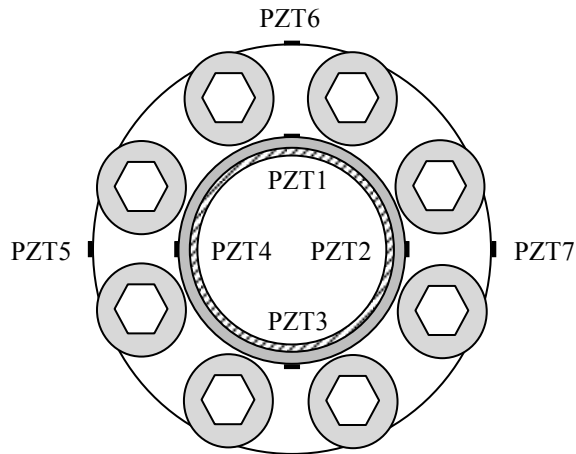
Figure 6-8 PZT sensor placement and numbering.
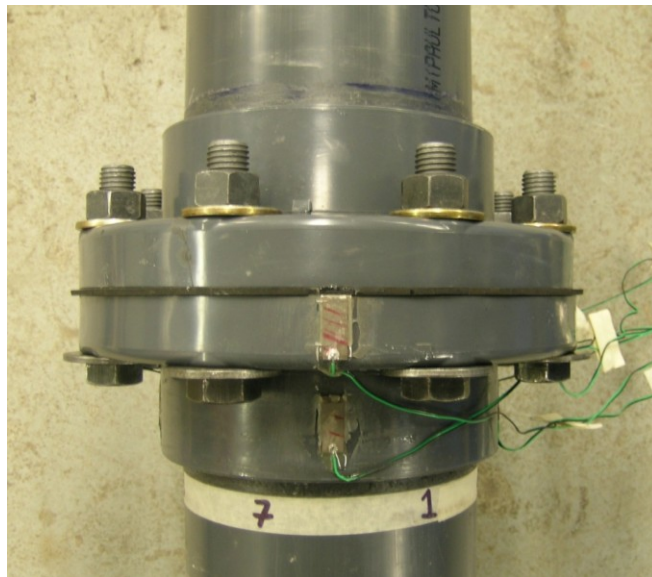
Figure 6-9 Sensor placement.

6.2 TESTING

The experimental set-up used the same data acquisition hardware and software as described in Chapter 5. A typical hammer impulse signal is depicted in Figure 6-10 (a). A typical sensor response is depicted in Figure 6-10 (b).
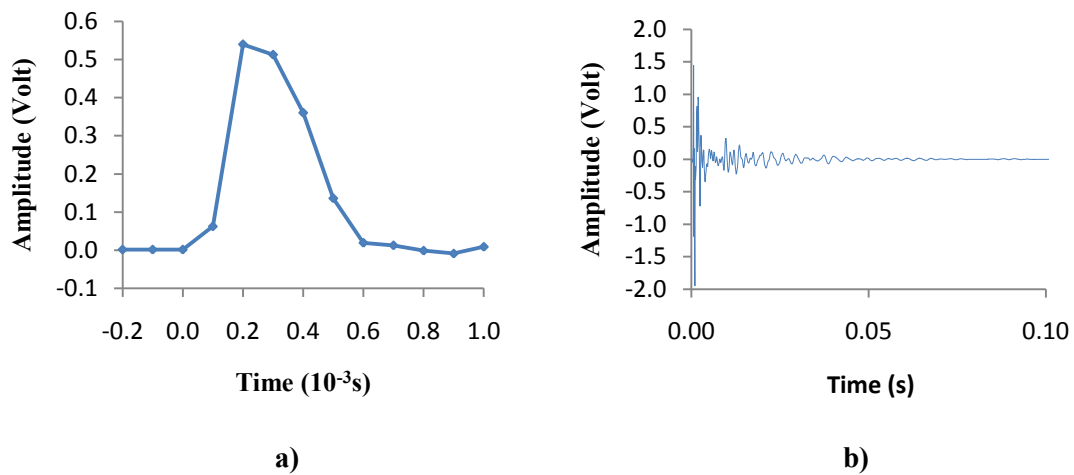
Figure 6-10 a) Typical impulse hammer signal **b)** Typical sensor response.

Two different damage scenarios were completed, each having a healthy case and multiple damage cases. Each of these damage scenarios was completed for the two different boundary conditions. The aluminum hammer tip was used for all scenarios. Seven impacts were completed for each impact location for all cases. According to the earlier experiments, seven impacts were chosen due to the probability being low that additional impacts would be necessary due to a lack of impact consistency. A list of all test cases considered is shown in Table 6-3.

Figure 6-11 is a schematic depicting the bolts included in the damage scenarios listed above. For each damage case, the indicated bolt was completely removed from the joint. An additional healthy case (HC 3-1) was also completed for each boundary condition for comparison purposes to investigate healthy state consistency.

Table 6-3 Damaged joint scenarios.

Scenario	State	Bolts Removed	Damage Case
Scenario 1	Healthy Pipe 1		HC 1-1
	Damage Case 1-1	Bolt #2	DC 1-1
	Damage Case 1-2	Bolt #2 and Bolt #8	DC 1-2
	Damage Case 1-3	Bolts #2, #8 and #5	DC 1-3
	Damage Case 1-4	Bolts #2, #8, #5 and #4	DC 1-4
Scenario 2	Healthy Pipe 2		HC 2-1
	Damage Case 2-5	Bolt #3	DC 2-5
	Damage Case 2-6	Bolt #3 and Bolt #8	DC 2-6
	Damage Case 2-7	Bolts#3, #8 and #5	DC 2-7
	Damage Case 2-8	Bolts #3, #8, #5 and #6	DC 2-8
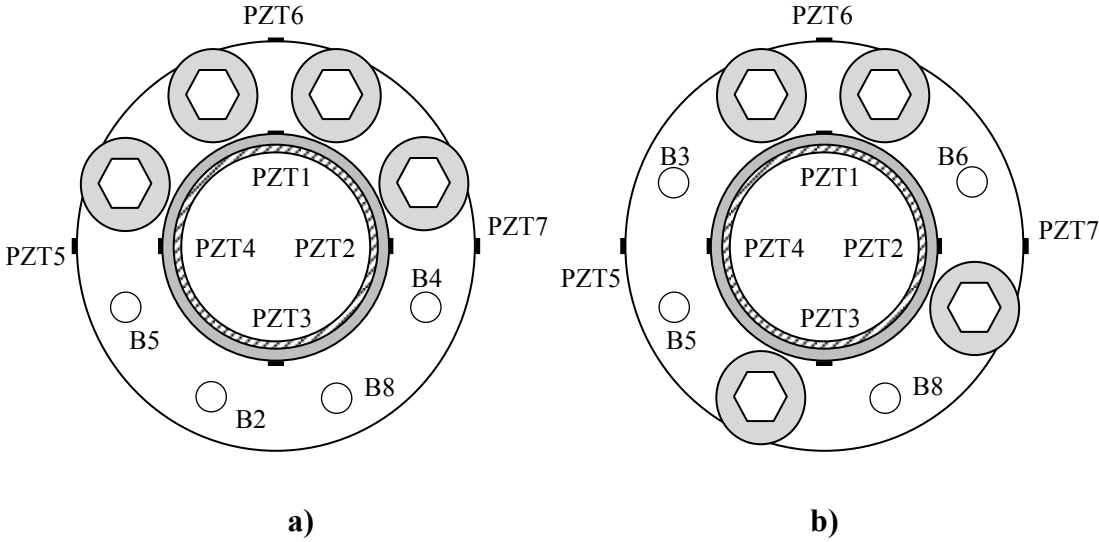
Figure 6-11 Joint damage scenarios **a)** Scenario 1 **b)** Scenario 2.

6.3 DATA ANALYSIS

The data analysis was completed in the same manner as for the experiments documented in Chapters 1 and 2. For all test cases, five impact signals were chosen for the calculation of the EMD average energy.

6.4 RESULTS

By analyzing the data using different frequency bands, it was found that a low-pass filter with a pass-band frequency of 2000 Hz provided the best resolution for the identification of damage for the free-free boundary condition. For the cantilevered boundary condition, it was determined that a low-pass filter with a pass-band frequency of 1500 Hz provided the best resolution for damage identification. These pass-bands were chosen based on the exhibition of damage progression, as well as consideration of the energy amplitude. However, these two pass-bands only marginally improved the EMD-EDI with respect to other pass-bands. It was also determined that the first IMF demonstrated the best damage resolution overall.

Figure 6-12 and Figure 6-13 illustrate the EMD-EDI calculated respectively for damage scenario 1 and 2 for the free-free boundary condition. Likewise, Figure 6-14 and Figure 6-15 illustrate the EMD-EDI calculated respectively for damage scenario 1 and 2 for the cantilevered boundary condition.

Boundary Condition: Free-Free
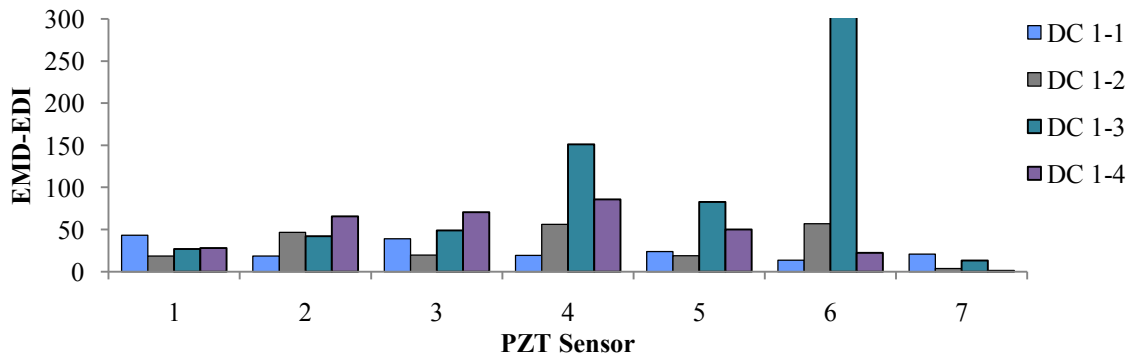
Figure 6-12 Damage scenario 1, 0-2000 Hz, IMF1.
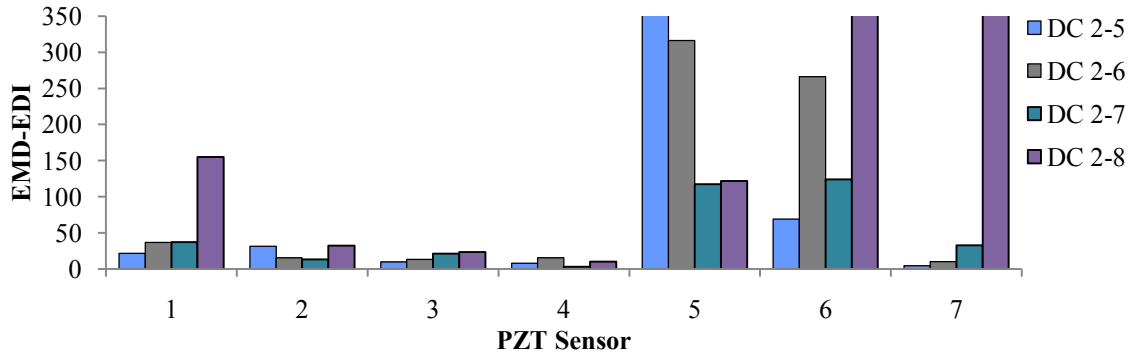
Figure 6-13 Damage scenario 2, 0-2000 Hz, IMF1.

Boundary Condition: Cantilevered
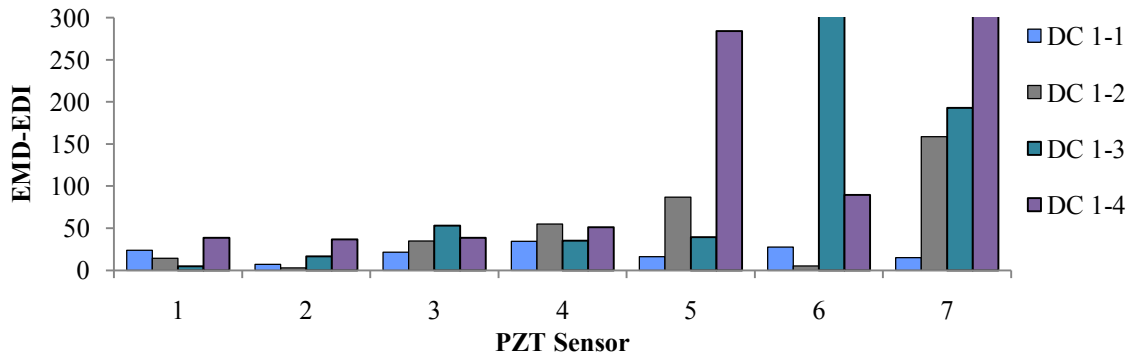
Figure 6-14 Damage scenario 1, 0-1500 Hz, IMF1.
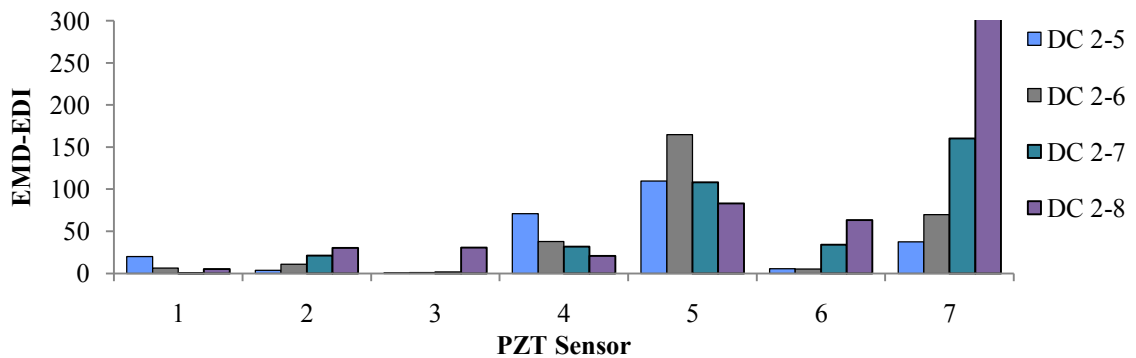
Figure 6-15 Damage scenario 2, 0-1500 Hz, IMF1.

6.5 CONSISTENCY

The same process was used for these experiments as explained in Chapter 3 to measure result consistency between impacts. In order to document the range of variability, Tables C-1 and C-2 in Appendix C list the variations for each healthy and

134

damage case. Table C-1 lists the values for the free-free boundary condition data and Table C-2 lists the values for the cantilevered boundary condition data. As seen, the EMD energies between different impacts were not consistent. During the experiments, it was extremely difficult to achieve impact consistency using the impulse hammer on the PVC pipe. This is in direct contrast to the earlier experimental work conducted on the steel pipes for which the impacts were much more consistent and the maximum difference remained under a value of 20%. The variation in consistency helps to explain the poor index results.

6.6 SET-UP RELIABILITY

In order to address the question of set-up reliability, three healthy cases were completed for each boundary condition as mentioned earlier. Eqn. 3-3 was used to calculate the variability between healthy states. The range of comparison values are listed in Table C-3 in Appendix C. It may be concluded from the values in the Table that it is very difficult to achieve consistency between the set-ups. The difference in EMD energies varies significantly, attributing to the poor resulting damage progression.

6.7 CONCLUSIONS

From comparing Figure 6-12 through 6-15, one can observed that overall the sensors located on the flange socket provided lower amplitude indices than the sensors on the flange itself. Furthermore, it is clear that PZT 7 gave the clearest indication of damage progression as evidenced by Figure 6-13, 6-14 and 6-15. Concerning boundary conditions, it appears that the cantilevered boundary condition resulted in a better prediction of damage progression. Unfortunately, due to the large inconsistencies in the excitation induced by the impact hammer, as discussed in section 6.5, these conclusions may be inherently flawed.

CHAPTER 7

CONCLUSION

7.1 CONCLUSIONS

The objective of this thesis was to explore the application of the Empirical Mode Decomposition Energy Damage Index, coupled with the use of piezoelectric sensors, to bolted pipeline joints. The EMD-EDI is a relatively new method developed for detecting the presence of damage in structures, including corrosion, cracks and support stiffness losses. The motive behind this research was to expand upon the previous work conducted using this method by focusing on a different type of structural damage than has been studied to date.

The EMD-EDI is based on the detection of changes within the dynamic characteristics of a structure due to damage. In the developed procedure, the free vibration response of the structure is monitored and collected through piezoceramic sensors, before and after the occurrence of damage. Subsequently, the Empirical Mode Decomposition, the key component in the Hilbert-Huang Transform, is used to decompose the free vibration signatures of the structure into a collection of oscillatory modes called Intrinsic Mode Functions. The EMD-EDI is then calculated based on the energy change of the IMFs measured from the healthy-state baseline. Accordingly, the index serves as a reflection of the deviations in the structural integrity of the system, thereby providing a means to detect the presence of damage.

To continue the effort focused on establishing the integrity and limitation of this novel damage detection method, a series of experimental testing on mechanically bolted joints was performed. Four different bolted joint systems were tested under different conditions including: a steel pipe with an 8-bolt flanged joint, a pressurized steel pipe with a 12-bolt flanged steel joint, an in-service steel pipe with a 12-bolt flanged joint and a PVC pipe with an 8-bolt flanged joint. The induced joint damage was a loss of clamping force

136

brought on through bolt loosening and/or bolt removal. Each of these experiments is briefly summarized below along with the appropriate conclusions.

7.1.1 Damage Detection of a Steel Pipeline Bolted Joint

Chapter 3 entailed the experimental testing performed on a simply supported steel pipe jointed at the mid-section using an 8-bolt flanged, gasketed joint. Varying degrees of joint damage were simulated by reducing the torque load on the bolts and/or removing them completely. Three different combinations of piezoceramic sensors and/or impact locations were explored in total.

The first session situated six sensors around the circumference of the pipe, at 250 mm from the joint, and used four impact locations for comparison purposes. By analyzing the data using different frequency bands, it was found that a low-pass filter with a pass-band frequency of 2000 Hz provided the best resolution for identification of damage. However, the results were poor in the context of identifying conclusive damage progressions.

The second session entailed removing the gasket from the first session and positioning new sensors in closer proximity to the joint. Two piezoceramic sensors were paced 25 mm from the flange, and four were placed directly on the flange face. In contrast to the last session, the frequency range of 0-2500 Hz yielded the best results in terms of damage index amplitude and damage progression with the excitation by an aluminium tip hammer yielding better results than the plastic tip.

It was concluded that the aluminum tip yielded improved damage detection capabilities than the plastic hammer tip. Furthermore, it was concluded that due to the variance in results between the four impact locations, further work was required. One important observation was that the majority of the results from the second session did not show damage progression for the first 5 damage cases. Therefore, only fully loosened bolts were considered in the later experiments. Finally, the decision to perform testing without a gasket yielded improved results overall. A possible reason would be that the presence of the gasket, and the type of gasket, may play a large role in the usefulness of this method.

The third session entailed placing four new sensors on the flange face on the other side of the joint with respect to the sensor locations from session 2. Additionally, two new impact locations were chosen closer to the joint in an effort to determine if a closer impact would result in improved damage detection.

The frequency range of 0-2000 Hz yielded the best results in terms of damage index amplitude and damage progression, with the added IMFs demonstrating the best resolution for damage detection. From a comparison of the different impact locations, it was observed that Impact Locations B and C gave the best results concerning damage progression. Therefore, it can be concluded that an impact location too close to the joint may negatively affect the index results. Furthermore, the side of the flange on which the sensors are mounted relative to the impact location does not seem to make any significant difference in the results.

Concerning the comparison between hammer tips, the two impulse hammer tips yielded approximately similar results overall with the plastic tip giving more consistent results concerning the variability in EMD energies among impacts. However, taking into account the results from session 2 that indicate a frequency bandwidth that surpasses 2 kHz may be required for improved damage resolution, it was concluded that the aluminium tip was the best choice for future damage detection trials.

7.1.2 Damage Detection of an In-Service Condensation Pipeline Joint

This experiment was performed in order to apply the EMD-EDI in a practical application of an in-service pipeline. A 12-bolt mechanical joint located in the underground tunnels at the Central Services Building at Dalhousie University, NS, was chosen for testing due to ease of access. To capture the dynamic response of the joint, eight piezoceramic sensors were bonded to the flange and pipe in the vicinity of the joint. Three different damage scenarios were explored, each involving a healthy case and multiple damage cases each involving complete removal of one or more bolts.

By analyzing the data using different frequency bands, it was found that a low-pass filter with a cutoff frequency of 2000 Hz provided the best resolution for identification of damage for each of the scenarios. The frequency band of 1000-2000 Hz also provided

good resolution for the second scenario. This choice was based on the evaluation of both IMFs. Several conclusions were made after the analysis of the results was completed.

It was concluded that the EMD-EDI can successfully detect the presence of damage. However, sensor placement, boundary conditions and impact locations have a significant influence on the results which should be carefully considered when choosing sensor and impact location. Moreover, the experimental results did not clearly indicate a relationship between the ability of a sensor to detect damage and its proximity to the damage, therefore further work in this area is required. The final conclusion was that the band-pass filter used for signal filtering should be applied carefully to avoid filtering out frequency components that contain meaningful information.

7.1.3 Damage Detection of a Pressurized Steel Pipeline Joint

Chapter 5 entailed experimental testing on a suspended steel pipe pressurized to 10 MPa with a 12-bolt flanged joint at the mid-point. Five PZT sensors were placed on the flange face and rim, and one sensor was placed on the pipe. Two impact locations were used, situated on the top and side of the pipe. Four different damage scenarios were completed, each having a healthy case and multiple damage cases.

By analyzing the data using different frequency bands, it was found that a low-pass filter with a pass-band frequency of 2000 Hz was one of the frequency ranges that provided the best resolution for identification of damage. The added IMFs gave better resolution than either IMF by itself. Further graphs supporting these conclusions may be found in Appendix B.

However, the results indicated inconsistency in the detection of damage progression. It is believed that a portion of this inconsistency is due to the variability inherent in using a hand held impulse hammer. It was also concluded that sensor placement and impact locations have a significant influence on the results. As such, further work is required to understand the most efficient locations for impact and senor placement.

139

7.1.4 Damage Detection of a PVC Pipeline Joint

Chapter 6 entailed experimental testing performed on a PVC pipe jointed at the mid-section using an 8-bolt flanged joint. Two damage scenarios were investigated including a damage pattern concentrated on bottom of the joint, as well as a random pattern. The influence of boundary conditions on the results was also investigated using free-free and cantilevered boundary conditions. To monitor the vibration of the system, four sensors were placed on the flange socket, and three sensors were placed on the flange rim. For the various damage cases, joint damage was simulated by completely removing the bolts from the flanges.

By analyzing the data using different frequency bands, it was found that a low-pass filter with a pass-band frequency of 2000 Hz provided the best resolution for the identification of damage for the suspended boundary condition. For the cantilevered boundary condition, it was determined that a low-pass filter with a pass-band frequency of 1500 Hz provided the best resolution for damage identification.

The conclusions reached for this experiment were as follows. The sensors located on the flange socket provided lower amplitude damage indices than the sensors on the flange. Concerning boundary conditions, it appears that the cantilevered boundary condition resulted in a better prediction of damage progression. Unfortunately, due to the large inconsistencies in the excitations induced by the hand-held impact hammer, these conclusions may not be entirely valid.

7.2 RECOMMENDATIONS FOR FUTURE WORK

Due to the presence of factors that caused problems during testing as well as inconsistencies in the results, below are some recommendations to improve upon the damage detection methodology of the EMD-EDI.

The first recommendation is to use an appropriate device to accurately measure bolt tension for future experimental damage cases that involve reducing bolt tension instead of completely removing the bolt from the joint. Taking into account the interaction between tensioned bolts, when one bolt is loosened to any degree it would affect the tension in the other bolts in the joint. Therefore, it is important to use a device to measure bolt tension and accurately gauge the actual damage introduced to the joint, as opposed to a perceived degree of damage. Furthermore, measuring the bolt tension will also allow greater accuracy when initially torquing the joint, thus yielding a more clearly defined healthy state. Examples of methods to employ are direct tension indicators and ultrasonic extensometers.

The implementation of a consistent excitation method is the second recommendation. The experimental work documented in this thesis required the use of a hand held impulse hammer. This method of excitation introduced inconsistency into the results. Additionally, in industrial applications, the use of an impulse hammer would be inefficient due to the time necessary for testing and the manpower required for personnel site visitation. Furthermore, depending on the location of the joint, manually exciting the pipe by hand may be impossible. Consequently, other excitation methods should be considered. For future experimental work, a consistent excitation method such as an electric hammer should improve results, especially in the case of the PVC pipeline.

Another recommendation for future work is the development of a method, or a rule-of-thumb, to determine the correct frequency range to use in the EMD-EDI. The band-pass filter used for signal filtering needs to be chosen carefully to avoid filtering out frequency components that contain meaningful information. However, it is inefficient to analyze the data for many frequency bands, and manually evaluate the results for the best frequency range. Accordingly, further insight into the relationship between the joint, damage type and the index will significantly decrease analysis time. Furthermore, the creation of a

Matlab code that would automatically determine the best frequency range to use would be extremely efficient. Additionally, the creation of an automated system in which the Matlab code would automatically apply the damage index upon the system acquiring damage data would be ideal.

The fourth recommendation is that more in-situ testing should be conducted for further validation of the method in a variety of situations. The majority of the testing completed so far has been conducted in a controlled laboratory setting. In-situ testing involves many variables including environmental conditions, external loadings, and unknown factors that may negatively affect the application of the method by inducing uncontrolled dynamic loading. An example of this would be the influence of noise produced by a system and its interaction with the excitation vibration signals.

The final recommendation is the use of an improved sensor system. It is a drawback to the current methodology that an inspector's presence is required at the site of the damage. As mentioned above, in real applications this may not be possible. Therefore, a wireless sensor system would be ideal for providing damage detection in cases that have inaccessible structures.

REFERENCES

Adeli, H., & Hung, S. (1995). *Machine learning – neural networks, genetic algorithms, and fuzzy systems.* John Wiley and Sons, Ltd., New York.

ANSI/ASME. (1985). *ANSI / ASME B36.19M-1985 - american national standard for welded and seamless wrought steel pipe* ANSI/ASME.

ASTM International. (2007). *ASTM A53 - standard specification for pipe, steel, black and hot-dipped, zinc-coated, welded and seamless*. West Conshohocken, PA: ASTM International.

Bibel, G. (1998). Tightening groups of fasteners in a structure and the resulting elastic interaction. In *Handbook of bolts and bolted joints,* J. H. Bickford, & S. Nassar (Eds.), (pp. 451). Marcel Dekker, Inc.: New York.

Bickford, J. H. (1995). *An introduction to the design and behavior of bolted joints.* Marcel Dekker, Inc.: New York.

Bickford, J. H., & Nassar, S. (Eds.). (1998). *Handbook of bolts and bolted joints*. Marcel Dekker, Inc.: New York.

Bickford, J. H. (1998a). Behavior of a bolted joint during assembly. In *Handbook of bolts and bolted joints,* J. H. Bickford, & S. Nassar (Eds.), (pp. 425). Marcel Dekker, Inc.: New York.

Bickford, J. H. (1998b). Torque control of assembly. In *Handbook of bolts and bolted joints,* J. H. Bickford, & S. Nassar (Eds.), (pp. 559). Marcel Dekker, Inc.: New York.

Brownjohn, J. M. W. (2007). Structural health monitoring of civil infrastructure. *Phil. Trans. R. Soc. A, 365*, 589-622.

Caccese, V., Mewer, R., & Vel, S. (2004). Detection of bolt load loss in hybrid composite/metal bolted connections. *Engineering Structures, 26*(7), 895.

143

Carden, E., & Fanning, P. (2004). Vibration based condition monitoring: A review. *Structural Health Monitoring, 3*(4), 355-377.

Chang, F. K. (1999). *Structural health monitoring: 2000*. Technomic Publishing Company, Lancaster, Pennsylvania.

Chattopadhyay, A., Das, S., & Coelho, C. (2007). Damage diagnosis using a kernel-based method. *Insight - Non-Destructive Testing and Condition Monitoring, 49*(8), 451-458.

Cheraghi, N., Riley, M. J., & & Taheri, F. (2005). A novel approach for detection of damage in adhesively bonded joints in plastic pipes based on vibration methods using piezoelectric sensors. In *Proceedings of the IEEE International Conference on Systems, Man and Cybernetics,* Hawaii, USA, 10-12 Oct., pp. 3472-3478.

Cheraghi, N., & Taheri, F. (2008). Application of the empirical mode decomposition for system identification and structural health monitoring. *International J. of Applied Mathematics and Engineering Sciences, 2*(1), 61-72.

Cheraghi, N., & Taheri, F. (2007). A damage index for structural health monitoring based on the empirical mode decomposition. *J. of Mechanics of Materials and Structures, 2*(1), 43-62.

Cheraghi, N., Riley, M. J., & Taheri, F. (2007). Application of hilbert-huang transform for evaluation of vibration characteristics of plastic pipes using piezoelectric sensors. *Structural Engineering Mechanics, 25*(6), 653-674.

Chopra, A. K. (2001). *Dynamics of structures: Theory and applications to earthquake engineering* (2nd ed.). Prentice-Hall, Inc.: Upper Saddle River, NJ.

CINDE. (2010). *Canadian institute for NonDestructive evaluation.* Retrieved May 27, from http://www.cinde.ca/ndt.shtml

Coelho, C. K., Das, S., Chattopadhyay, A., Papandreou-Suppappola, A., & Peralta, P. (2007). Detection of fatigue cracks and torque loss in bolted joints. In *Proceedings of SPIE: Health Monitoring of Structural and Biological Systems 2007,* California, USA, 19-22 March.

Corbett, R. (1998). Stretch control. In *Handbook of bolts and bolted joints,* J. H. Bickford, & S. Nassar (Eds.), (pp. 571). Marcel Dekker, Inc.: New York.

Doebling, S. W., Farrar, C. R., Prime, M. B., & Shevitz, D. W. (1996). *Damage identification and health monitoring of structural and mechanical systems from changes in their vibration characteristics: A literature review.* Report No. LA-13070-MS, Los Alamos National Laboratory.

Doebling, S. W., Farrar, C. R., & Prime, M. B. (1998). A summary review of vibration-based damage identification methods. *The Shock and Vibration Digest, 30*(2), 91-105.

Energy Institute (Great Britain). (2007). *Guidelines for the management of the integrity of bolted joints for pressurised systems.* (2nd ed.). Energy Institute: London.

Farrar, R., Doeblíng, S. W., & Charles, D. (2001). Vibration-based structural damage identification. *Philosophical Transactions of the Royal Society A: Mathematical, Physical and Engineering Sciences, 359*(1778), 131-149.

Farrar, C., & Worden, K. (2007). An introduction to structural health monitoring. *Philosophical Transactions of the Royal Society A: Mathematical, Physical and Engineering Sciences, 365*(1851), 303-315.

Fasel, T., Kennel, M., Todd, M., Clayton, E., & Park, G. (2009). Damage state evaluation of experimental and simulated bolted joints using chaotic ultrasonic waves. *Smart Structures and Systems, 5*(4), 329-344.

Fasel, T. R., Olson, C. C., Todd, M. D., & Kundu, T. (2008). Optimized guided wave excitations for health monitoring of a bolted joint. In *Proceedings of SPIE: Health Monitoring of Structural and Biological Systems 2008,* California, USA, 10-13 March.

Hess, D. P. (1998). Vibration and shock induced loosening. In *Handbook of bolts and bolted joints,* J. H. Bickford, & S. Nassar (Eds.), (pp. 757). Marcel Dekker, Inc.: New York.

Huang, N. E., Shen, Z., Long, S. R., Wu, M. C., Shih, H. H., Zheng, Q., Nai-Chyuan, Y., Tung, C. C., & Liu, H. H. (1998). The empirical mode decomposition and the hilbert spectrum for nonlinear and non-stationary time series analysis. *Philosophical Transactions of the Royal Society A: Mathematical, Physical and Engineering Sciences, 454*(1971), 903-995.

Industrial Fasteners Institute: Division VI Aerospace Fasteners. (1995). *Test application handbook relating to mechanical fasteners*. Industrial Fasteners Institute: Cleveland, Ohio.

Ipex Inc. (2010). *Industrial products, process piping systems, xirtec PVC & corzan CPVC.* Retrieved March, 2010, from http://www.ipexinc.com/

Jiang, Y., Zhang, M., & Lee, C. (2003). A study of early stage self-loosening of bolted joints. *Journal of Mechanical Design, 125*(3), 518.

Johnson, E. A., Lam, H. F., Katafygiotis, L. S., & Beck, J. L. (2004). Phase I IASC-ASCE structural health monitoring benchmark problem using simulated data. *Journal of Engineering Mechanics, 130*(1), 3-15.

Junker, G. (1972). Criteria for self-loosening of fasteners under vibration. *Aircraft Engineering and Aerospace Technology, 44*(10), 14.

Kitaura, M., & Miyajima, M. (1996). Damage to water supply pipelines. *Soils and Foundations,* January, 325-333.

Krawczuk, M. (2002). Application of spectral beam finite element with a crack and iterative search technique for damage detection. *Finite Elements in Analysis and Design, 38*(6), 537-548.

Kull, F. (1998). Bolt fatigue. In *Handbook of bolts and bolted joints,* J. H. Bickford, & S. Nassar (Eds.), (pp. 699). Marcel Dekker, Inc.: New York.

Lee, L. S., Karbhari, V. M., & Sikorsky, C. (2004). *Investigation of integrity and effectiveness of RC bridge deck rehabilitation with CFRP composites.* No. SSRP-2004/08: University of California., Retrieved from http://svctwww1.dot.ca.gov/hq/esc/earthquake_engineering/Research/SSRP_200.pdf

Leo, D. J. (2007). *Engineering analysis of smart material systems*. John Wiley and Sons, Ltd.: New Jersey.

Lin, S., Yang, J. N., & Zhou, L. (2005). Damage identification of a benchmark building for structural health monitoring. *Smart Materials & Structures, 14*(3), S162-S169.

Liu, J., Wang, X., Yuan, S., & & Li, G. (2006). On hilbert-huang transform approach for structural health monitoring. *Journal of Intelligent Material Systems and Structures, 17*(8-9), 721-728.

Lopes JR, V., Park, G., Cudney, H., & Inman, D. (2000). Impedance-based structural health monitoring with artificial neural networks. *Journal of Intelligent Material Systems and Structures, 11*(3), 206-214.

Loutridis, S. (2004). Damage detection in gear systems using empirical mode decomposition. *Engineering Structures, 26*(12), 1833-1841.

Lovell, P. A., & Pines, D. J. (1998). Damage assessment in a bolted lap joint. In *Proceedings SPIE: Smart Structures and Materials 1998: Smart Systems for Bridges, Structures, and Highways,* California, USA, 4-5 March, 112-126.

Mascarenas, D. L., Park, G., & Farrar, C. R. (2005). Monitoring of bolt preload using piezoelectric active devices. In *Proceedings of SPIE: Health Monitoring and Smart Nondestructive Evaluation of Structural and Biological Systems IV,* California, USA, 7-9 March, 129-136.

Melhem, H.G. & Nagaraja, S. (1996). Machine learning and its application to civil engineering systems. *Civil Engineering and Environmental Systems*, 13(4), 259-279.

Metzger, D. (2004). Bolted joint integrity management: Implementing industry best practice. In *Proceedings of the 12th International Conference on Nuclear Engineering,* Virginia, USA, 25-29 April, 179-184.

Michaelides, P. G., & Fassois, S. D. (2008). Damage detection and localization in the joints of a thin plate via a statistical power spectral density based method. In *Proceedings of the 4th European Workshop on Structural Health Monitoring,* Krakow, Poland, July, 937-944.

Milanese, A., Marzocca, P., Nichols, J., Seaver, M., & Trickey, S. (2008). Modeling and detection of joint loosening using output-only broad-band vibration data. *Structural Health Monitoring, 7*(4), 309.

Moniz, L., Nichols, J., Nichols, C., Seaver, M., Trickey, S., & Todd, M. (2005). A multivariate, attractor-based approach to structural health monitoring. *Journal of Sound and Vibration, 283*(1-2), 295-310.

Nichols, J. M. (2003). Using state space predictive modeling with chaotic interrogation in detecting joint preload loss in a frame structure experiment. *Smart Materials Structures, 12*(4), 580-601.

Nichols, J. M., Trickey, S. T., Seaver, M., Motley, S. R., & Eisner, E. D. (2007). Using ambient vibrations to detect loosening of a composite-to-metal bolted joint in the presence of strong temperature fluctuations. *Journal of Vibration and Acoustics, Transactions of the ASME, 129*(6), 710-717.

Noble, R. (2006). Integrity of bolted joints; hydrocarbon leak reduction by joint-integrity management. *APPEA Journal, 46*(1), 603-609.

Noman, A. (2008). *Application of vibration based methods and statistical pattern recognition techniques to structural health monitoring* (M.A.Sc. dissertation). Dept. of Building, Civil and Environmental Engineering, Concordia University, Canada. Retrieved from ProQuest Dissertations & Theses Database. (UMI No. AAT MR45523)

Okugawa, M., & Tanaka, T. (2007). Effect on detection sensitivity for smart washer configuration, and ambient temperature characteristics on bolted joint. In *Proceedings of SPIE: Health Monitoring of Structural and Biological Systems 2007,* California, USA, 19-22 March.

Pai, N. G., & Hess, D. P. (2002). Three-dimensional finite element analysis of threaded fastener loosening due to dynamic shear load. *Engineering Failure Analysis, 9*(4), 383-402. Retrieved from http://dx.doi.org/10.1016/S1350-6307(01)00024-3

Park, G., & Inman, D. J. (2005). Impedance-based structural health monitoring. In *Damage prognosis for aerospace, civil and mechanical systems,* D. J. Inman, C. R. Farrar, V. Lopes Jr. & V. Steffen Jr. (Eds.), (pp. 275). John Wiley and Sons, Ltd.: Great Britain.

Park, G., Muntges, D. E., & Inman, D. J. (2003). Self-repairing joints employing shape-memory alloy actuators. *Journal of the Minerals, Metals and Materials Society, 55*(12), 33-37.

Park, S., Yun, C., & Roh, Y. (2005). PZT-induced lamb waves and pattern recognitions for on-line health monitoring of jointed steel plates. In *Proceedings of SPIE: Smart Structures and Materials 2005: Sensors and Smart Structures Technologies for Civil, Mechanical, and Aerospace Systems,* California, USA, 7-10 March, 364-375.

Park, S., Yun, C., Roh, Y., & Lee, J. (2006). PZT-based active damage detection techniques for steel bridge components. *Smart Materials and Structures, 15*(4), 957-966.

Park, G., Muntges, D. E., & Inman, D. J. (2001). Self-monitoring and self-healing jointed structures. *Key Engineering Materials, 204-205*, 75-84.

Peairs, D. M., Park, G., & Inman, D. J. (2002). Reducing the cost of impedance-based structural health monitoring. In *Proceedings of SPIE: Smart Nondestructive Evaluation for Health Monitoring of Structural and Biological Systems,* California, USA, 18-19 March, pp. 301-310.

Peairs, D. M., Park, G., & Inman, D. J. (2004). Improving accessibility of the impedance-based structural health monitoring method. *Journal of Intelligent Material Systems and Structures, 15*(2), 129-140. Retrieved from http://dx.doi.org/10.1177/1045389X04039914

Pines, D., & Salvino, L. (2006). Structural health monitoring using empirical mode decomposition and the hilbert phase. *Journal of Sound and Vibration, 294*(1-2), 97-124.

Quek, S. T., Tua, P. S., & Wang, Q. (2003). Detecting anomalies in beams and plate based on the hilbert-huang transform of real signals. *SMART MATERIALS AND STRUCTURES, 12*(Part 3), 447-460. Retrieved from stacks.iop.org/SMS/12/447

Quek, S. T., Wang, Q., Zhang, L., & Ang, K. K. (2001). Sensitivity analysis of notch detection in beams by wavelet technique. *International J. of Mechanical Sciences, 43*, 2899-2910.

Rezaei, D. (2010). *Experimental and computational validation of a novel structural health monitoring strategy based on the hilbert-huang transform.* (Doctoral dissertation). Dept. of Civil and Resource Engineering, Dalhousie University, Canada.

Rezaei, D., & Taheri, F. (2010a). Health monitoring of pipeline girth weld using empirical mode decomposition. *Smart Materials and Structures, 19*(5).

Rezaei, D., & Taheri, F. (2010b). Damage identification in beams using empirical mode decomposition. *Journal of Structural Health Monitoring,* in press.

Rezaei, D., & Taheri, F. (2009). Experimental validation of a novel structural damage detection method based on empirical mode decomposition. *Smart Materials and Structures, 18*(4).

Riley, M. J. (2005). Investigation into the feasibility of implementing piezoelectric patches for sensing and actuation of structural components (Doctoral dissertation). Dept. of Civil Engineering, Dalhousie University, Canada.

Ritdumrongkul, S., Abe, M., Fujino, Y., & Miyashita, T. (2004). Quantitative health monitoring of bolted joints using a piezoceramic actuator-sensor. *Smart Materials and Structures, 13*(1), 20-29.

Ritdumrongkul, S., & Fujino, Y. (2006). Identification of the location and level of damage in multiple-bolted-joint structures by PZT actuator-sensors. *Journal of Structural Engineering, 132*(2), 304-311.

Rutherford, A., Park, G., & Farrar, C. (2007). Non-linear feature identifications based on self-sensing impedance measurements for structural health assessment. *Mechanical Systems and Signal Processing, 21*(1), 322-333.

Rytter, A. (1993). *Vibration based inspection of civil engineering structures* (Doctoral dissertation). Dept. of Building Technology and Structural Engineering, Aalborg University, Denmark. Retrieved from ProQuest Dissertations & Theses Database.

Shi, Z. (2000). Structural damage detection from modal strain energy change. *Journal of Engineering Mechanics, 126*(12), 1216-1223.

Sohn, H., Farrar, C. R., Hemez, F. M., Czarnecki, J. J., Shunk, D. D., Stinemates, D. W., & Nadler, B. R. (2003). *A review of structural health monitoring literature: 1996–2001* No. LA-13976-MS, Los Alamos National Laboratory, Los Alamos, NM.

Stinemates, D. W., Farrar, C. R., Bennett, J. G., & Sohn, H. (2002). Structural health monitoring system design using finite element analysis. In *Proceedings of SPIE: Smart Nondestructive Evaluation for Health Monitoring of Structural and Biological Systems,* California, USA, 18-19 March, 169-178.

Sturdevant, G. A. (1998). Hydraulically powered wrenches. In *Handbook of bolts and bolted joints,* J. H. Bickford, & S. Nassar (Eds.), (pp. 479). Marcel Dekker, Inc.: New York.

Todd, M., Erickson, K., Chang, L., Lee, K., & Nichols, J. (2004). Using chaotic interrogation and attractor nonlinear cross-prediction error to detect fastener preload loss in an aluminum frame. *Chaos, 14*(2), 387-399.

Todd, M. D., Nichols, J. M., Nichols, C. J., & Virgin, L. N. (2004). An assessment of modal property effectiveness in detecting bolted joint degradation: Theory and experiment. *Journal of Sound and Vibration, 275*(3-5), 1113-1126. Retrieved from http://dx.doi.org/10.1016/j.jsv.2003.10.037

Worden, K., Farrar, C., Manson, G., & Park, G. (2007). The fundamental axioms of structural health monitoring. *Philosophical Transactions of the Royal Society A: Mathematical, Physical and Engineering Sciences, 463*(2082), 1639.

Xu, Y. L., & Chen, J. (2004). Structural damage detection using empirical mode decomposition: Experimental investigation. *Journal of Engineering Mechanics, 130*(11), 1279-1288.

Yan, Y., Cheng, L., Wu, Z., & Yam, L. (2007). Development in vibration-based structural damage detection technique. *Mechanical Systems and Signal Processing, 21*(5), 2198-2211.

Yu, L., Link, M., Law, S., & Zhang, L. (1999). Structural damage identification procedure with application to a frame structure with bolted joints. In *Proceedings of the 17th International Modal Analysis Conference,* Florida, USA, 8-11 February, 1387-1394.

APPENDIX A

SUPPLEMENTARY RESULTS FROM CHAPTER 3

A.1 TABLES

Table A-1 Session 1 EMD energy variability, 0-2000 Hz, IMF 1.

Location /Sensor	HC 1-1	HC 1-2	DC 1-1	DC 1-2	DC 1-3	DC 1-4
Location A	(*maximum values are highlighted)					
PZT1	4.16%	4.12%	5.31%	2.86%	3.65%	2.13%
PZT2	2.29%	3.10%	10.05%	3.31%	3.87%	3.33%
PZT3	6.08%	3.11%	19.81%	3.61%	4.38%	3.88%
PZT4	1.10%	3.83%	7.63%	1.92%	2.63%	2.85%
PZT5	7.85%*	5.88%	8.03%	2.84%	3.00%	3.61%
PZT6	6.28%	3.34%	3.72%	1.96%	0.54%	2.22%
Maximum	**7.85%**	**5.88%**	**19.81%**	**3.61%**	**4.38%**	**3.88%**
Location B						
PZT1	3.62%	5.58%	2.51%	3.08%	4.88%	3.89%
PZT2	1.69%	4.47%	6.88%	4.89%	4.92%	1.55%
PZT3	5.56%	4.57%	2.51%	0.49%	3.28%	4.34%
PZT4	1.34%	5.41%	3.01%	2.73%	2.93%	3.00%
PZT5	5.75%	3.68%	5.33%	2.86%	6.12%	2.37%
PZT6	3.85%	2.92%	4.13%	1.17%	2.21%	3.17%
Maximum	**5.75%**	**5.58%**	**6.88%**	**4.89%**	**6.12%**	**4.34%**
Location C						
PZT1	3.60%	2.13%	5.60%	6.19%	1.13%	4.12%
PZT2	0.43%	1.64%	3.14%	6.22%	2.68%	1.32%
PZT3	1.45%	2.93%	5.28%	2.85%	0.77%	1.93%
PZT4	0.27%	1.29%	5.15%	7.45%	2.78%	1.38%
PZT5	1.52%	3.42%	4.22%	5.30%	1.82%	2.07%
PZT6	0.99%	2.29%	3.93%	5.56%	2.41%	0.54%
Maximum	**3.60%**	**3.42%**	**5.60%**	**7.45%**	**2.78%**	**4.12%**
Location D						
PZT1	1.00%	4.12%	1.14%	0.73%	2.70%	2.37%
PZT2	1.27%	3.10%	1.94%	0.65%	1.47%	2.44%
PZT3	0.22%	3.11%	1.19%	2.05%	2.62%	3.06%
PZT4	1.50%	3.83%	1.54%	1.18%	2.08%	3.73%
PZT5	3.03%	5.88%	0.98%	1.52%	2.56%	2.60%
PZT6	0.93%	3.34%	0.36%	1.73%	2.48%	3.82%
Maximum	**3.03%**	**5.88%**	**1.94%**	**2.05%**	**2.70%**	**3.82%**
Average						
PZT1	3.09%	3.99%	3.64%	3.21%	3.09%	3.13%
PZT2	1.42%	3.08%	5.50%	3.77%	3.24%	2.16%
PZT3	3.33%	3.43%	7.20%	2.25%	2.76%	3.30%
PZT4	1.05%	3.59%	4.33%	3.32%	2.61%	2.74%
PZT5	4.54%	4.72%	4.64%	3.13%	3.38%	2.66%
PZT6	3.01%	2.97%	3.04%	2.60%	1.91%	2.44%

Table A-2 Session 1 EMD energy variability, 0-2000 Hz, IMF 2.

Location /Sensor	HC 1-1	HC 1-2	DC 1-1	DC 1-2	DC 1-3	DC 1-4
Location A			(*maximum values are highlighted)			
PZT1	5.60%*	3.80%	3.24%	2.18%	6.12%	7.79%
PZT2	3.88%	1.77%	6.80%	4.07%	3.30%	10.21%
PZT3	2.15%	2.77%	11.84%	1.20%	4.24%	7.14%
PZT4	1.82%	4.88%	6.02%	1.56%	4.22%	8.68%
PZT5	4.14%	4.65%	5.40%	4.06%	2.22%	9.37%
PZT6	3.43%	1.98%	5.41%	1.42%	2.83%	10.34%
Maximum	**5.60%**	**4.88%**	**11.84%**	**4.07%**	**6.12%**	**10.34%**
Location B						
PZT1	4.81%	6.43%	2.20%	3.73%	7.71%	2.13%
PZT2	7.72%	1.48%	5.24%	4.91%	7.58%	2.37%
PZT3	5.57%	7.33%	1.22%	3.37%	6.83%	3.78%
PZT4	4.45%	2.88%	1.80%	6.56%	5.53%	2.06%
PZT5	7.04%	3.03%	5.01%	2.38%	7.64%	3.33%
PZT6	7.26%	8.94%	6.55%	3.23%	6.11%	2.69%
Maximum	**7.72%**	**8.94%**	**6.55%**	**6.56%**	**7.71%**	**3.78%**
Location C						
PZT1	2.30%	6.68%	2.34%	11.48%	2.20%	4.14%
PZT2	2.66%	10.14%	6.17%	7.51%	3.52%	1.24%
PZT3	4.88%	8.36%	2.49%	6.49%	4.31%	2.26%
PZT4	1.64%	8.68%	2.82%	7.78%	2.74%	3.24%
PZT5	5.17%	2.83%	6.73%	6.34%	0.61%	2.62%
PZT6	4.04%	4.23%	5.18%	6.34%	6.39%	4.88%
Maximum	**5.17%**	**10.14%**	**6.73%**	**11.48%**	**6.39%**	**4.88%**
Location D						
PZT1	3.04%	8.78%	5.13%	7.06%	2.33%	2.07%
PZT2	3.04%	6.67%	1.40%	4.69%	2.29%	2.40%
PZT3	6.05%	7.08%	3.90%	6.82%	1.70%	2.43%
PZT4	1.18%	5.40%	4.28%	4.86%	3.02%	8.40%
PZT5	4.33%	6.69%	5.90%	5.64%	5.13%	7.60%
PZT6	4.01%	5.89%	5.61%	8.48%	5.28%	7.08%
Maximum	**6.05%**	**8.78%**	**5.90%**	**8.48%**	**5.28%**	**8.40%**
Average						
PZT1	3.94%	6.42%	3.23%	6.11%	4.59%	4.03%
PZT2	4.33%	5.02%	4.90%	5.29%	4.18%	4.05%
PZT3	4.66%	6.38%	4.86%	4.47%	4.27%	3.90%
PZT4	2.27%	5.46%	3.73%	5.19%	3.88%	5.59%
PZT5	5.17%	4.30%	5.76%	4.60%	3.90%	5.73%
PZT6	4.68%	5.26%	5.69%	4.87%	5.15%	6.25%

Table A-3 Session 1 result repeatability, healthy states, 0-2000 Hz.

Location A	IMF 1	IMF 2
PZT1	75.35%	5.09%
PZT2	34.97%	3.89%
PZT3	97.22%	58.43%
PZT4	68.01%	7.53%
PZT5	19.18%	6.90%
PZT6	62.44%	9.15%
Location B		
PZT1	4.89%	9.42%
PZT2	0.23%	2.41%
PZT3	81.37%	63.39%
PZT4	1.71%	0.81%
PZT5	5.24%	1.49%
PZT6	2.57%	4.80%
Location C		
PZT1	0.15%	1.50%
PZT2	1.44%	4.16%
PZT3	1.50%	1.90%
PZT4	2.92%	1.69%
PZT5	1.32%	5.02%
PZT6	1.38%	4.92%
Location D		
PZT1	3.09%	6.95%
PZT2	3.73%	1.55%
PZT3	2.05%	2.09%
PZT4	5.13%	8.43%
PZT5	1.71%	2.85%
PZT6	1.62%	0.33%

*Variations over 20% are highlighted

Table A-4 Session 2 EMD energy variability, 0-2500 Hz, IMF 1, aluminium tip.

Location /Sensor	HC 2-1 (%)	HC 2-2 (%)	HC 2-3 (%)	HC 2-4 (%)	DC 2-1 (%)	DC 2-2 (%)	DC 2-3 (%)	DC 2-4 (%)	DC 2-5 (%)	DC 2-6 (%)	DC 2-7 (%)	DC 2-8 (%)	DC 2-9 (%)
Loc. A													
PZT7	3.58	2.51	3.10	2.69	4.93	4.33	2.25	4.25	4.26	2.59	4.48	5.01	4.81
PZT8	2.49	3.29	3.41	2.85	2.74	2.26	4.23	4.77	3.66	3.03	6.74	4.03	7.53
PZT10	4.18	2.62	3.08	3.20	1.02	2.57	1.68	4.75	4.40	3.54	3.74	6.42	6.44
PZT11	6.59	3.84	5.25	3.48	2.95	2.51	2.74	2.70	4.93	1.47	5.40	4.01	5.81
PZT12	3.08	4.45	2.68	2.65	4.75	2.65	1.91	3.39	2.58	2.66	6.22	7.38	6.17
Max	6.59	4.45	5.25	3.48	4.93	4.33	4.23	4.77	4.93	3.54	6.74	7.38	7.53
Loc. B													
PZT7	3.37	4.09	4.18	2.62	4.65	3.52	2.91	4.66	3.26	7.39	4.26	2.75	5.32
PZT8	2.56	4.16	3.72	1.39	6.04	3.17	1.65	2.63	1.00	5.44	3.34	4.23	5.60
PZT10	3.18	4.99	4.45	2.34	3.65	3.72	2.56	3.11	1.43	5.36	3.00	2.33	5.32
PZT11	1.91	6.52	4.38	3.30	4.27	0.93	2.03	1.58	2.48	2.72	6.56	4.72	6.02
PZT12	3.85	5.41	5.56	3.85	7.67	4.09	3.34	3.28	2.89	3.04	1.85	1.54	3.79
Max	3.85	6.52	5.56	3.85	7.67	4.09	3.34	4.66	3.26	7.39	6.56	4.72	6.02
Loc. C													
PZT7	5.09	3.19	3.77	4.57	8.73	5.39	5.39	3.19	5.55	3.48	4.79	5.78	3.44
PZT8	4.27	4.11	1.48	3.14	8.19	1.93	5.15	6.58	6.06	4.16	3.53	6.81	4.35
PZT10	6.59	2.85	3.35	3.65	9.07	4.76	4.43	3.86	4.08	4.70	3.14	5.95	3.78
PZT11	11.19	2.65	3.37	2.12	6.94	2.72	3.06	2.80	3.86	3.56	3.61	5.68	5.40
PZT12	5.16	1.81	4.03	5.79	8.51	2.26	5.91	4.06	5.46	2.88	3.55	2.78	4.49
Max	11.19	4.11	4.03	5.79	9.07	5.39	5.91	6.58	6.06	4.70	4.79	6.81	5.40
Loc. D													
PZT7	6.47	2.79	5.09	3.26	6.73	4.10	6.84	5.99	6.28	5.09	6.92	3.89	6.91
PZT8	8.68	4.44	6.85	6.13	5.73	3.15	2.64	4.22	3.99	7.24	6.71	4.90	8.29
PZT10	3.01	5.18	3.27	5.88	8.30	2.19	3.57	3.17	5.97	7.28	5.11	3.30	3.93
PZT11	2.89	6.35	5.66	5.35	4.15	3.24	5.72	5.03	6.61	3.39	2.64	6.79	3.00
PZT12	3.76	5.35	4.46	4.88	4.19	4.55	3.45	5.34	5.63	6.21	5.92	6.01	5.36
Max	8.68	6.35	6.85	6.13	8.30	4.55	6.84	5.99	6.61	7.28	6.92	6.79	8.29
Average													
PZT7	4.63	3.14	4.03	3.28	6.26	4.34	4.35	4.52	4.84	4.64	5.11	4.36	5.12
PZT8	4.50	4.00	3.86	3.38	5.68	2.63	3.42	4.55	3.68	4.97	5.08	4.99	6.44
PZT10	4.24	3.91	3.54	3.77	5.51	3.31	3.06	3.72	3.97	5.22	3.75	4.50	4.87
PZT11	5.65	4.84	4.66	3.56	4.58	2.35	3.39	3.03	4.47	2.79	4.55	5.30	5.06
PZT12	3.96	4.26	4.18	4.29	6.28	3.39	3.65	4.01	4.14	3.70	4.38	4.43	4.95

Maximum values are highlighted

Table A-5 Session 2 EMD energy variability, 0-2500 Hz, IMF 1, plastic tip.

Location /Sensor	HC 2-1 (%)	HC 2-2 (%)	HC 2-3 (%)	HC 2-4 (%)	DC 2-1 (%)	DC 2-2 (%)	DC 2-3 (%)	DC 2-4 (%)	DC 2-5 (%)	DC 2-6 (%)	DC 2-7 (%)	DC 2-8 (%)	DC 2-9 (%)
Loc. A													
PZT7	7.84	5.62	3.85	5.61	7.13	1.59	1.36	7.13	10.17	16.82	10.32	10.94	15.20
PZT8	4.68	6.18	6.34	5.80	7.41	2.11	3.10	5.18	8.31	14.86	6.39	14.23	13.92
PZT10	5.71	3.09	8.45	4.92	3.95	2.82	3.07	6.97	2.63	16.30	4.74	10.01	15.20
PZT11	5.04	4.04	6.81	5.41	6.43	2.19	4.01	4.70	4.60	8.54	5.38	7.59	13.92
PZT12	4.46	4.10	10.29	5.80	6.60	1.64	2.01	5.97	3.43	7.97	4.49	4.91	0.00
Max	7.84	6.18	10.29	5.80	7.41	2.82	4.01	7.13	10.17	16.82	10.32	14.23	15.20
Loc. B													
PZT7	3.71	5.79	2.09	1.70	3.85	4.63	4.63	6.75	4.88	4.46	53.90	6.51	8.36
PZT8	3.50	4.49	1.89	1.77	6.03	4.11	5.06	8.02	6.86	6.29	53.24	6.60	7.76
PZT10	4.67	3.56	5.05	1.53	2.09	4.76	5.56	6.89	4.21	4.05	34.18	7.24	10.16
PZT11	5.01	2.53	2.89	2.88	2.31	4.07	3.66	6.00	4.96	5.12	22.92	5.04	6.88
PZT12	5.93	4.11	9.73	1.03	2.83	3.83	2.84	3.64	2.97	3.46	8.74	2.17	5.55
Max	5.93	5.79	9.73	2.88	6.03	4.76	5.56	8.02	6.86	6.29	53.90	7.24	10.16
Loc. C													
PZT7	2.21	4.04	3.01	2.38	1.08	5.00	3.34	15.32	7.50	13.03	13.86	31.54	26.02
PZT8	2.30	5.90	2.23	2.95	4.15	13.19	4.18	14.44	6.08	15.58	17.05	25.34	22.76
PZT10	3.09	5.22	4.62	2.79	2.64	9.64	6.13	4.17	5.09	8.87	16.46	20.12	26.21
PZT11	3.24	4.28	1.66	3.84	1.54	7.69	4.58	4.77	6.84	7.52	10.14	13.09	5.24
PZT12	2.15	7.27	5.39	1.71	3.39	2.88	5.48	4.04	2.71	4.97	7.85	3.58	8.26
Max	3.24	7.27	5.39	3.84	4.15	13.19	6.13	15.32	7.50	15.58	17.05	31.54	26.21
Loc. D													
PZT7	2.53	2.04	5.31	3.50	3.35	4.95	3.95	29.39	12.91	9.90	34.94	22.85	7.95
PZT8	3.94	4.59	9.99	3.34	2.65	5.49	4.61	29.34	13.93	11.99	20.19	25.98	11.48
PZT10	3.11	2.87	6.10	2.98	4.46	5.10	2.33	21.57	7.02	8.10	29.26	17.02	10.64
PZT11	2.90	3.05	8.21	4.37	3.09	4.60	4.00	9.40	6.15	5.85	10.71	5.55	4.36
PZT12	2.31	3.55	17.38	5.52	4.41	5.03	3.54	3.89	3.24	3.96	8.89	10.19	6.29
Max	3.94	4.59	17.38	5.52	4.46	5.49	4.61	29.39	13.93	11.99	34.94	25.98	11.48
Avg,													
PZT7	4.07	4.37	3.57	3.30	3.85	4.04	3.32	14.65	8.87	11.05	28.26	17.96	14.38
PZT8	3.60	5.29	5.11	3.47	5.06	6.23	4.24	14.24	8.79	12.18	24.22	18.04	13.98
PZT10	4.15	3.68	6.06	3.06	3.29	5.58	4.27	9.90	4.74	9.33	21.16	13.60	15.55
PZT11	4.05	3.47	4.89	4.12	3.34	4.64	4.06	6.22	5.64	6.75	12.29	7.82	7.60
PZT12	3.71	4.76	10.70	3.51	4.31	3.35	3.47	4.39	3.09	5.09	7.49	5.21	5.02

Maximum values are highlighted

Table A-6 Session 2 result repeatability, healthy cases, 0-2500 Hz, IMF1, aluminium tip.

	0-2500 Hz						
	Case 2 with Case 1	Case 3 with Case 1	Case 4 with Case 1		Case 3 with Case 2	Case 4 with Case 2	Case 4 with Case 3
Location A							
PZT7	0.38%	3.20%	2.69%		3.58%	2.31%	5.88%
PZT8	1.93%	4.63%	3.85%		6.55%	5.77%	0.79%
PZT10	7.96%	5.66%	4.83%		13.55%	3.14%	10.46%
PZT11	0.45%	2.44%	4.85%		1.98%	5.30%	7.28%
PZT12	0.88%	7.51%	1.66%		8.38%	0.79%	9.16%
Location B							
PZT7	7.25%	3.39%	0.05%		3.87%	7.30%	3.43%
PZT8	7.64%	6.97%	0.14%		14.54%	7.78%	6.84%
PZT10	4.09%	0.83%	7.51%		4.92%	3.43%	8.33%
PZT11	0.42%	2.12%	3.09%		2.54%	2.67%	5.21%
PZT12	2.61%	10.04%	7.31%		7.45%	4.71%	2.75%
Location C							
PZT7	2.05%	7.59%	6.72%		9.62%	8.76%	0.87%
PZT8	2.93%	9.41%	5.31%		12.30%	8.22%	4.12%
PZT10	6.96%	5.63%	5.89%		12.54%	1.08%	11.48%
PZT11	0.74%	4.33%	5.06%		5.07%	5.81%	0.74%
PZT12	0.81%	0.53%	2.01%		1.34%	2.82%	1.47%
Location D							
PZT7	2.44%	7.46%	11.54%		9.88%	13.94%	4.11%
PZT8	1.06%	4.45%	7.25%		5.51%	8.31%	2.81%
PZT10	12.03%	6.47%	2.93%		18.36%	9.14%	9.38%
PZT11	5.64%	0.13%	2.46%		5.51%	8.09%	2.59%
PZT12	2.51%	2.03%	7.99%		4.53%	10.48%	5.98%

Table A-7 Session 2 result repeatability, healthy cases, 0-2500 Hz, IMF1, plastic tip.

|	0-2500 Hz					
	Case 2 with Case 1	Case 3 with Case 1	Case 4 with Case 1	Case 3 with Case 2	Case 4 with Case 2	Case 4 with Case 3
Location A						
PZT7	9.02%	6.13%	1.14%	2.90%	10.14%	7.27%
PZT8	11.64%	1.53%	0.74%	13.14%	12.37%	0.79%
PZT10	4.58%	7.46%	4.73%	11.99%	0.16%	12.15%
PZT11	6.93%	5.43%	1.73%	1.51%	5.21%	3.71%
PZT12	1.39%	16.95%	0.36%	18.30%	1.76%	16.60%
Location B						
PZT7	15.49%	5.50%	2.54%	10.07%	13.00%	2.97%
PZT8	14.50%	3.66%	3.28%	18.07%	11.27%	6.94%
PZT10	1.63%	8.47%	5.46%	10.08%	3.83%	13.86%
PZT11	8.39%	6.72%	4.79%	1.68%	3.62%	1.94%
PZT12	3.63%	11.30%	2.04%	14.87%	5.66%	9.28%
Location C						
PZT7	3.74%	6.27%	6.69%	9.99%	10.41%	0.42%
PZT8	4.89%	10.73%	7.28%	15.53%	12.12%	3.48%
PZT10	12.29%	0.04%	8.12%	12.33%	4.22%	8.16%
PZT11	3.44%	1.79%	0.56%	1.65%	4.00%	2.35%
PZT12	1.30%	23.64%	0.99%	22.41%	0.31%	22.70%
Location D						
PZT7	8.65%	3.75%	9.32%	12.36%	17.82%	5.59%
PZT8	3.85%	12.92%	12.83%	16.70%	16.60%	0.10%
PZT10	13.46%	6.94%	1.52%	20.21%	14.95%	5.43%
PZT11	5.26%	4.62%	5.26%	9.86%	10.49%	0.64%
PZT12	1.77%	36.31%	7.86%	34.77%	9.61%	42.95%

Variations over 20% are highlighted

159

Table A-8 Session 3 EMD energy variability, 0-2000 Hz, IMF 1, aluminium tip.

Location /Sensor	HC 3-1	DC 3-1	DC 3-2	DC 3-3
Location A				
PZT10	10.09%	3.50%	6.18%	6.24%
PZT11	6.70%	3.84%	0.97%	3.59%
PZT12	8.63%	7.47%	3.35%	2.55%
PZT13	9.49%	4.48%	2.16%	5.21%
PZT14	4.02%	0.61%	2.25%	1.63%
PZT15	8.65%	6.99%	3.02%	2.51%
PZT16	8.14%	1.94%	4.16%	1.35%
Maximum	**10.09%**	**7.47%**	**6.18%**	**6.24%**
Location B				
PZT10	6.80%	4.82%	4.45%	4.11%
PZT11	2.26%	3.05%	2.83%	2.42%
PZT12	7.02%	3.66%	7.87%	6.72%
PZT13	7.94%	4.90%	6.90%	7.76%
PZT14	4.93%	6.61%	4.96%	10.44%
PZT15	6.03%	7.87%	8.65%	7.72%
PZT16	2.97%	2.45%	7.49%	4.53%
Maximum	**7.94%**	**6.61%**	**7.87%**	**10.44**
Location C				
PZT10	5.51%	5.99%	0.43%	3.18%
PZT11	4.39%	5.14%	5.45%	5.91%
PZT12	1.84%	1.35%	7.08%	10.62%
PZT13	5.28%	4.77%	5.65%	9.62%
PZT14	7.76%	3.04%	6.61%	7.80%
PZT15	4.15%	6.93%	6.21%	4.59%
PZT16	3.03%	3.25%	4.03%	3.17%
Maximum	**7.76%**	**5.99%**	**7.08%**	**10.62**
Location D				
PZT10	8.80%	2.13%	4.99%	4.04%
PZT11	11.80%	3.04%	4.11%	6.75%
PZT12	7.08%	3.30%	5.27%	10.21%
PZT13	8.53%	5.72%	3.38%	6.07%
PZT14	8.45%	6.91%	4.46%	7.61%
PZT15	9.32%	7.08%	2.34%	2.91%
PZT16	5.81%	5.35%	6.34%	7.83%
Maximum	**11.80%**	**6.91%**	**5.27%**	**10.21**

Table A-9 Session 3 EMD energy variability, 0-2000 Hz, IMF 1, plastic tip.

Location /Sensor	HC 3-1	DC 3-1	DC 3-2	DC 3-3
Location A				
PZT10	6.66%	2.09%	2.18%	2.30%
PZT11	6.09%	2.10%	3.52%	3.80%
PZT12	5.52%	2.07%	2.90%	2.64%
PZT13	5.13%	1.57%	0.99%	0.96%
PZT14	3.99%	2.16%	1.90%	2.32%
PZT15	7.17%	1.35%	3.65%	2.25%
PZT16	4.42%	1.96%	3.53%	0.42%
Maximum	**6.66%**	**2.16%**	**3.52%**	**3.80%**
Location B				
PZT10	4.71%	2.07%	6.69%	2.33%
PZT11	3.31%	0.93%	6.91%	2.12%
PZT12	3.22%	4.32%	5.55%	1.94%
PZT13	1.56%	1.93%	5.86%	2.25%
PZT14	3.95%	2.23%	7.00%	0.64%
PZT15	3.03%	2.31%	5.67%	1.12%
PZT16	4.39%	1.06%	4.25%	1.72%
Maximum	**4.71%**	**4.32%**	**7.00%**	**2.33%**
Location C				
PZT10	6.11%	2.23%	4.02%	0.92%
PZT11	5.37%	2.53%	4.08%	1.90%
PZT12	3.29%	4.78%	4.72%	2.22%
PZT13	3.99%	2.02%	3.21%	1.74%
PZT14	5.04%	0.64%	2.39%	2.31%
PZT15	2.83%	1.49%	4.26%	1.62%
PZT16	4.40%	1.17%	4.50%	1.22%
Maximum	**6.11%**	**4.78%**	**4.72%**	**2.31%**
Location D				
PZT10	3.46%	3.15%	3.30%	1.60%
PZT11	3.70%	4.02%	4.56%	2.23%
PZT12	5.43%	3.15%	4.13%	1.34%
PZT13	3.80%	4.76%	3.34%	1.82%
PZT14	3.41%	2.84%	4.63%	1.58%
PZT15	2.16%	3.95%	4.64%	0.95%
PZT16	3.87%	3.78%	3.67%	2.10%
Maximum	**5.43%**	**4.76%**	**4.63%**	**2.23%**

Table A-10 Session 3 EMD energy variability, 0-2000 Hz, IMF 2, aluminium tip.

Location /Sensor	HC 3-1	DC 3-1	DC 3-2	DC 3-3
Location A				
PZT10	16.29%	11.76%	5.29%	4.75%
PZT11	14.11%	9.54%	4.74%	0.98%
PZT12	9.15%	6.92%	4.76%	9.45%
PZT13	18.67%	3.76%	5.26%	12.84%
PZT14	18.99%	17.40%	8.41%	10.11%
PZT15	19.70%	14.54%	6.33%	11.07%
PZT16	21.14%	19.62%	10.60%	5.13%
Maximum	**18.99%**	**17.40%**	**8.41%**	**12.84%**
Location B				
PZT10	14.40%	4.50%	10.23%	8.95%
PZT11	7.70%	3.95%	5.15%	8.76%
PZT12	2.17%	11.88%	4.89%	5.08%
PZT13	12.54%	5.62%	9.74%	6.05%
PZT14	18.14%	13.81%	7.94%	7.35%
PZT15	21.14%	11.24%	8.03%	8.18%
PZT16	6.83%	2.30%	4.60%	12.49%
Maximum	**18.14%**	**13.81%**	**10.23%**	**8.95%**
Location C				
PZT10	4.44%	3.75%	9.59%	4.40%
PZT11	9.50%	8.09%	10.10%	3.91%
PZT12	11.57%	18.90%	9.79%	6.12%
PZT13	10.63%	10.79%	10.17%	3.90%
PZT14	13.12%	10.66%	13.06%	11.53%
PZT15	17.59%	11.43%	11.62%	18.88%
PZT16	10.56%	4.68%	13.09%	10.46%
Maximum	**13.12%**	**18.90%**	**13.06%**	**11.53%**
Location D				
PZT10	12.62%	3.16%	7.11%	5.96%
PZT11	5.87%	17.25%	15.53%	10.75%
PZT12	12.73%	1.47%	4.13%	3.75%
PZT13	6.92%	2.12%	9.88%	9.36%
PZT14	10.65%	7.84%	9.10%	6.91%
PZT15	13.57%	12.37%	6.47%	5.64%
PZT16	12.01%	4.75%	10.73%	5.73%
Maximum	**12.73%**	**17.25%**	**15.53%**	**10.75%**

Table A-11 Session 3 EMD energy variability, 0-2000 Hz, IMF 2, plastic tip.

Location /Sensor	HC 3-1	DC 3-1	DC 3-2	DC 3-3
Location A				
PZT10	4.03%	5.66%	3.61%	2.97%
PZT11	2.48%	2.13%	5.00%	2.01%
PZT12	5.81%	4.26%	1.53%	4.95%
PZT13	5.40%	1.08%	4.92%	0.91%
PZT14	7.73%	2.83%	3.13%	1.58%
PZT15	3.04%	2.56%	7.00%	4.93%
PZT16	3.66%	2.94%	1.66%	2.91%
Maximum	**7.73%**	**5.66%**	**5.00%**	**4.95%**
Location B				
PZT10	3.29%	1.26%	4.08%	6.39%
PZT11	6.77%	2.77%	3.97%	3.86%
PZT12	4.52%	5.84%	3.45%	2.70%
PZT13	6.45%	2.60%	4.35%	4.32%
PZT14	2.08%	2.73%	8.17%	3.59%
PZT15	3.10%	3.06%	2.14%	2.46%
PZT16	3.71%	3.21%	4.77%	6.24%
Maximum	**6.77%**	**5.84%**	**8.17%**	**6.39%**
Location C				
PZT10	3.93%	2.83%	3.42%	2.68%
PZT11	1.24%	6.75%	1.26%	1.34%
PZT12	1.52%	4.07%	3.54%	3.04%
PZT13	4.88%	4.07%	2.10%	2.76%
PZT14	3.54%	3.66%	0.18%	1.77%
PZT15	6.83%	5.66%	4.95%	1.86%
PZT16	3.35%	2.47%	1.09%	0.59%
Maximum	**4.88%**	**6.75%**	**3.54%**	**3.04%**
Location D				
PZT10	5.26%	2.23%	4.90%	4.89%
PZT11	4.76%	1.42%	2.29%	1.30%
PZT12	3.02%	5.23%	4.73%	3.21%
PZT13	3.25%	2.19%	1.72%	2.43%
PZT14	3.15%	2.29%	3.98%	3.93%
PZT15	3.92%	2.95%	2.79%	1.39%
PZT16	2.27%	3.11%	4.73%	1.81%
Maximum	**5.26%**	**5.23%**	**4.90%**	**4.89%**

A.2 GRAPHS
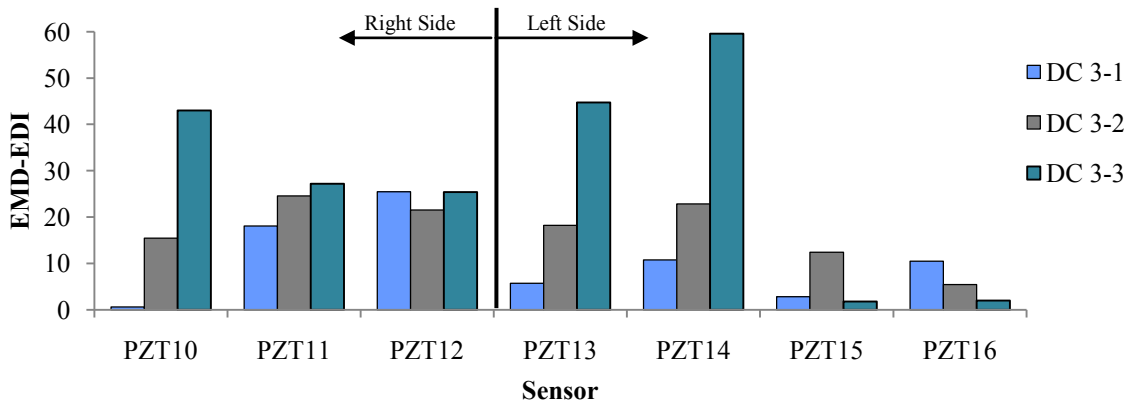
Figure A-1 EMD-EDI, session 3, location B, 0-2000 Hz, IMF2, aluminium tip.
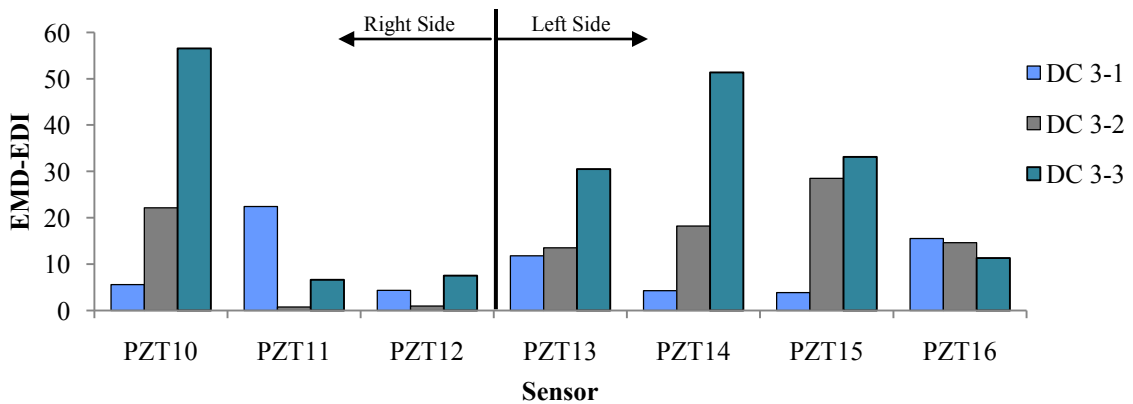
Figure A-2 EMD-EDI, session 3, location C, 0-2000 Hz, IMF2, aluminium tip.
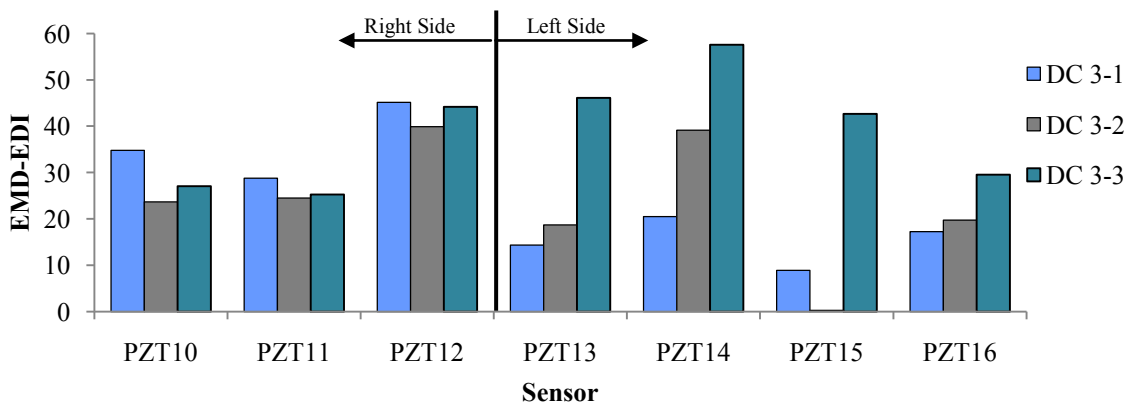
Figure A-3 EMD-EDI, session 3, location E, 0-2000 Hz, IMF2, aluminium tip.
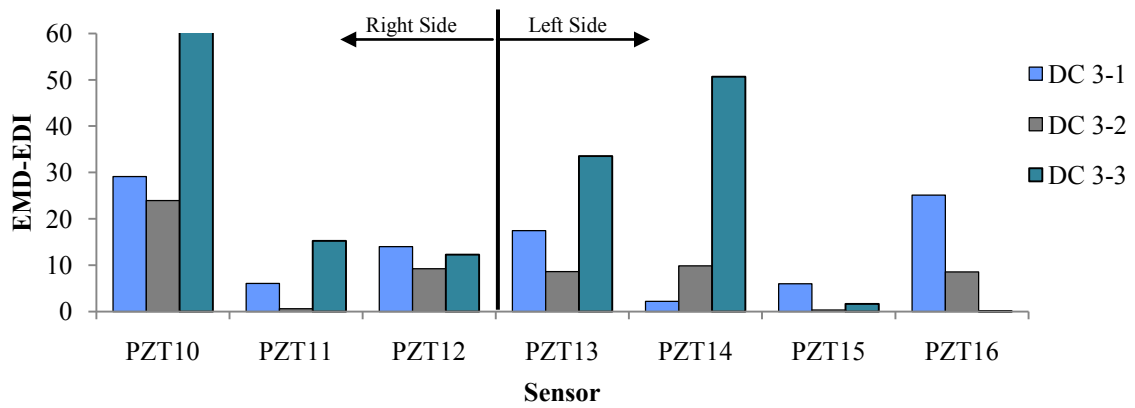
Figure A-4 EMD-EDI, session 3, location F, 0-2000 Hz, IMF2, aluminium tip.
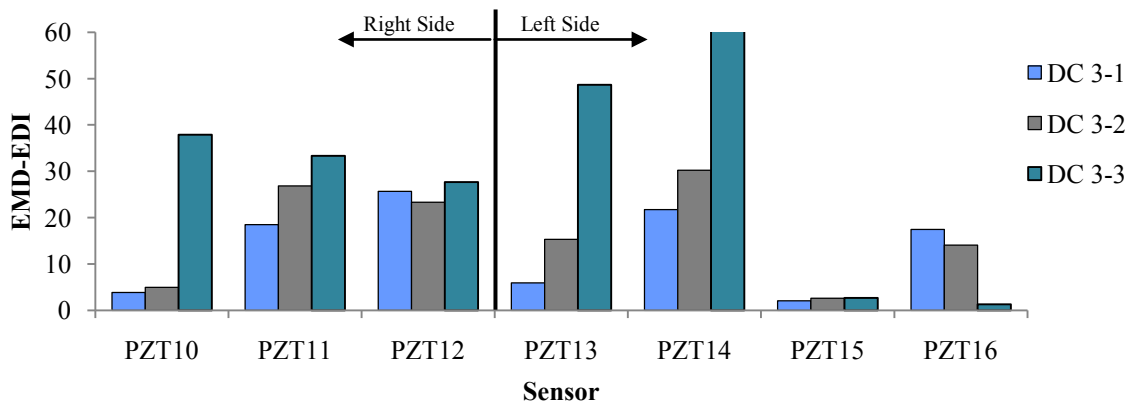
Figure A-5 EMD-EDI, session 3, location B, 0-2000 Hz, IMF2, plastic tip.
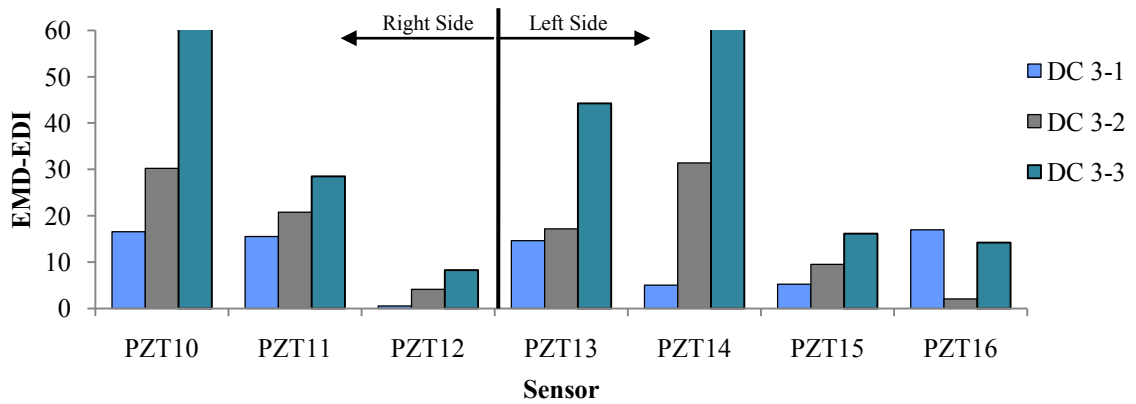
Figure A-6 EMD-EDI, session 3, location C, 0-2000 Hz, IMF2, plastic tip.
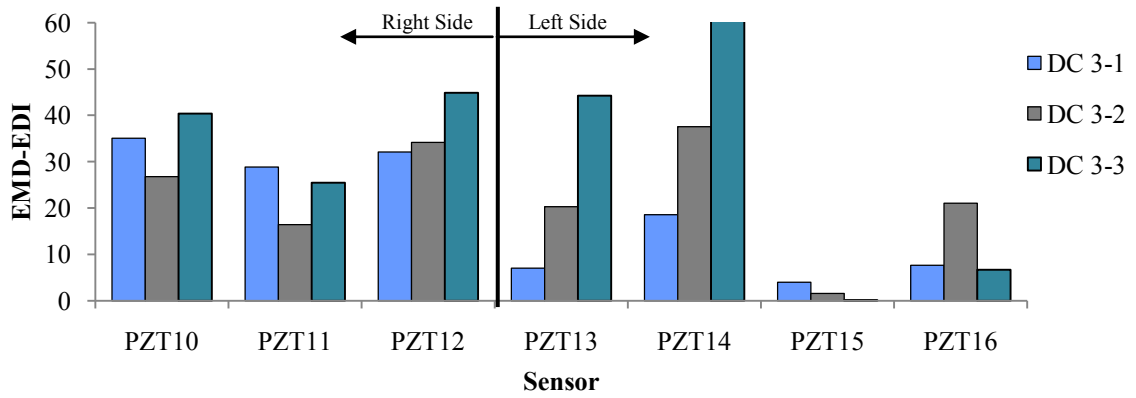
Figure A-7 EMD-EDI, session 3, location E, 0-2000 Hz, IMF2, plastic tip.
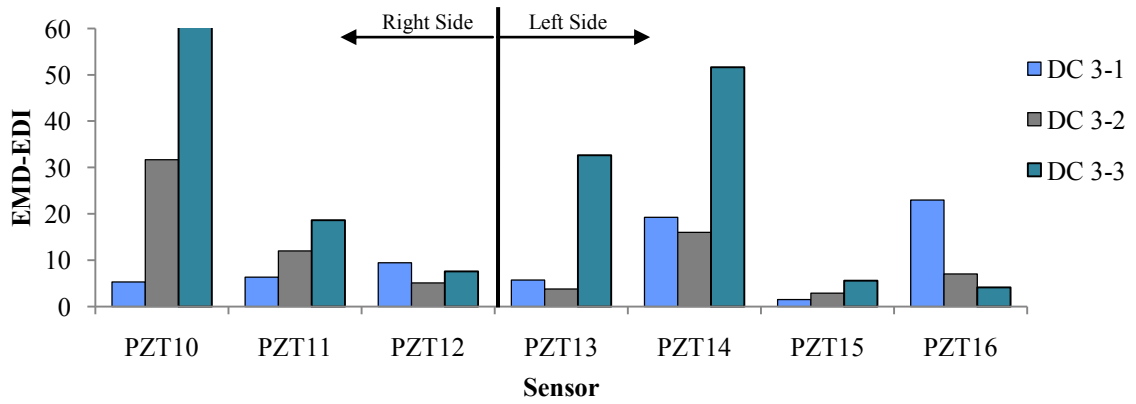
Figure A-8 EMD-EDI, session 3, location F, 0-2000 Hz, IMF2, plastic tip.
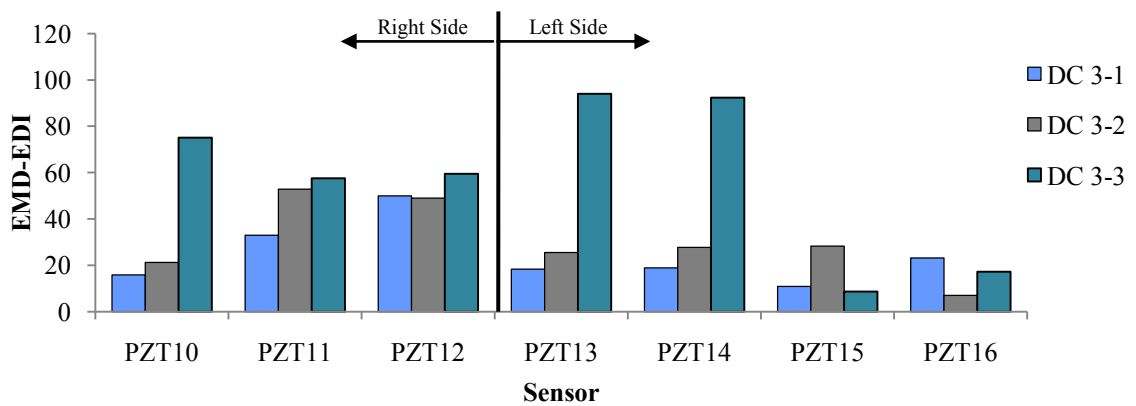
Figure A-9 EMD-EDI, session 3, location B, 0-2000 Hz, combined IMFs, aluminium tip.

166
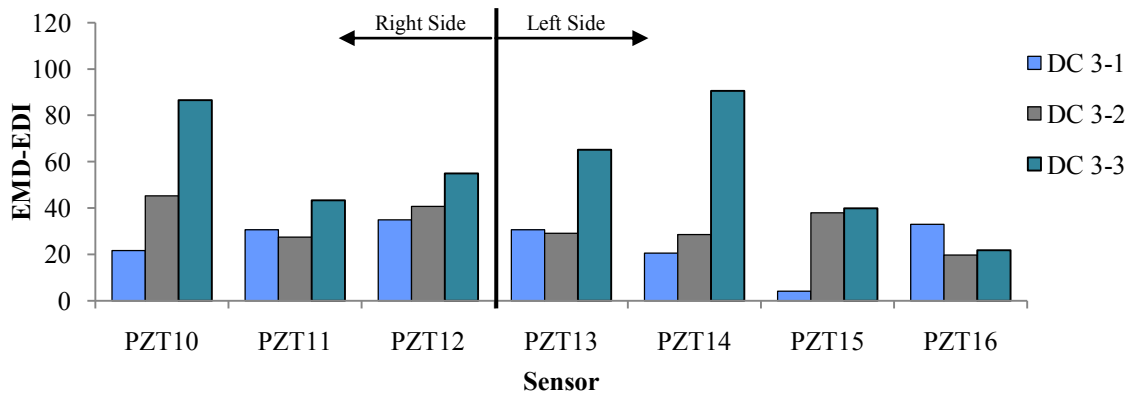
Figure A-10 EMD-EDI, session 3, location C, 0-2000 Hz, combined IMFs, aluminium tip.
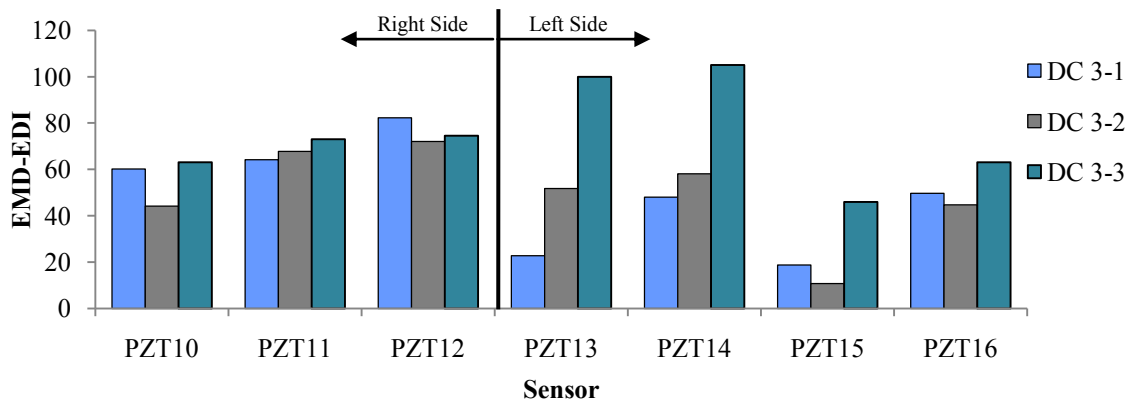
Figure A-11 EMD-EDI, session 3, location E, 0-2000 Hz, combined IMFs, aluminium tip.
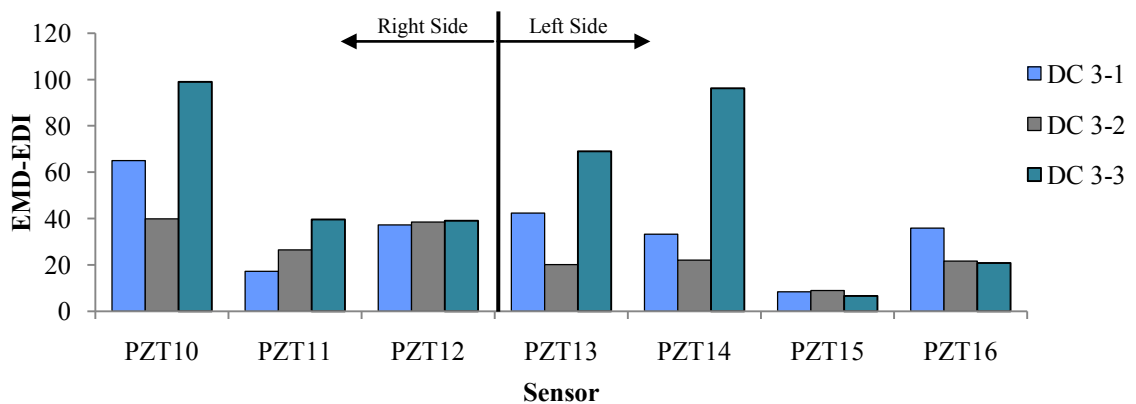
Figure A-12 EMD-EDI, session 3, location F, 0-2000 Hz, combined IMFs, aluminium tip.
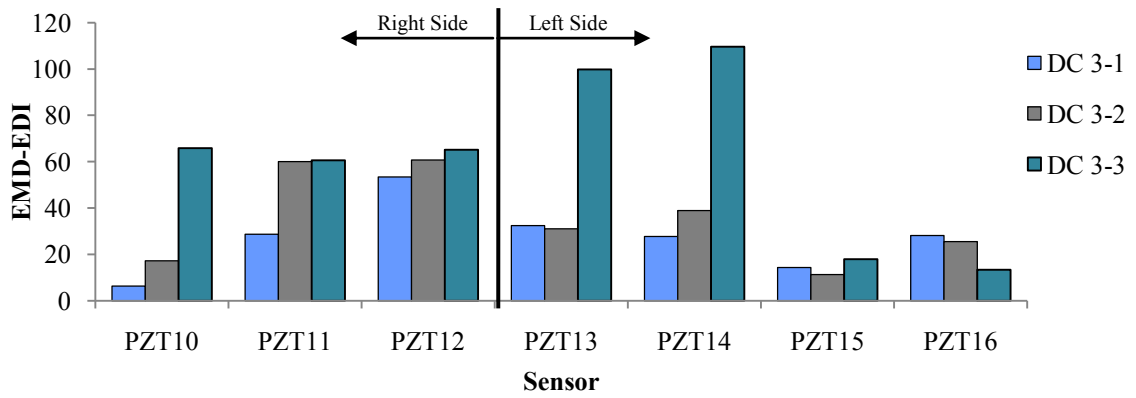
Figure A-13 EMD-EDI, session 3, location B, 0-2000 Hz, combined IMFs, plastic tip.
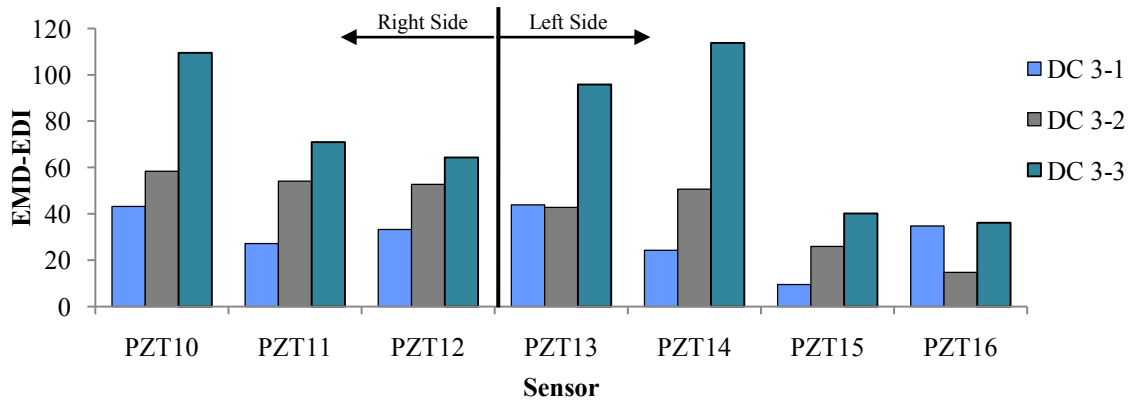
Figure A-14 EMD-EDI, session 3, location C, 0-2000 Hz, combined IMFs, plastic tip.
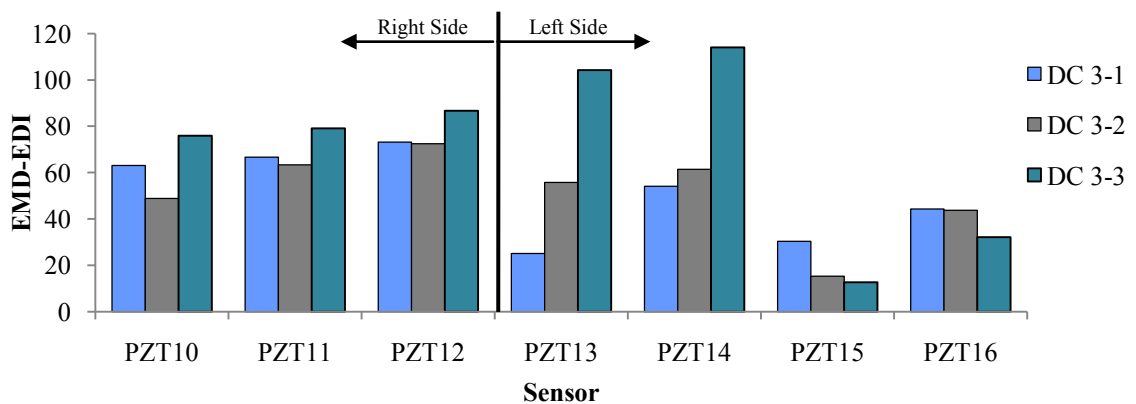
Figure A-15 EMD-EDI, session 3, location E, 0-2000 Hz, combined IMFs, plastic tip.
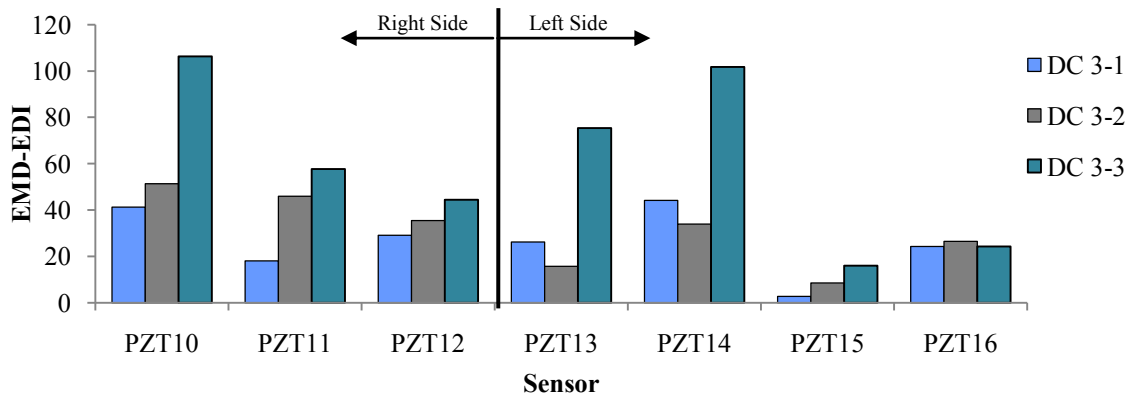
Figure A-16 EMD-EDI, session 3, location F, 0-2000 Hz, combined IMFs, plastic tip.

APPENDIX B

SUPPLEMENTARY RESULTS FROM CHAPTER 5

B.1 GRAPHS
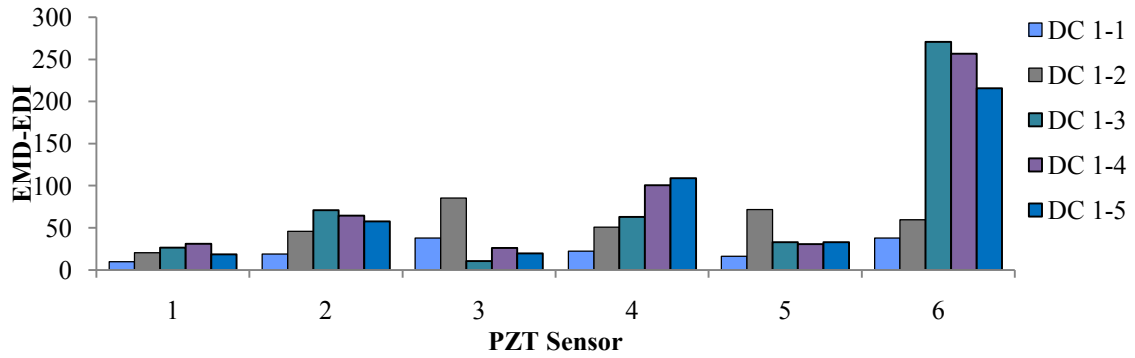
Figure B-1 EMD-EDI, damage scenario 1, location A, 0-1500 Hz, combined IMFs.
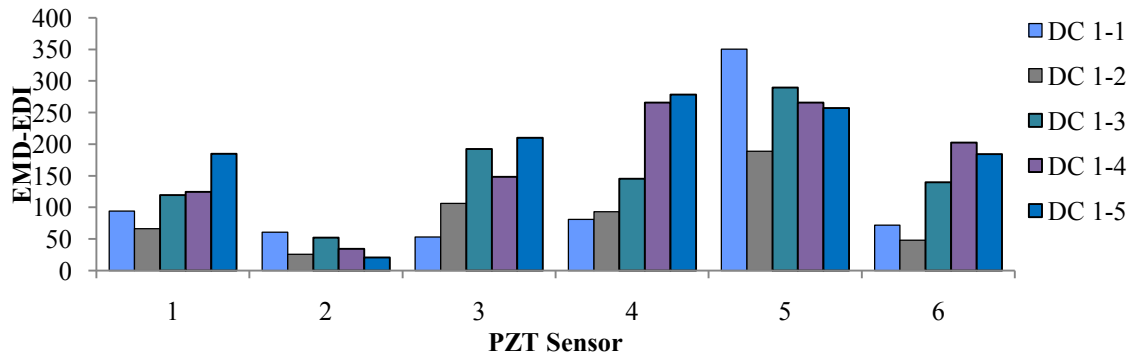
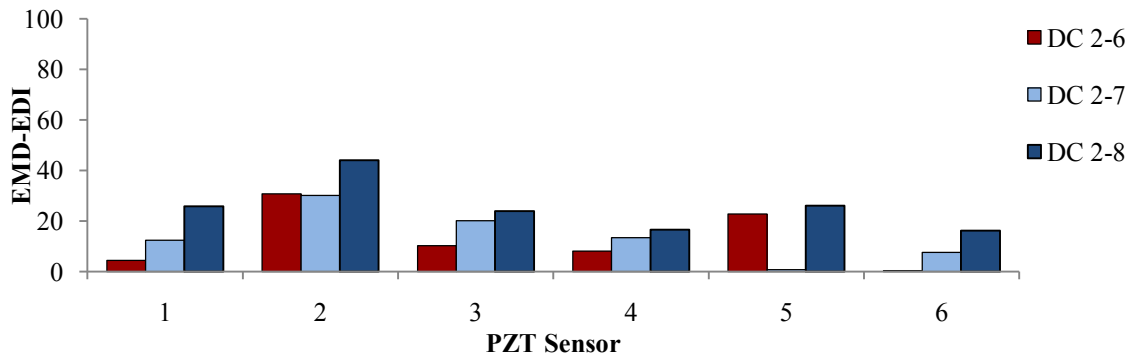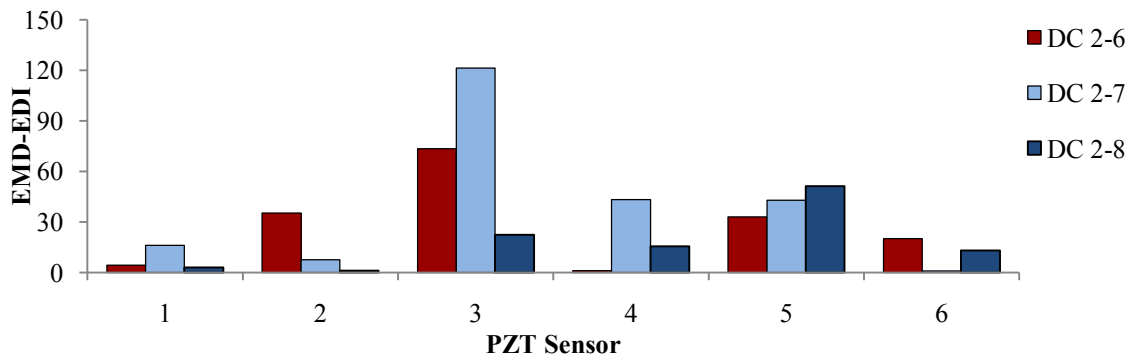**Figure B-2** EMD-EDI, damage scenario 1, location S, 500-2000 Hz, combined IMFs.
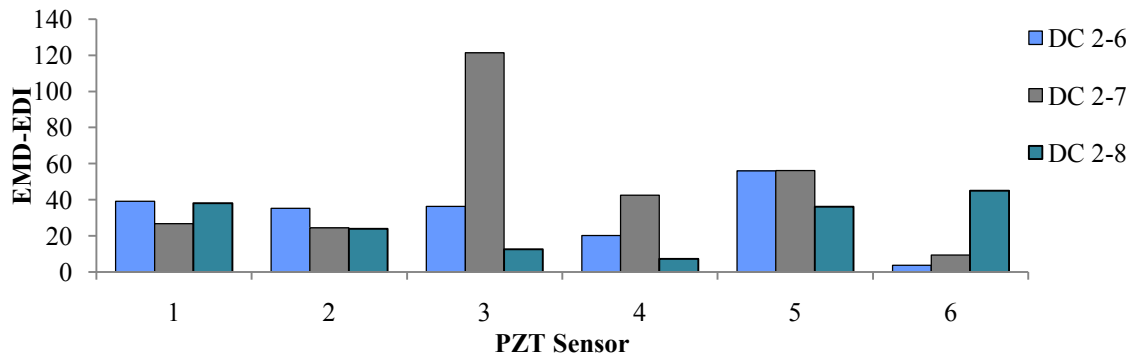
Figure B-3 EMD-EDI, damage scenario 2, location S, 0-1500 Hz, combined IMFs.
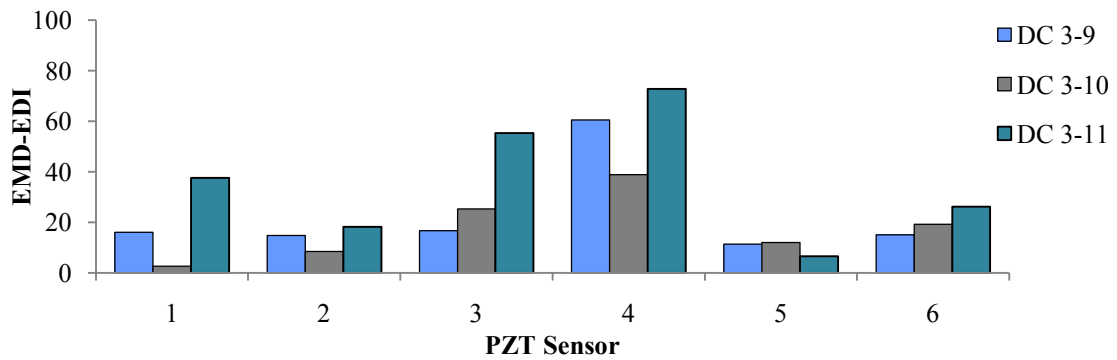
Figure B-4 EMD-EDI, damage scenario 3, location A, 0-1500 Hz, combined IMFs.
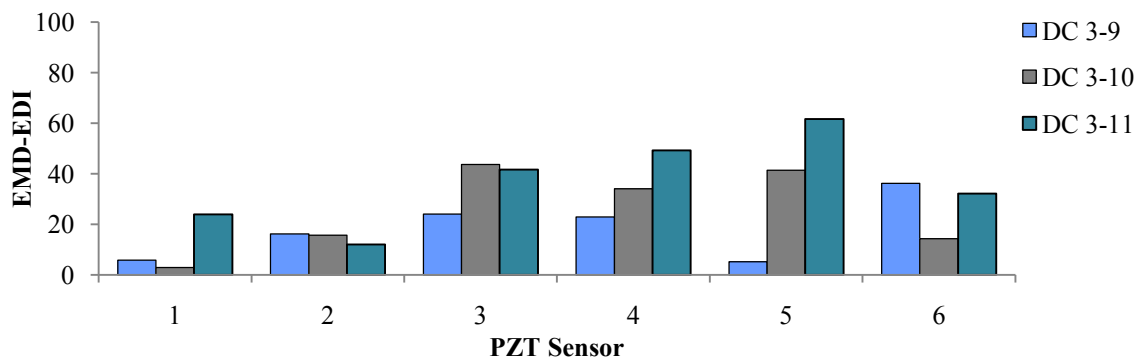
Figure B-5 EMD-EDI, damage scenario 3, location S, 0-1500 Hz, combined IMFs.
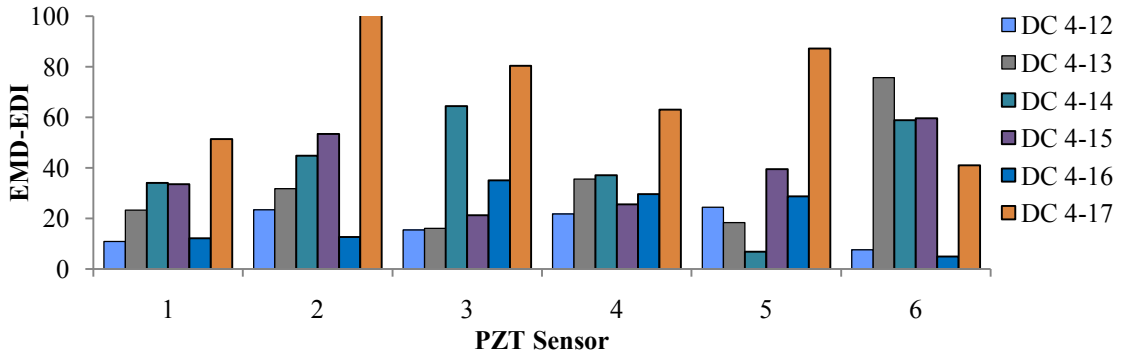
Figure B-6 EMD-EDI, damage scenario 4, location A, 0-2500 Hz, combined IMFs.
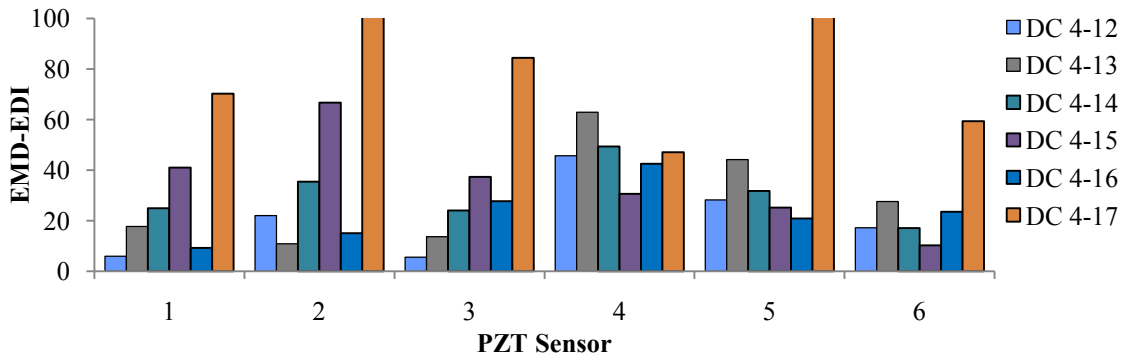
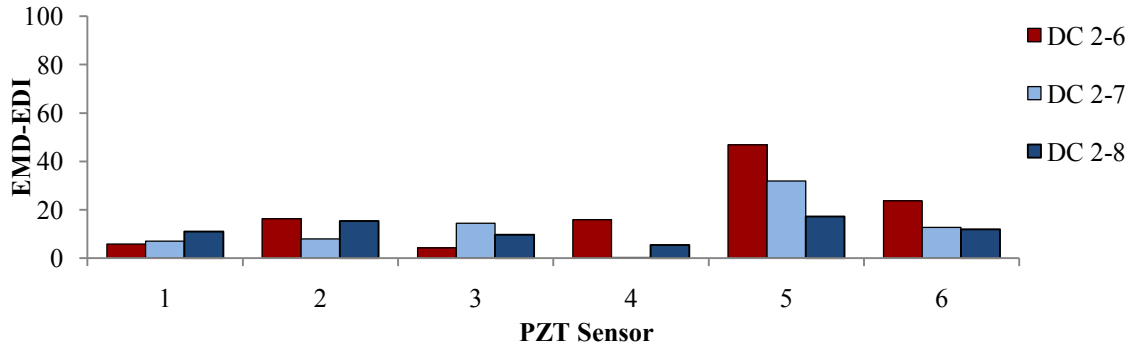**Figure B-7** EMD-EDI, damage scenario 4, location S, 0-2500 Hz, combined IMFs.
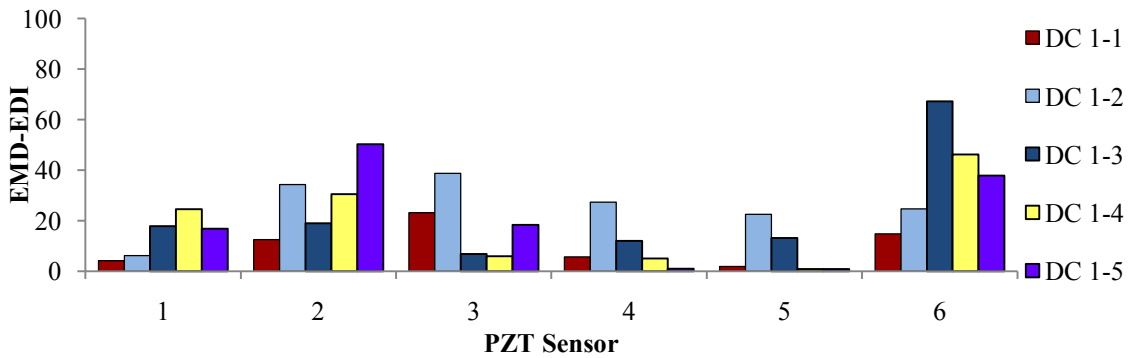
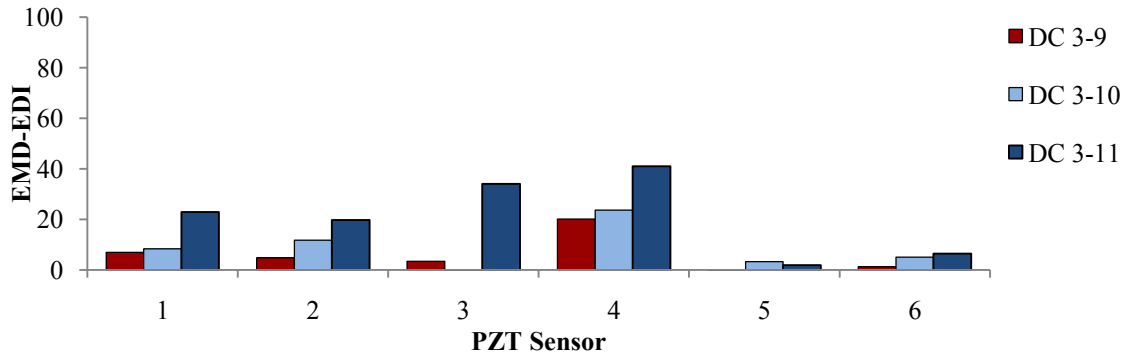**Figure B-8** EMD-EDI, damage scenario 1, location A, 0-2000 Hz, IMF1.
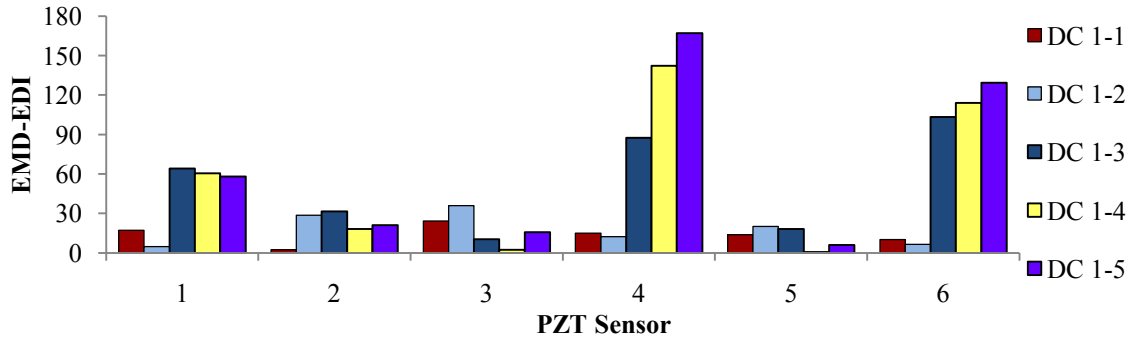
Figure B-9 EMD-EDI, damage scenario 1, location A, 0-2000 Hz, IMF2.
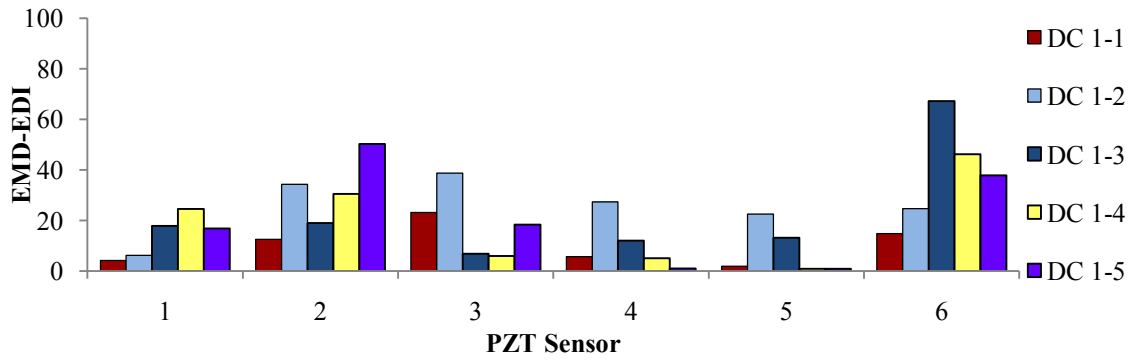
Figure B-10 EMD-EDI, damage scenario 1, location S, 0-2000 Hz, IMF1.
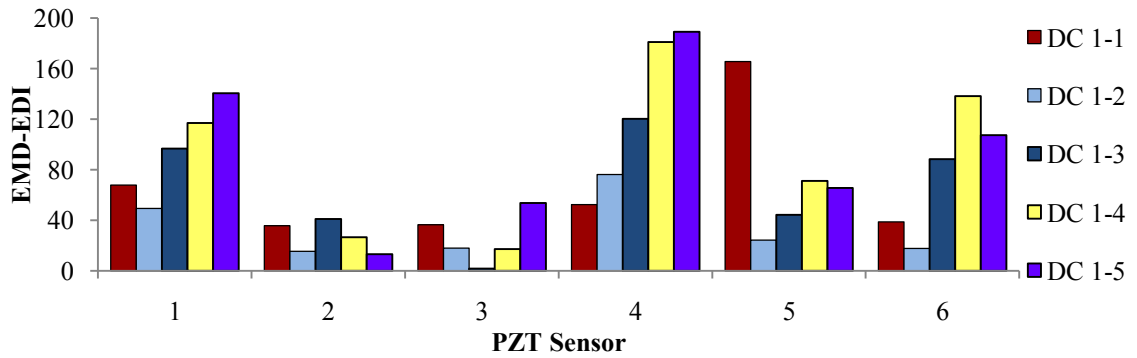
Figure B-11 EMD-EDI, damage scenario 1, location S, 0-2000 Hz, IMF2.
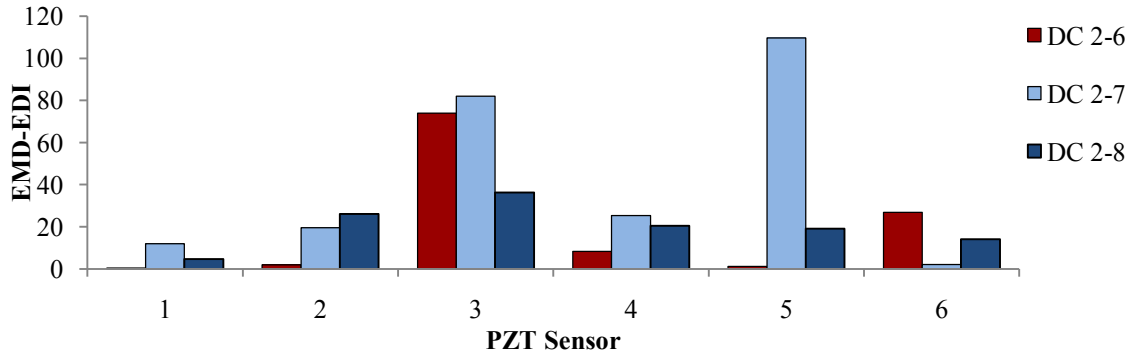
Figure B-12 EMD-EDI, damage scenario 2, location A, 0-2000 Hz, IMF1.

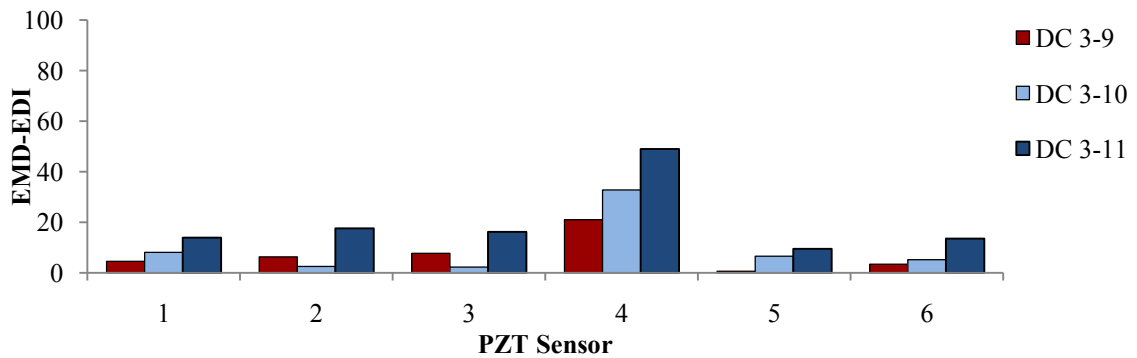**Figure B-13** EMD-EDI, damage scenario 2, location A, 0-2000 Hz, IMF2.

Figure B-14 EMD-EDI, damage scenario 2, location S, 0-2000 Hz, IMF1.
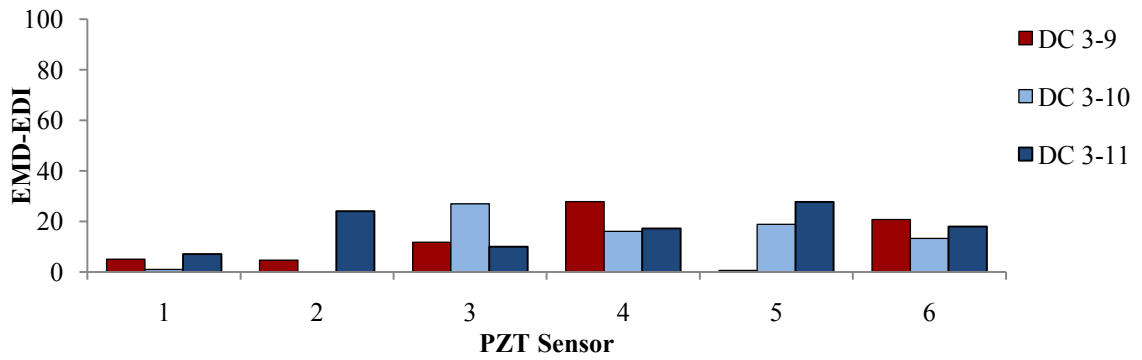
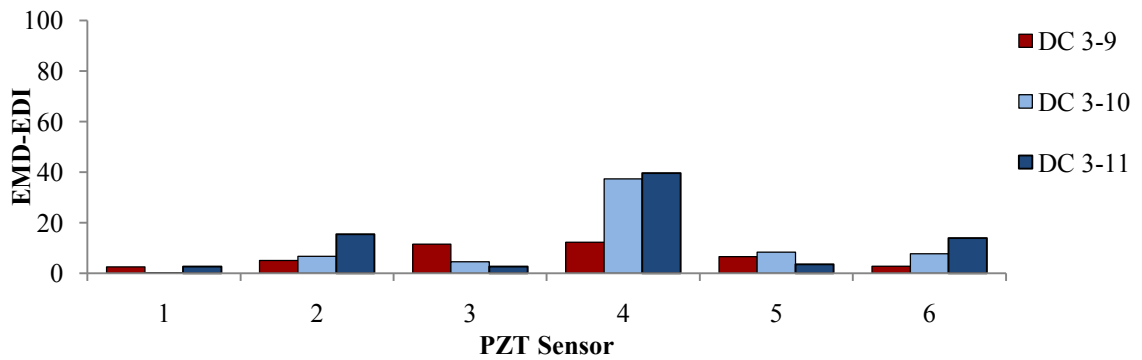**Figure B-15** EMD-EDI, damage scenario 2, location S, 0-2000 Hz, IMF2.

Figure B-16 EMD-EDI, damage scenario 3, location A, 0-2000 Hz, IMF1.

Figure B-17 EMD-EDI, damage scenario 3, location A, 0-2000 Hz, IMF2.

175

Figure B-18 EMD-EDI, damage scenario 3, location S, 0-2000 Hz, IMF1.

Figure B-19 EMD-EDI, damage scenario 3, location S, 0-2000 Hz, IMF2.

Figure B-20 EMD-EDI, damage scenario 4, location A, 0-2000 Hz, IMF1.
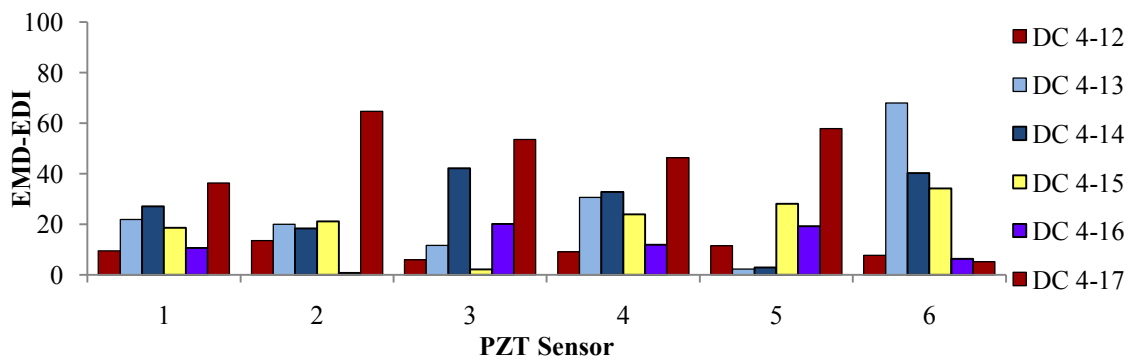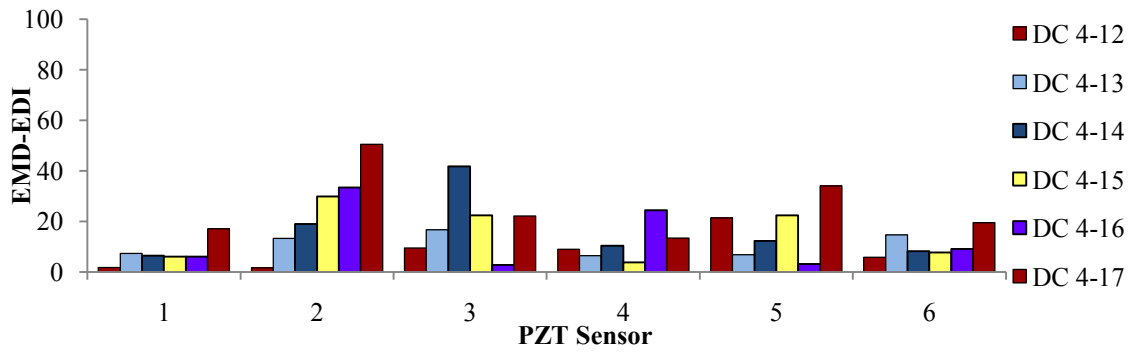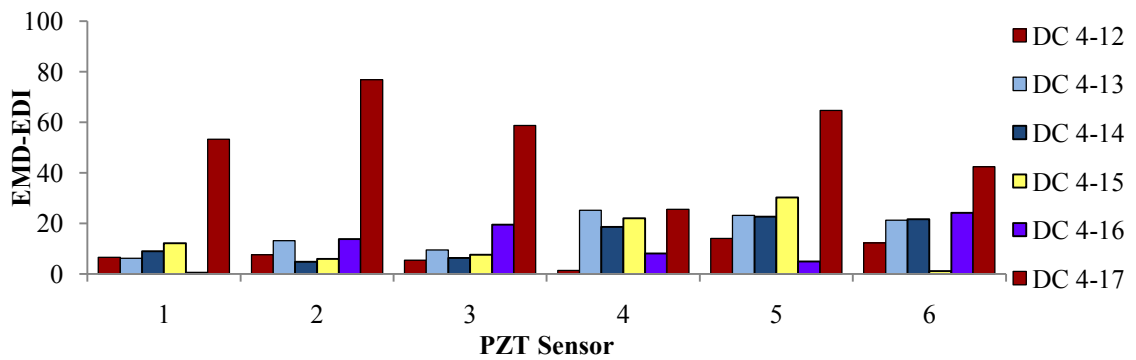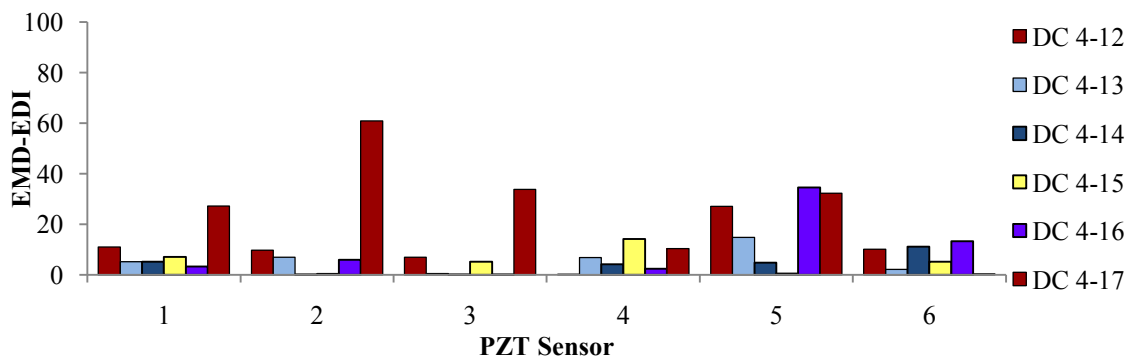
Figure B-21 EMD-EDI, damage scenario 4, location A, 0-2000 Hz, IMF2.

Figure B-22 EMD-EDI, damage scenario 4, location S, 0-2000 Hz, IMF1.

Figure B-23 EMD-EDI, damage scenario 4, location S, 0-2000 Hz, IMF2.

APPENDIX C

SUPPLEMENTARY RESULTS FROM CHAPTER 6

C.1 TABLES

Table C-1 EMD energy variability, 0-2000 Hz, IMF 1.

Boundary Condition: Free-free				
Scenario 1				
Sensor	HC 1-1	DC 1-1	DC 1-2	DC 1-3	DC 1-4
	(%)	(%)	(%)	(%)	(%)
PZT1	19.97	15.34	62.15	63.14	24.13
PZT2	5.78	16.90	35.71	13.75	7.45
PZT3	15.90	19.90	53.47	49.24	14.19
PZT4	11.14	9.59	50.62	19.80	10.58
PZT5	25.08	15.80	35.30	30.62	24.01
PZT6	12.41	41.94	14.93	55.71	22.54
PZT7	16.47	15.90	15.73	21.26	8.63
Max	25.08	41.94	62.15	63.14	24.13

Scenario 2				
Sensor	HC 2-1	DC 2-5	DC 2-6	DC 2-7	DC 2-8
	(%)	(%)	(%)	(%)	(%)
PZT1	33.25	40.53	19.66	29.90	57.25
PZT2	22.19	28.49	35.76	17.53	23.91
PZT3	18.41	18.00	18.29	31.63	40.11
PZT4	7.61	12.22	10.09	8.27	17.43
PZT5	40.69	33.45	7.10	23.60	25.21
PZT6	25.84	17.95	17.96	15.65	14.55
PZT7	15.99	10.17	4.43	17.76	19.19
Max	40.69	40.53	35.76	31.63	57.25

Table C-2 EMD energy variability, 0-1500 Hz, IMF 1.

Boundary Condition: Cantilevered

Scenario 1

Sensor	HC 1-1 (%)	DC 1-1 (%)	DC 1-2 (%)	DC 1-3 (%)	DC 1-4 (%)
PZT1	26.72	11.34	41.90	7.48	8.23
PZT2	48.63	40.98	30.49	9.23	17.11
PZT3	28.64	11.60	22.10	7.05	7.28
PZT4	48.89	53.72	41.11	9.88	18.20
PZT5	23.56	11.95	49.47	7.76	7.06
PZT6	21.59	21.30	28.37	6.12	20.06
PZT7	32.46	12.53	28.92	6.47	7.78
Max	48.89	53.72	49.47	9.88	8.23

Scenario 2

Sensor	HC 2-1 (%)	DC 2-5 (%)	DC 2-6 (%)	DC 2-7 (%)	DC 2-8 (%)
PZT1	14.27	46.93	19.35	24.96	17.09
PZT2	19.25	38.43	39.48	18.66	50.58
PZT3	25.14	24.50	20.36	21.28	7.64
PZT4	54.54	52.62	53.16	15.53	58.23
PZT5	83.92	31.50	18.94	42.22	19.30
PZT6	64.53	36.69	27.65	22.13	11.61
PZT7	37.69	17.87	27.27	29.14	16.82
Max	83.92	52.62	53.16	42.22	58.23

Table C-3 Result repeatability, healthy states, 0-2000 Hz.

Boundary Condition: Free-free

Sensor	Case 1 & Case 2	Case 2 & Case 3	Case 1 & Case 3
PZT1	14.7%	28.2%	14.0%
PZT2	16.3%	43.1%	28.8%
PZT3	9.0%	20.2%	11.4%
PZT4	6.7%	44.0%	38.4%
PZT5	6.3%	25.1%	19.1%
PZT6	18.6%	20.0%	37.2%
PZT7	31.9%	8.6%	39.5%
Max	31.9%	44.0%	39.5%

Boundary Condition: Cantilevered

Sensor	Case 1 & Case 2	Case 2 & Case 3	Case 1 & Case 3
PZT1	1.0%	13.7%	14.6%
PZT2	8.4%	11.7%	19.8%
PZT3	0.7%	4.9%	4.3%
PZT4	9.1%	11.2%	20.1%
PZT5	29.5%	48.4%	22.1%
PZT6	6.4%	17.7%	23.8%
PZT7	11.3%	2.5%	8.8%
Max	29.5%	48.4%	23.8%

APPENDIX D

COPYRIGHT RELEASE REQUEST
& STUDENT CONTRIBUTION TO MANUSCRIPT